A MODEL FOR MAGNETIC BUBBLES IN ION IMPLANTED TYPE OF CHANNELS

A MODEL FOR MAGNETIC BUBBLES IN ION IMPLANTED TYPE OF CHANNELS

by

SAMI HAKIM MIKHAIL

B.E.Eng., M.Sc.

A Thesis

Submitted to the Faculty of Graduate Studies

in Partial Fulfilment of the Requirements

for the Degree

Master of Engineering

McMaster University

December 1975

Master of Engineering
(Electrical Engineering)

McMaster University
Hamilton, Ontario

TITLE: A MODEL FOR MAGNETIC BUBBLES IN ION IMPLANTED TYPE OF CHANNELS.

AUTHOR: SAMI HAKIM MIKHAIL
B.E.Eng.(Cairo University, 1972)
M.Sc.(The American University in Cairo, 1974)

SUPERVISOR: Dr. W. Kinsner
(Assistant Professor)

NUMBER OF PAGES: x , 146

SCOPE AND CONTENTS:

The purpose of this thesis is to present a model for magnetic domains wholly situated inside an ion implanted channel. In this model, ion implantation is assumed to change the saturation magnetization, the wall energy density, and the in-plane susceptibility. As a result the channel and the domain induce magnetic pole distributions on the channel walls which interact with the bubble domain, altering its geometry and energy. An analysis for a circular domain with variable penetration and location in the channel, as well as a variational formulation for a generally deformable domain of fixed penetration in the implanted channel, are presented. The latter case has been programmed and the results obtained are discussed. The case of a domain penetrating into the unimplanted region outside the channel is also considered.

ACKNOWLEDGEMENTS

I would like to thank Dr. E. Della Torre for supervising the initial stages of this work, and for his comments.

My heart felt thanks go to Dr. W. Kinsner for suggesting the topic, and for his continuous encouragement and active supervision of this thesis through all its phases.

I am grateful to Dr. J.W. Bandler for allowing me to use his program packages.

Special thanks go to my colleagues Mr. W. Ishak and H.L. Abdel Malek for their help and lively discussions.

I would like to thank the National Research Council and the Defence Research Board for financial support.

I would further like to thank Mrs. R. Henderson for her excellent typing of this thesis.

TABLE OF CONTENTS PAGE

TABLE OF CONTENTS Continued. PAGE

LIST OF VARIABLES

M_1 - Saturation magnetization of the nonimplanted region of the bubble supporting material.

M_2 - Saturation magnetization of the ion implanted layer of the bubble supporting material.

σ_1 - Magnetic domain-wall energy density for the nonimplanted region of the material.

σ_2 - Magnetic domain-wall energy density for the ion implanted layer of the material.

σ' - Magnetic domain-wall energy density of the bubble cap.

q_1 - Magnetic quality factor of the nonimplanted material.

q_2 - Magnetic quality factor of the ion implanted material.

χ_t - In-plane magnetic susceptibility.

ρ - Volume magnetic charge density.

T - Thickness of bubble material uniform plate.

r_i - The ith radial variable parameter of the magnetic bubble domain.

δ - Displacement of bubble co-ordinate origin along y axis from the channel central plane of symmetry (i.e., from xy plane).

2w - Width of the ion implanted channel.

D - Depth of the ion implanted channel.

Δ - Width of the side walls of the channel.

H_D - Demagnetizing field.

H_w - Equivalent bubble wall field.

H_B - External uniform bias field.

H_{cw} - Field due to channel wall induced poles.

H_{cB} - Channel bases demagnetizing field correction.

$\bar{H}_z$ - z-averaged, z-component of the total field acting at a bubble domain wall.

p_i - Magnetic pressure at a point i.

LIST OF FIGURES

LIST OF TABLES

PAGE

CHAPTER 1

QUALITATIVE ANALYSIS OF ION IMPLANTATION OF FERRIMAGNETIC THIN FILMS

1.1 Introduction

In recent years, considerable interest has arisen in the potential ability of magnetic domains in thin film ferrimagnetic materials (e.g. orthoferrites, garnets, etc.) to act as memory units, due to their stability, reliability and alleged superior performance in moderate speed memory systems. A trend to attain a high packing density can be observed; in the case of ferrimagnetic domain memories, such as garnets [21] and recently certain amorphous films [6,19] which can support domains in the micron and submicron range, packing densities of 10^6 bits per sq. inch are prophicied.

Unfortunately, in the case of garnets, the so called domain wall may not be of the simple type, namely the Bloch type or the Néel type, but is actually a mixed type wall which changes from Bloch type to Néel type in cycles around the domain boundary [4]. Domains with this type of the wall are called "hard bubbles" [2].

Hard bubbles have anomalous dynamic properties. Unlike "soft bubbles" that propagate along the direction of the field gradient, hard bubbles move at an angle (or several possible angles)

to this direction; this could be the direction that requires the least energy to start flipping the spins, effectively moving the whole domain. Since statistically we could have walls with one, two, and in general n cycles; with various probabilities, it is impossible to guarantee a unique direction of motion of a hard bubble. Furthermore, walls may unwind at high field gradients decreasing the number of cycles changing suddenly the direction of propagation.

Such unreliable propagation properties act as a deterrent to the technical exploitation of garnets in magnetic memories, however, it has been reported by several workers [3,4,5] that multilayer garnet films and the ion implantation of garnet films could supress such hard bubbles by rendering them "soft" and inducing them to behave like normal ones. The physical mechanism of such a process is not yet properly understood, although several endeavours have been made [3,4] based on the assumption that the ion implanted layer has its spins almost aligned in-plane rather than normal to the crystal surface along the originally easy axis of magnetization. This normally leads to bubble capped by a 90° wall at the interface of the implanted and nonimplanted regions of the bubble material, and not penetrating through the implanted region [3,4]. Recently however, it has been reported [11] that in some cases ion implantation changes the material magnetic quality factor q to a lower value, and

it has been reported that a layer of low q on top of a layer of higher q film facilitates the supression of hard bubbles [11,22]. No physical reasoning exists for this latter behavior.

In the fabrication of magnetic domain memory arrays, one does not have to implant all the crystal substrate only the channels through which the domain is to propagate need be implanted. Therefore, ion implanted channels are of importance in potential engineering applications [8,9,15], and a model for the magnetic domain inside an ion implanted channel could be very significant. Up to date, an adequate model has not been published and the published experimental data concerning the changes in magnetic parameters induced by ion implantation is scarce. The model presented in this thesis will incorporate all the possible parameter changes in sight, leaving future work to decide which and how much each parameter changes.

In the following section we shall endeavour to give a physical interpretation of the mechanism by which ion implantation alters the magnetic properties of a crystalline ferrimagnetic material. The conclusions that are drawn concerning the changes in the various physical parameters are consistent with the observed [23].

1.2 Ferrimagnetism and Ion Implantation

Ferromagnetism is a collective phenomenon arising from the overlap of outer atomic orbitals, and the electron-electron interactions

of those electrons occupying those orbitals. For conducting ferromagnetic materials (e.g., Fe,Co,Ni) the orbital overlap is big, resulting in the formation of a narrow conduction band, and the picture is that of an electron-hole pair of opposite spin, their relative motions being such that they reside on the same atomic site most of the time [18,20]. On the other hand, for a variety of insulating ferrimagnetic materials (such as garnets) the well established picture of the "Heisenberg exchange interaction" seems to represent the situation well. The relative importance of the various aforementioned contributions to the collective phenomenon of ferromagnetism remains a controversial matter.

The Hamiltonian for an electron in a solid has the form

$$H = \sum_i \left[\frac{1}{2m} p_i^2 + V(\vec{r}_i) \right] + \frac{1}{2} \sum_{i \neq j} \frac{e^2}{|\vec{r}_i - \vec{r}_j|} \qquad (1.2.1)$$

where $V(\vec{r})$ is the potential energy of the ion-electron interaction, while the last term represents the one electron-electron interactions. If we represent the one electron part by $h(r_i)$ and the interaction term by $\frac{1}{2} \sum_{ij} v_{ij}$, we can recast (1.2.1) in the second quantization notation

$$H = \sum_{\mu\nu} \langle \mu | h | \nu \rangle a_\mu^+ a_\nu + \frac{1}{2} \sum_{\substack{\mu\nu \\ \sigma\tau}} \langle \mu\nu | v | \sigma\tau \rangle a_\mu^+ a_\nu^+ a_\tau a_\sigma \qquad (1.2.2)$$

where

$$< \mu|h|\nu > = \int \phi_\mu^*(\vec{r})h(\vec{r})\phi_\nu(\vec{r})d\vec{r} \qquad (1.2.3)$$

and

$$< \mu\nu|v|\sigma\tau > = \int \phi_\mu^*(\vec{r})\phi_\nu^*(\vec{r}')v(\vec{r}-\vec{r}')\phi_\sigma(\vec{r}')\phi_\tau(\vec{r})d\vec{r}d\vec{r}'$$

The a_γ^+ and a_γ are the creation and annihilation operators of an electron in state γ. The complete set of functions ϕ will now be chosen as Bloch functions ψ_k^i, where i is the band index. If σ is the spin variable, then, for each Bloch function, we shall have two creation and destruction operators corresponding to the spin up and spin down. Furthermore, if ε_{ik} are the single-electron eigenvalues $< \psi_k^i|h|\psi_k^i>$ we may write

$$H = \sum_{k,i,\sigma} \varepsilon_k^i a_{ki\sigma}^+ a_{ki\sigma}$$

$$+ \frac{1}{2} \sum_{k_1,k_2,k_1',k_2'} \sum_{i_1,i_2,i_1',i_2'} \sum_{\sigma,\sigma'} < k_1 i_1 k_2 i_2 \frac{e^2}{r} | k_1' i_1' k_2' i_2' >$$

$$a^+_{k_1,i_1\sigma_1} \quad a^{+\prime}_{k_2 i_2 \sigma_2} \quad a_{k_2' i_2' \sigma_2'} \quad a_{k_1' i_1' \sigma_1'} \qquad (1.2.4)$$

where

$$< k_1 i_1 k_2 i_2 | \frac{1}{r} | k_1' i_1' k_2' i_2' > = e^2 \int \frac{\psi^*_{k_1}{}^{i_1}(\vec{r})\psi_{k_2}{}^{i_2}(\vec{r}')\psi_{k_1}{}^{i_1'}(\vec{r})\psi_{k_2}{}^{i_2'}(\vec{r}')}{|\vec{r}-\vec{r}'|} d\vec{r}' d\vec{r} \qquad (1.2.5)$$

It is seen that it would be very difficult and impractical to handle the sum over all bands. However, for 3d electrons in transition metals we may deal with five sub-bands, and it would be convenient to follow Kubo and Hubbard and treat the case of an isolated 5-band, using an approximated Hamiltonian with a one band label only which will be dropped.

To emphasize the atomic aspect of the problem we now work in a Wannier function representation. The Wannier function w is defined by

$$\psi_k(\vec{r}) = \frac{1}{N^{1/2}} \sum_{\ell} w(\vec{r}-\vec{R}_\ell) \exp i\vec{k}\cdot\vec{R}_\ell \qquad (1.2.6)$$

where $\vec{R}_\ell$ is a lattice vector and N is the number of atoms per unit volume. Using the result

$$\sum_{\vec{k}} \exp i\vec{k}.(\vec{R}_\ell-\vec{R}_j) = N\delta_{\ell j}, \qquad (1.2.7)$$

where $\delta_{\ell j}$ is the Kronecker delta symbol.

One could obtain the inverse tranformation

$$w(\vec{r}-\vec{R}_\ell) = N^{-1/2} \sum_{\vec{k}} \psi_k(\vec{r}) \exp -i\vec{k}.\vec{R}_\ell$$

Corresponding to this relation we define

$$\left.\begin{aligned} a^+_{\ell\sigma} &= N^{-1/2} \sum_k a^+_{k\sigma'}, \exp -i\vec{k}.\vec{R} \\ a_{\ell\sigma} &= N^{-1/2} \sum_k a_{k\sigma} \exp i\vec{k}.\vec{R} \end{aligned}\right\} \qquad (1.2.8)$$

We can now write the approximated one band Hamiltonian as

$$H = \sum_{ij} \varepsilon_{ij} a^+_{i\sigma} a_{j\sigma} + \frac{1}{2} \sum_{\substack{ij\sigma\sigma \\ k\ell}}{}' \langle ij|\frac{1}{r}|k\ell\rangle a^+_{\ell\sigma} a^+_{k\sigma} a_{k\sigma'} a_{\ell\sigma} \qquad (1.2.9)$$

where

$$\varepsilon_{ij} = \int w^*(\vec{r}-\vec{R}_i) h(\vec{r}) w(\vec{r}-\vec{R}_j) d\vec{r} \qquad (1.210a)$$

and

$$\langle ij|\frac{1}{r}|k\ell\rangle = e^2 \int \frac{w^*(\vec{r}-\vec{R}_i) w^*(\vec{r}-\vec{R}_j) w(\vec{r}-\vec{R}_k) w(\vec{r}-\vec{R}_\ell)}{|\vec{r}-\vec{r}'|} \qquad (1.2.10b)$$

The Hamiltonian can be split up into one center integrals and two center integrals of various kinds. Since the decomposition is mathematically trivial, we only comment on the one center integral with $i=k=j=\ell$; that is,

$$\frac{1}{2}\sum_{i\sigma\sigma'} \langle ii|\frac{1}{r}|ii\rangle\, a^{+}_{i\sigma}\, a^{+}_{i\sigma'}\, a_{i\sigma'} a_{i\sigma} = \sum_{i\sigma} \langle ii|\frac{1}{r}|ii\rangle a^{+}_{i\sigma}\, a_{i\sigma} a^{+}_{i-\sigma}\, a_{i-\sigma}$$

since we cannot create two particles of the same spin at the same site. Introducing the number operation

$$a^{+}_{i\sigma}\, a_{i\sigma} = n_{i\sigma}$$

for electrons of spin σ and on the ith lattice side, the decomposition of H takes the form,

$$H = \sum_{ij}\sum_{\sigma} \epsilon_{ij} a^{+}_{i\sigma}\, a_{j\sigma} + \frac{I}{2}\sum_{i\sigma} n_{i\sigma} n_{i-\sigma} + \frac{1}{2}\sum_{ij\sigma\sigma'} \sum \langle ij|\frac{1}{r}|ij\rangle\, n_{i\sigma} n_{j\sigma'}\,,$$

$$-\frac{1}{2}\sum_{ij}\sum_{\sigma\sigma'} J_{ij} a^{+}_{i\sigma}\, a_{i\sigma'} a^{+}_{j\sigma'}\, a_{j\sigma} + \sum_{ij}\sum_{\sigma\sigma'} \langle ii|\frac{1}{r}|jj\rangle\, a^{+}_{i\sigma}\, a^{+}_{i\sigma'} a_{j\sigma'} a_{j\sigma} \quad (1.2.11)$$

where

$$I = e^2 \int \frac{|w(\vec{r})|^2 |w(\vec{r}\,')|^2}{|\vec{r}-\vec{r}\,'|} \quad (1.2.12a)$$

and

$$J_{ij} = e^2 \int \frac{w^*(\vec{r}-\vec{r}_i)\, w(\vec{r}-\vec{R}_j)\, w^*(\vec{r}\,'-\vec{R}_j)\, w(\vec{r}\,'-\vec{R}_i)}{|\vec{r}-\vec{r}\,'|}\, d\vec{r}\,' d\vec{r} \quad (1.2.12b)$$

The magnitude of I is largest as compared to the integrals concerned if the electrons are truly localized, and J_{ij} are the customary direct exchange integrals. Of the other terms, since $n_i = \sum_\sigma n_{i\sigma}$, the third term is $\frac{1}{2}\sum_{ij} \langle ij|\frac{1}{r}|ij\rangle\, n_i n_j$ with no spin dependence and is not important in magnetism. The effect of the last term is to remove antiparallel spin pairs from one site to a previously vacant one. This term will play no part in our considerations.

The integral I in the second term of the Hamiltonian (1.2.11) is essentially the interaction energy between two spins on the same atom, so if I is very large we can expect a state of lowest energy in which all atoms are singly occupied (taking a system of N electron and N atoms). The wave function is then a Slater determinant composed of Wannier functions, or equivalently the ψ_k' s; every state $\vec{k}$ in the Brillouin zone is singly occupied and the material is an insulator. As $I \to \infty$, the exchange term J_{ij} completely determines the state of the system. Since the states differ only in their spin configuration, it ought to be possible to write H solely in terms of spin operators provided it operates on modified functions of the form

$$|\sigma_1,\ldots\sigma_N\rangle = a^+_{1\sigma(1)}\, a^+_{2\sigma(2)} \;\cdots\; a^+_{N\sigma(N)}\,|0\rangle \qquad (1.2.13)$$

By casting the spin operators $\sigma_{i\sigma(i)}$ in a spinor form, using the Pauli matrices, we obtain an expression for the exchange term in the form

$$H_H = -\frac{1}{4}\sum_{ij} J_{ij}\,\vec{\sigma}_i.\vec{\sigma}_j \tag{1.2.14}$$

the familiar Heisenberg Hamiltonian. Inspection of Eqn. (1.2.12a) for J_{ij} shows it to be positive leading to ferromagnetism. In equation (1.2.11) we can interpret $\varepsilon_{ij}(i\neq j)$ as the energy required to take an electron from site j to site i and shall refer to it as the hopping energy. If we allow I to become infinite (as in the Heisenberg model), the energy involved in such a hopping process with one electron/atom becomes prohibitive, and the only contribution from the first term comes from $\varepsilon_{ij}(i=j) = \varepsilon$.

If one considers a large but finite I, then the "hopping Hamiltonian"

$$H_h = \sum_{ij}{}' \varepsilon_{ij} \sum_{\sigma} a^{+}_{i\sigma}\, a_{j\sigma} \tag{1.2.15}$$

can be taken as a perturbation on zeroth order function $|\xi_o>$, which is a linear combination of terms of the form (1.2.13). The prime in (1.2.15) indicates that $i\neq j$. Standard Rayleigh-Schrödinger perturbation theory then gives a second order energy

$$E^{(2)} = \sum_{\alpha} \frac{\langle \xi_o | H_h | \xi_\alpha \rangle \langle \xi_\alpha | H_h | \xi_o \rangle}{E_o - E_\alpha} \tag{1.2.16}$$

From Eqn. (1.2.15) if $\langle \xi_\alpha | H_h | \xi_o \rangle$ is non-zero, $|\xi_\alpha\rangle$ describes a state in which there is an antiparallel spin pair. By definition the self-energy of such a pair is I, so $E_o - E_\alpha \cong I$ because I is very large. Thus we find that

$$E^{(2)} = \frac{-\sum_{\alpha} \langle \xi_o | H_h | \xi_\alpha \rangle \langle \xi_\alpha | H_h | \xi_o \rangle}{I} = -\frac{\langle \xi_o | H_h^2 | \xi_o \rangle}{I} \tag{1.2.17}$$

Similarly we can handle high order terms, yielding an expansion in the inverse powers of I. We see that when operating on functions of the form (1.2.13) we can take an effective hopping Hamiltonian

$$H_{eff} = H_h - \frac{H_h^2}{I} + \frac{H_h^3}{I^2} \cdots \tag{1.2.18}$$

which can be expressed as

$$H_{eff} = \frac{1}{2} \sum_{ij} \frac{|\varepsilon_{ij}|^2}{I} \{\vec{\sigma}_i \cdot \vec{\sigma}_j - 1\} \tag{1.2.19}$$

This is a positive term opposing $-J_{ij}$ in (1.2.14), so that $J_{ijeff} = (J_{ij} - \frac{|\varepsilon_{ij}|^2}{2I})$ may become effectively negative if $|\varepsilon_{ij}|^2/I$ is large enough.

Let us now imagine that the crystal is ion bombarded with a light ion (e.g., H, He) and that the ions rest interstitially. The orbital overlap of the implanted ions and the host ions will be negligible; however, the implanted ions will tend to distort the lattice. Since the implanted region of the crystal cannot expand in the plane of the thin film crystal, being hindered by the non-implanted region, the expansion occurs along the normal to the plane along the easy axis of magnetization. This distortion implies a reduction in the orbital overlap of the host atoms along this direction, which originally had the largest orbital overlap. This would lead to an increase in the localizability and hence an increase in I accompanied by a decrease in J_{ij}, along the easy axis of magnetization. Consequently, J_{eff} along this direction would decrease.

On averaging these local effects over the whole lattice, a decrease in the microscopic magnetization parameter M_s is to be observed.

Due to relativisitc corrections we have to add an extra term to our Hamiltonian Eqn. (2.1.1), known as the spin-orbit coupling term, given by

$$H_{Ls} = \frac{h}{4m^2c^2} \vec{\sigma}\cdot(\vec{\nabla}V(\vec{r})x\vec{p}\psi) \qquad (1.2.20)$$

where $V(\vec{r})$ is the lattice potential as felt by the electron and $\vec{p}$ is the linear momentum operator on ψ.

If we assume for the moment that $V(\vec{r})$ is spherically symmetric for an isolated ion, then

$$\vec{\nabla}V(\vec{r}) = \frac{\vec{r}}{r}\left(\frac{dV(\vec{r})}{dr}\right)$$

and

$$\frac{1}{r}\left(\frac{dV}{dr}\right)(\vec{r}\times\vec{p})\cdot\vec{\sigma} = \frac{1}{r}\left(\frac{dV}{dr}\right)(\vec{L}\cdot\vec{\sigma}) \qquad (1.2.21)$$

where L is the orbital angular momentum.

The part of the Hamiltonian given by (1.2.20) is the contribution to the socalled "anisotropy energy" [7,10], and is basically due to the assymetry of the overlap of electron distributions on the neighbouring ions.

The appearance of anisotropy in mixed rare-earth garnets strongly suggests the well known Van Vleck pair ordering phenomenon [20]. It was shown by Callen [7] that the noncubic anisotropy observed under the growth faces of certain mixed garnet crystals is due to the preferential occupation, by one of the two types of rare earth ions, in particular rare earth sites. The effect depends on the co-ordination of rare earth ions with its second nearest tetrahedral ion neighbours.

The existence of randomly distributed interstitial ions slightly blurs the originally well defined lattice potentials, hence slightly decreasing $(\vec{\nabla}V(r))$, as well as decreasing the orbital symmetry along the easy axis and hence decreasing $(\vec{L}.\vec{\sigma})$. The overall effect is a decrease in the spin-orbit coupling energy and hence the miroscopic "anisotropy energy" of the crystal.

As we use ferrimagnetic cyrstal films whose main anisotropy axis is normal to the crystal film plane, the spin projection along this axis (and magnetization) should decrease and the in-plane spin component should increase, and the in-plane susceptibility should increase although it would still be anisotropic in general, all as a result of the ion implantation. The microscopic wall energy density parameter σ_w should also decrease, as a result of the previous changes.

It should be pointed out that the previous qualitative reasoning applies to materials where the implanted part of the crystal prefers to expand along the easy axis (negative magnetostriction), in some cases the crystal may energetically favour an in-plane expansion, and the reverse of the above conclusions would be true with some reservations.

In garnets, the outer atomic orbitals of the rare earth ions do not directly overlap, and the exchange integrals, with the atomic orbitals replacing the Wannier functions, are zero. However, the outer atomic orbitals of the rare earth ions overlap with the hybridized s-p orbitals of the intervening oxygen atoms (ligands), leading to an effective exchange better known as "superexchange". The previous analysis holds equally well here if we realize that the $\vec{R}_\ell$'s are the position vectors of the rare earth ions only, the Wannier functions are then a blend of the rare earth ion and oxygen orbitals, and do lead to an effective nonzero exchange integral between the rare earth ions.

CHAPTER 2

THE GENERALLY DEFORMABLE DOMAIN IN AN ION IMPLANTED CHANNEL

In this chapter, we shall formulate an approximate variational method [14] to compute the general shape of a magnetic domain wholly situated in an ion implanted channel of constant depth and width with parallel vertical channel sides (a straight channel) as shown in Fig. 2.1. The model is based on three important assumptions.

The magnetic domain in this analysis will be assumed to penetrate through the whole thickness of the bubble supporting thin-film plate. This could also embrace the case where the domain penetrates through the nonimplanted region of the thin film and is capped by a 90° domain wall at the interface of the implanted and nonimplanted regions [3,4] by mere adaptation of the parameters, as will be shown in Sec. 2.5.

We shall further assume the uniformity of all physical parameters in both the implanted and the nonimplanted regions of the bubble supporting material. This is equivalent to approximating the ion implantation "damage" profile for parameter change by a step function, starting at the bubble material upper surface up to a depth D after which the parameter changes become negligible. This is a reasonable approximation of the actual smooth damage profile, which, if considered, would lead to an effective volume pole density distribution through the material thickness that would greatly complicate the analysis and would

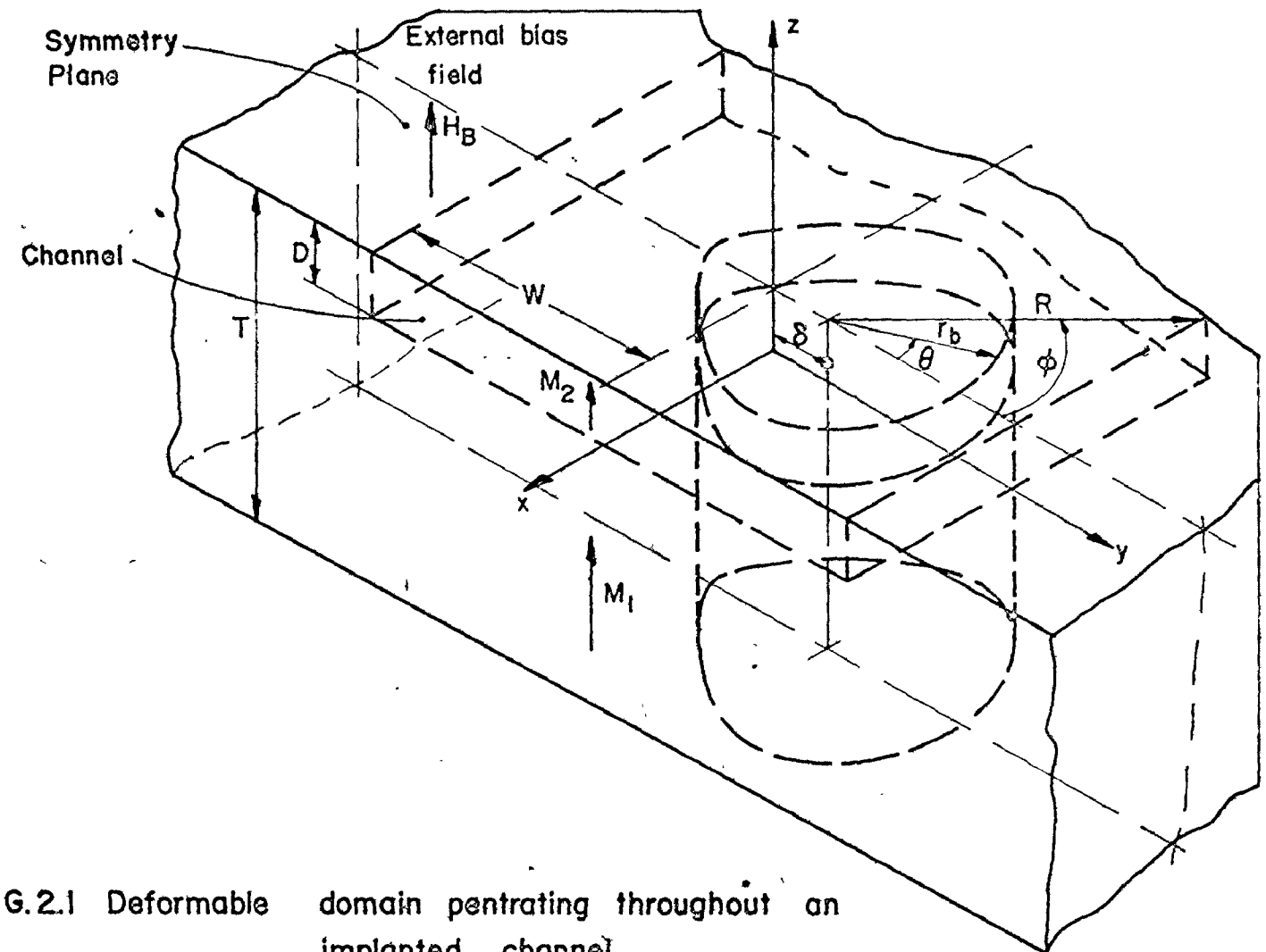

FIG. 2.1 Deformable domain pentrating throughout an implanted channel

increase numerical computations time considerably.

Furthermore, we assume that the magnetic domain wall is deformable in the x and y directions (see Fig. 2.2) but not along the z direction (see Fig. 2.3); thus we shall consider a right cylindrical domain whose uniform cross section, through the thickness of the material has a variable geometry. This assumption is merely an approximation of a bubble wall along the z direction. In fact, the cross section is nonuniform along the z direction. The assumption is, however, adequate and follows the models of other workers [1,13,14].

We shall now study the equilibrium of such a wall under the influence of the various pressures acting on it. It can be shown [14] that such a problem reduces to that of finding the variational minimum of the functional given by

$$F = \int_{\ell} \left\{\frac{dp}{d\ell}\right\}^2 d\ell$$

where p is the pressure at the domain boundary and ℓ is the length along the boundary perimeter. Such a problem can further be reduced to finding the minimum of the approximate discretized functional Φ

$$\Phi = \sum_{i=1}^{N} p_i^2$$

where p_i are the pressures on the magnetic domain wall at N discrete sampling points. Since we have already assumed a nondeformable domain

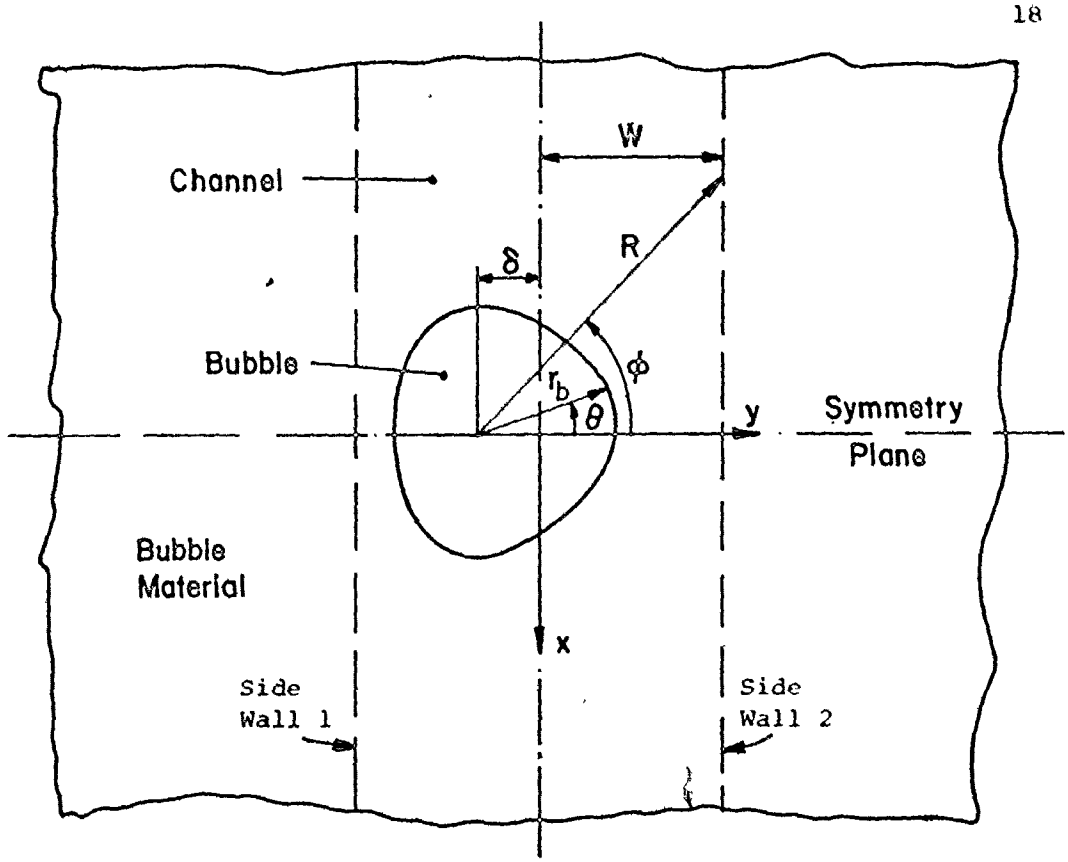

FIG. 2.2 Top view of a cylindrical bubble in an implanted channel.

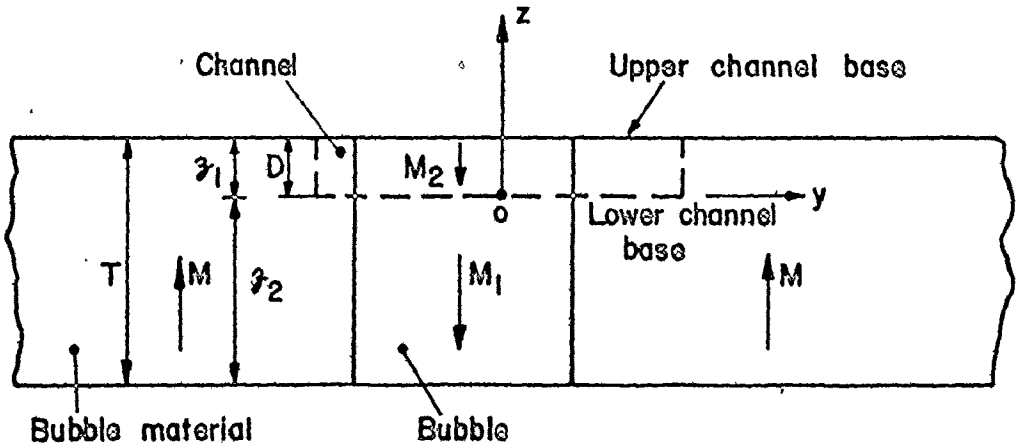

FIG. 2.3 Cross-section of a cylindrical bubble in an implanted channel in the symmetry plane y z.

wall along the z-direction, the pressures p_i would be the average domain wall pressures along the domain height; in this case, the N sampling points would be given by the (x,y) co-ordinates on the domain boundary.

If $p_i = p_i(v_1, v_2, \ldots, v_M)$ the problem reduces to finding the minimum of the approximate functional Φ, that is

$$\text{Min:} \quad \Phi = \sum_{i=1}^{N} p_i^2$$

subject to,

$$f_\ell(v_1, v_2, \ldots v_M) \geq 0 \qquad \ell = 1, 2, \ldots, k$$

where k is the number of constraints.

The problem has now been formally converted to a nonlinear, constrained problem that can be handled numerically.

2.1 The Physical Model

Let us consider a magnetic domain-supporting material plate of thickness T along the z-direction and of infinite extension in the xy-plane with a rectangular channel implanted to a depth D and of uniform width 2w (see Figs. 2.1 to 2.3). Let us further assume a magnetic domain wholly situated inside the channel at all times and that ion implantation has the effect of producing a change in the in-plane magnetic susceptibility given by

$$\chi_t = \chi_{t_f} - \chi_{t_o} = \frac{1}{4\pi}\left(\frac{1}{q_f} - \frac{1}{q_o}\right) \qquad (2.1.1)$$

where χ_{t_f} and χ_{t_o} are the in-plane susceptibilities of the implanted and non-implanted material respectively

and q is the "quality factor" given by [1]

$$q = \frac{Ha}{4\pi Ms} \tag{2.1.2}$$

where Ha is the magnetic anisotropy field.

The veritcal side walls of the channel (Figs. 2.1 and 2.3) will now have induced pole distributions due to both the implanted channel bases of width 2w each (i.e., the upper base on the top surface and the lower base at a depth D from the upper surface, as shown in Fig. 2.3), and the bubble configuration inside the channel. The induced poles on the two channel walls 1 and 2, in turn, induce further pole distributions on each other and we finally obtain the net pole density distributions on the channel walls given by

$$\left.\begin{aligned} P_1(x_1,z_1) &= P_{o1}(x_1,z_1) - \chi_t \int_{-\infty}^{\infty} dx_2 \int_0^D \frac{2wP_2(x_2,z_2)\,dz_2}{[(x_1-x_2)^2+4w^2+(z_1-z_2)^2]^{3/2}} \\ P_2(x_2,z_2) &= P_{o2}(x_2,z_2) - \chi_t \int_{-\infty}^{\infty} dx_2 \int_0^D \frac{2wP_1(x_1,z_1)\,dz_1}{[(x_1-x_2)^2+4w^2+(z_1-z_2)^2]^{3/2}} \end{aligned}\right\} \tag{2.1.3}$$

where $P_{oi}(x_i,z_i)$ are the induced pole density distributions attributed to the following two sources: (a) the empty channel bases with no domain, and (b) the bubble domain. The terms P_{oi} can be obtained by

superposition of the contributions (a) and (b).

As the channel has an infinite length along the x-direction, it would be convenient to change the coordinate system to a new set of variables such that the limits of integrations in (2.1.3) become finite. We shall change from the Cartesian co-ordinates (x,y,z) to the circular cylindrical co-ordinate system of the bubble (r,θ,z). We now recast Eqns. (2.1.3) into the more convenient form.

$$P_1(\phi_1,z_1) = P_{o1}(\phi_1,z_1)-\chi_t\int_{-\pi/2}^{\pi/2} d\phi_2\int_0^D \frac{2w(w+\delta)\sec^2\phi_2 P_2(\phi_2,w)\, dz_2}{[([w-\delta]\tan\phi_1-[w+\delta]\tan\phi_2)^2+4w^2+(z_1-z_2)^2]^{3/2}} \tag{2.1.4a}$$

$$P_2(\phi_2,z_2) = P_{o2}(\phi_2,z_2)-\chi_t\int_{-\pi/2}^{\pi/2} d\phi_1\int_0^D \frac{2w(w-\delta)\sec^2\phi_1 P_1(\phi_1,z_1)\, dz_1}{[(\{w-\delta\}\tan\phi_1-\{w+\delta\}\tan\phi_2)^2+4w^2+(z_1-z_2)^2]^{3/2}} \tag{2.1.4b}$$

where δ is the deviation of the bubble co-ordinate center from the channel center. Equations (2.1.4) constitute a pair of coupled linear integral equations of the Fredholm type with identical non-singular kernels. The simplest approach to solving (2.1.4) numerically is to discretize the pole distributions $P_1(\phi_1,z_1)$ and $P_2(\phi_2,z_2)$ and to use the property of mirror symmetry about the yz-plane. Hence we can write the discretized pair of equations as

$$\left.\begin{aligned} P_1(\phi_i,z_j) &= P_{o1}(\phi_i,z_j) + \sum_{k,\ell} K^{(1)}_{ik,j\ell} P_2(\phi_k,z_\ell) \\ P_2(\phi_i,z_j) &= P_{o2}(\phi_i,z_j) + \sum_{k,\ell} K^{(2)}_{ik,j\ell} P_\ell(\phi_k,z_\ell) \end{aligned}\right\} \qquad (2.1.5a)$$

where

$$K^{(1,2)}_{ik,j\ell} = \frac{\chi_t^{2w(w\pm\delta)\sec^2\phi_k}}{[(\{w\mp\delta\}\tan\phi_i-\{w\pm\delta\}\tan\phi_k)^2+4w^2+(z_\ell-z_j)^2]^{3/2}} \qquad (2.1.5b)$$

We can obtain more insight into the problem by taking the pole distributions $P_{1,2}$ as multidimensional vectors and the kernel K as a square matrix, hence we can express (2.1.5) in matrix form. Taking into account the symmetry of K, that is,

$$\tilde{K} = \tilde{K}_1 = \tilde{K}_2^T \qquad (2.1.6)$$

yields

$$\tilde{P}_1 = \tilde{P}_{o1} + \tilde{K}\tilde{P}_2 \qquad (2.1.7a)$$

$$\tilde{P}_2 = \tilde{P}_{o2} + \tilde{K}^T\tilde{P}_1 \qquad (2.1.7b)$$

or

$$\tilde{P}_1 = (1-\tilde{K}\tilde{K}^T)^{-1}(\tilde{P}_{o1}+\tilde{K}\tilde{P}_{o2}) \qquad (2.1.8a)$$

$$\tilde{P}_2 = (1-\tilde{K}^T\tilde{K})^{-1}(\tilde{P}_{o2}+\tilde{K}^T\tilde{P}_{o1}) \qquad (2.1.8b)$$

where the wiggle denotes a matrix. A direct solution of Eqns. (2.1.8a) and (2.1.8b) by inverting and multiplying the matrices becomes numerically inaccurate as the dimensions of the matrices become large. Thus, an iterative self-correcting solution is desired. Such an approach has been used in obtaining subsequent results.

2.2 The Problem Formulation

Let us now return to the nonlinear approximate objective functional Φ which can be written as

$$\Phi = \Phi[r_b(\theta);\delta] \tag{2.2.1}$$

where we have assumed that the generally deformable magnetic domain geometry can be described by the single-valued cyclic-function $r_b(\theta)$. Such single-valued functions can be expanded in an orthogonal series

$$r_b(\theta) = \sum_n C_n \, f_n(\theta) \tag{2.2.2}$$

Here, the set $\{f_n(\theta)\}$ is an infinite set of functions satisfying the orthonormality condition

$$\int f_n(\theta) f_m(\theta) d\theta = \delta_{mn} \tag{2.2.3}$$

where δ_{mn} is the Kronecker symbol, and the completeness relation

$$\sum_n f_n(\theta) f_n(\theta_o) = \delta(\theta-\theta_o) \tag{2.2.3b}$$

where δ is the Dirac delta function.

The functions (2.2.2) form a subset of the set of all functions. For a given set of orthonormal functions $f_n(\theta)$ they are determined uniquely by the infinite set of expansion coefficients C_n. Introducing (2.2.2) into the functional (2.2.1) we obtain a function of an infinite set $\{C_n\}$. Hence we can write

$$\Phi[r_b(\theta),\delta] = \Phi[\{C_n\};\delta] \tag{2.2.4}$$

We shall choose our infinite set of orthogonal functions to be the set $\{\cos n\theta, \sin n\theta\}$, where n is an integer including zero. The expansion (2.2.2) now becomes

$$r_b(\theta) = \sum_{n=0}^{\infty} C_n \cos[n(\theta-\theta_n)] \tag{2.2.5}$$

where θ is the angle measured from the y-axis (Fig. 2.2). Due to the mirror symmetry about the yz-plane, we have

$$r_b(\theta) = r_b(-\theta) \tag{2.2.6}$$

and hence, for that special case of the straight channel, $\theta_n = 0$ (all n), and Eqn. (2.2.5) becomes

$$r_b(\theta) = \sum_{n=0}^{\infty} C_n \cos[n\theta] \tag{2.2.7}$$

For computational purposes we should use a truncated cosine expansion with N+1 terms, and accordingly we select (N+1) radial parameters sampling points in the range $\theta=0$ to $\theta=\pi$. While any (N+1) distinct sampling points would be satisfactory, we shall divide the range from $\theta=0$ to $\theta=\pi$ into (π/N) equal angular spacings and use the values of $r_b(\theta=n\pi/N)$ for $[n=0,N]$ as the N+1 radial parameters, which would uniquely determine the (N+1) coefficients C_n of the truncated expansion (2.2.7).

The N+1 radial parameters r_i are subject to the constraints $r_i \geq 0$, and $r_i|\cos(\theta_i)| \leq (\bar{w}+\delta)$, the latter expressing the condition that all radial parameters are inside the channel. While the latter conditions do not guarantee that the entire domain remains inside the channel, they act as weak constraints, forcing the bubble to remain in the channel.

By expanding $r_b(\theta)$ by a truncated cosine series

$$r_b(\theta) = \sum_{n=0}^{N} C_n \cos[n\theta] \tag{2.2.8}$$

we can determine the expansion coefficients C_n in terms of the radial parameters r_m from the matrix equation

$$r_m = \sum_{n=1}^{N+1} C_n A_{mn} \tag{2.2.9a}$$

where

$$A_{m,n} = \cos[(n-1)\theta_m] \tag{2.2.9b}$$

The matrix equation can be written as

$$\tilde{R} = \tilde{A}\tilde{C} \tag{2.2.10a}$$

It can be shown that $\tilde{A}$ is nonsingular, and therefore

$$\tilde{C} = \tilde{A}^{-1}\tilde{R} \tag{2.2.10b}$$

where $\tilde{C}$ and $\tilde{R}$ are column vectors made of the (N+1) coefficients and radial parameters respectively. From (2.2.10b), the coefficients C_n are expressed as a linear combination of the variables, the radial parameters r_m. The functional given by Eqn. (2.2.4) can now be written as

$$\Phi[r_b(\theta),\delta] \cong \Phi[\{r_m\};\delta] \tag{2.2.11}$$

Furthermore, from Eqn. (2.2.10b), we have

$$\frac{\partial C_i}{\partial r_j} = A_{ij}^{-1} \tag{2.2.12}$$

In the formulation, we shall need various derivatives $r(\theta)$ with respect to θ and r_j. It can be shown that

$$\frac{d}{d\theta}(r_b(\theta)) = \sum_{n=1}^{N+1} -(n-1)C_n \sin[(n-1)\theta] \tag{2.2.13a}$$

$$\frac{d^2}{d\theta^2}(r_b(\theta)) = \sum_{i=1}^{N+1} -(n-1)^2 C_n \cos[(n-1)\theta] \tag{2.2.13b}$$

and

$$\frac{d}{dr_j}[r_b(\theta)] = \sum_{n=1}^{N+1} A_{n,j}^{-1} \cos[(n-1)\theta] \tag{2.2.14a}$$

$$\frac{d}{dr_j}[\frac{d}{d\theta}(r_b(\theta))] = -\sum_{n=1}^{N+1} (n-1)A_{n,j}^{-1} \sin[(n-1)\theta] \tag{2.2.14b}$$

$$\frac{d}{dr_j}[\frac{d^2}{d\theta^2}(r_b(\theta))] = -\sum_{n=1}^{N+1} (n-1)^2 A_{n,j}^{-1} \cos[(n-1)\theta] \tag{2.2.14c}$$

Let us now return to the problem of calculating the average pressure on a magnetic wall. This is given by

$$\bar{p} = \frac{1}{T}\int \Delta\vec{M}\cdot\vec{H}dz \tag{2.2.15}$$

where $\Delta\vec{M}$ is the change in magnetization on crossing the domain wall, and $\vec{H}$ is the net field at the wall at the point of crossing. In the most general sense, we can have

$$\Delta\vec{M} = \vec{1}_x\{\Delta\chi_{xx}H_x+\Delta\chi_{xy}H_y+\Delta\chi_{xz}H_y+\Delta M_{ox}\}$$

$$+ \vec{1}_y\{\Delta\chi_{yx}H_x+\Delta\chi_{yy}H_y+\Delta\chi_{yz}H_z+\Delta M_{oy}\} \qquad (2.2.16)$$

$$+ \vec{1}_z\{\Delta\chi_{zx}H_x+\Delta\chi_{zy}H_y+\Delta\chi_{zz}H_z+\Delta M_{oz}\}$$

where $\Delta\chi$ is the change in magnetic susceptibility on crossing the domain wall, and $\Delta\vec{M}_o$ is the field independent part of the magnetization. If we employ matrix notation we can combine (2.2.15) and (2.2.16) into

$$\bar{p} = \frac{1}{T}\int(\tilde{H}^T:\Delta\tilde{\chi}:\tilde{H}+\Delta\tilde{M}_o^T\tilde{H})\,dz \qquad (2.2.17)$$

where $\tilde{H}$ and $\Delta\tilde{M}_o$ are column matrices and $\Delta\tilde{\chi}$ is a 3x3 susceptibility change matrix. It will be assumed that in Eqn. (2.2.16), $\Delta\vec{M} \cong \vec{1}_z\Delta M_{oz}$ and hence Eqn. (2.2.17) reduces to

$$\bar{p} = \frac{1}{T}\int\Delta M_{oz}H_z\,dz \qquad (2.2.18)$$

As ΔM_{oz} is a constant, the problem reduces to finding an average equivalent magnetic field $\bar{H}_z$ acting along a vertical wall line at the various pressure sampling locations; that is,

$$\bar{H}_z = \bar{H}_{Dz} + \bar{H}_{\sigma z} + \bar{H}_{Ez} + \bar{H}_{CB} + \bar{H}_{Cw} \qquad (2.2.19)$$

where

$\bar{H}_{Dz}$ is the z-averaged, z-component of the demagnetization field,

$\bar{H}_{\sigma z}$ is the equivalent domain wall field,

$\bar{H}_{CB}$ is the averaged channel bases demagnetization correction,

$\bar{H}_{Bz}$ is the external uniform bias field, and

$\bar{H}_{Cw}$ is the average field due to the channel wall induced poles.

It should be clear, that the number and angular locations at which we compute the radial parameters r_i, taken as the active variables, are not necessarily the same sampling locations at which we calculate the pressures and in general, they are different.

We are now ready to proceed with the formulation of the various aspects of the problem.

2.3 Initial Induced Pole Density and Pole Density Gradients

We have assumed (Ch.1) that the ion implantation of a ferrimagnetic domain-supporting thin film changes the in-plane magnetic susceptibility χ of the implanted region in the material, as well as the saturation magnetization. Let us further assume that the change in the latter is linear and takes place over a transition region of width Δ, (Fig. 2.4) while the chane in χ, the in-plane susceptibility, is a step change in the middle of the transition region Δ. In general, the change in χ through the transition region Δ will lead to an effective volume pole density. However, as Δ is a small fraction of the ion implanted depth (due to the side scattering of implanted ions and ion diffusion) one can consider an effective surface pole density distribution on the channel walls.

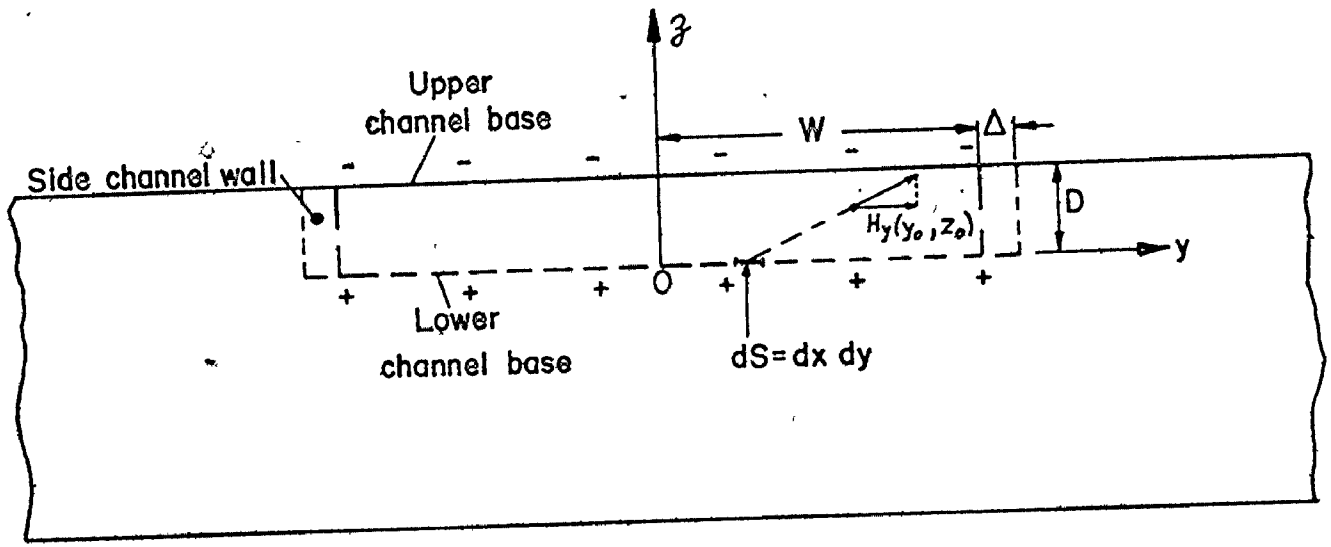

FIG. 2.4 In-plane magnetic field due to channel bases.

As mentioned in Sec. 2.1, two sources are responsible for the pole density distributions along the walls of the implanted channel: the bases of the bubble free channel, and the magnetic bubble domain inside the channel. Explicit expressions for these contributions will be given in the following two subsections.

2.3.1 Empty Channel Induced Pole Density

The in-plane magnetic field, arising due to the implantation of a channel, will induce poles on the vertical side channel walls (see Fig. 2.4). This field could be attributed to the corresponding changes in the pole densities of the channel bases (Fig. 2.4). The geometry of this problem suggests the use of the Cartesian co-ordinate system.

From the pole theory, the in-plane magnetic field component normal to the channel wall at (x_o, y_o, z_o) due to a surface element dxdy of a channel base at (x,y,z) is given by

$$dH(x_o, y_o, z_o) = \begin{cases} \dfrac{(M_1-M_2)(y_o-y)\,dxdy}{[(x-x_o)^2+(y-y_o)^2+(z-z_o)^2]^{3/2}} & -w \leq y \leq w \\[2ex] \dfrac{(M_1-M_2)(y_o-y)[(|y|-w')/\Delta]\,dxdy}{[(x-x_o)^2+(y-y_o)^2+(z-z_o)^2]^{3/2}} & w \leq |y| \leq (w+\Delta) \\[2ex] 0 & |y| \geq |w+\Delta| \end{cases} \qquad (2.3.1)$$

where $w' = w+\Delta$

where M_1 and M_2 are the magnetizations in the material and the channel respectively, and Δ is the thickness of the side walls of the implanted channel.

The total in-plane, pole-inducing field due to a channel base of width 2w and at a depth z at the point (y_o, z_o) on the channel wall is given by

$$H_y(y_o,z_o) = (M_1-M_2)\int_{-\infty}^{\infty} dx \left[\int_{-w}^{w} \frac{dy\,(y_o-y)}{[(x-x_o)^2+(y-y_o)^2+(z-z_o)^2]^{3/2}} \right.$$

$$\left. + \frac{1}{\Delta}\int_{w}^{w+\Delta} \frac{dy\,(y_o-y)\,(y-w')}{w[(x-x_o)^2+(y-y_o)^2+(z-z_o)^2]^{3/2}} + \frac{1}{\Delta}\int_{-(w+\Delta)}^{-w} \frac{-dy\,(y_o-y)\,(w'+y)}{[(x-x_o)^2+(y-y_o)^2(z-z_o)^2]^{3/2}} \right]$$

$$= 2(M_1-M_2)\left[\int_{-w}^{w} \frac{dy\,(y_o-y)}{[z'^2+(y_o-y)^2]} + \frac{1}{\Delta}\int_{w}^{w+\Delta} \frac{dy\,(y_o-y)\,(y-w')}{[z'^2+(y_o-y)^2]} \right.$$

$$\left. - \frac{1}{\Delta}\int_{-(w+\Delta)}^{-w} \frac{dy\,(y_o-y)\,(y+w')}{[z'^2+(y-y_o)^2]} \right]$$

$$= 2(M_1-M_2)\left[-\ln\left(\frac{z'^2+(y_o-w)^2}{z'^2+(y_o+w)^2}\right) - \frac{(y_o-w)}{\Delta}\ln\left(\frac{z'^2+(y_o-w'-\Delta)^2}{z'^2+(y_o-w')^2}\right)\right.$$

$$+ \frac{1}{\Delta} \{(y_o-y) - z' \tan^{-1}(\frac{y_o-y}{z})\}\Bigg|_{w}^{w+\Delta} - \frac{(y_o+w')}{\Delta} \ln\left(\frac{z'^2+(y_o+w'+\Delta)^2}{z'^2+(y_o+w')^2}\right)$$

$$+ \frac{1}{\Delta} \{(y_o-y) - z' \tan^{-1}(\frac{y_o-y}{z})\}\Bigg|_{-w}^{-w-\Delta} \qquad (2.3.2a)$$

where $z' = z_o - z$.

If the lower channel base is taken as the zero reference for measuring z, (see Figs. 2.1 and 2.3) then the total pole inducing field, due to the empty channel, at a point (y_o, z_o) on the channel wall is

$$H_{yind}(y_o,z_o) = 2(M_1-M_2)\Bigg[-\ln\left(\frac{z_o^2+(y_o-w)^2}{z_0^2+(y_o+w)^2}\right) + \ln\left(\frac{(D-z_o)^2+(y_o-w)^2}{(D-z_o)^2+(y_o+w)^2}\right)$$

$$- \frac{(y_o-w')}{\Delta} \ln\left(\frac{z_o^2+(y_o-w'-\Delta)^2}{z_o^2+(y_o-w')^2}\right) + \frac{(y_o-w')}{\Delta} \ln\left(\frac{(D-z_o)^2+(y_o-w'-\Delta)^2}{(D-z_o)^2+(y_o-w')^2}\right)$$

$$- \frac{(y_o+w')}{\Delta} \ln\left(\frac{z_o^2+(y_o+w'+\Delta)^2}{z_o^2+(y_o+w')^2}\right) + \frac{(y_o+w)}{\Delta} \ln\left(\frac{(D-z_o)^2+(y_o+w'+\Delta)^2}{(D-z_o)^2+(y_o+w')^2}\right)$$

$$+ \frac{z_o}{\Delta} \left[\tan^{-1}\left(\frac{y_o-w'}{z_o}\right) - \tan^{-1}\left(\frac{y_o-w'-\Delta}{z_o}\right) + \tan^{-1}\left(\frac{y_o+w'}{z_o}\right) - \tan^{-1}\left(\frac{y_o+w'+\Delta}{z_o}\right)\right]$$

$$\left. - \frac{(D-z_o)}{\Delta} \left[\tan^{-1}\left(\frac{y_o-w'}{D-z_o}\right) + \tan^{-1}\left(\frac{y_o+w'}{D-z_o}\right) - \tan^{-1}\left(\frac{y_o-w'-\Delta}{D-z_o}\right) - \tan^{-1}\left(\frac{y_o+w'+\Delta}{D-z_o}\right)\right]\right]$$

(2.3.2b)

Let us now proceed to calculate the volume pole density distribution through the channel walls. This is given by the equation

$$\rho(x_o,y_o,z_o) = -\mathrm{div}_o[\chi(y_o)\vec{H}_{ind}] = -\vec{\nabla}_o\cdot[\chi(y_o)\vec{H}_{ind}] = -[\chi(y_o)\vec{\nabla}_o\cdot\vec{H}_{ind}+\vec{H}_{ind}\cdot \vec{\nabla}_o\chi(y_o)] = \vec{H}_{ind}\cdot(\vec{\nabla}_o\chi(y_o))$$

(2.3.3a)

where $\rho(x_o,y_o,z_o)$ is the volume pole density at the channel side walls. Since $\chi(y_o)$ changes only along the y direction Eqn. (2.3.3a) can be written as

$$\rho(x_o,y_o,z_o) = H_{yind}\frac{\partial}{\partial y_o}(\chi(y_o)) \qquad (2.3.3b)$$

Since we have already assumed a step change in $\chi(y_o)$ at $|y_o| = w+\Delta/2$, the volume density becomes

$$\rho(y_o,z_o) = H_{yind}(y_o,z_o)\delta(|y_o|-[w+\frac{\Delta}{2}])\chi_t \qquad (2.3.3c)$$

where δ is the Dirac delta function and χ_t is given by Eqn. (2.1.1).

The mean surface pole density on the channel wall is obtained by integrating $\rho(y_o,z_o)$ across the transition region Δ. Hence, we get

$$P_{ok}^{(1)}(z_o) = \int_{|y| = w}^{|y| = w+\Delta} \rho(y_o,z_o)dy_o = \chi_t H_{yind}(w+\frac{\Delta}{2},z_o) \tag{2.3.4}$$

where k=1,2.

It should be pointed out that if $\Delta=0$, the induced surface pole density on the channel walls would become infinite at $z_o=0$ and $z_o=D$, a physically impossible situation.

In conclusion, the surface pole density due to the bubble free (empty) channel is independent of the bubble domain configuration and hence does not contribute to the pole density gradients with respect to the domain parameters.

2.3.2 Bubble Domain Induced Pole Density

The second source, inducing an effective magnetic pole density distribution, is the magnetic domain wholly situated inside the ion implanted channel. The bubble induced pole density is superimposed on that induced by the bubble-free channel. The geometry of the problem suggests the use of the cylindrical coordinate system. The in-plane magnetic field component normal to channel wall k(k=1,2) at

the point (ϕ_o, z_o) (see Sec. 2.1 and Figs. 2.1 and 2.2) due to the incremental surface element $rdrd\theta$ of the bubble surface pole densities at (r,θ) is given by [1]

$$dH^{(k)}_{ind\,y}(\phi_o, z_o) \quad \sum_{i=1}^{3} M_i^* \frac{(R_k\cos\phi_o - r\cos\theta)}{[r^2+R_k^2-2rR_k\cos(\theta-\phi_o)+(z_i-z_o)^2]^{3/2}} \qquad (2.3.5a)$$

where

$$M_1^* = -M_1, M_2^* = M_2,\ M_3^* = M_1-M_2 \quad ; \quad z_1 = T-D,\ z_2 = D,\ z_3 = 0,$$

$$R_k = \{w+\frac{\Delta}{2}+(2k-3)\delta\}/|\cos\phi_o| \ , \qquad (2.3.5b)$$

and δ is the y-displacement of the origin of the cylindrical coördinate system with respect to the Cartesian systems. The bubble induced pole density distribution $P^{(2)}_{ok}(\phi_o, z_o)$ is obtained by integrating (2.3.5) a over the entire domain surface densities and multiplying by the change in the in-plane susceptibility χ_t. Hence

$$P^{(2)}_{ok}(\phi_o, z_o) = \chi_t \int_0^{2\pi} d\xi \int_0^{r_b(\theta)} \sum_{i=1}^{3} M_i^* \frac{[R_k\cos\phi_o - r\cos(\xi+\phi_o)]rdr}{[r^2+R_k^2-2rR_k\cos\xi+(z_i-z_o)^2]^{3/2}} \qquad (2.3.6a)$$

where $\xi=\theta-\phi_o$. One can rewrite this equation into the more convenient form

$$P_{ok}^{(2)}(\phi_o,z_o) = \chi_t \int_0^{2\pi} d\xi \int_0^{r_b(\theta)} \left\{ \sum_{i=1}^{3} M_i^* \right.$$

$$\left. \times \frac{\{R_k\cos\phi_o(r-R_k\cos\xi)dr+R_k^2\cos\phi_o\cos\xi dr-r^2\cos(\phi_o+\xi)dr\}}{[r^2+R_k^2-2rR_k\cos\xi+(z_i-z_o)^2]^{3/2}} \right\}$$

$$= \chi_t \int_0^{2\pi} d\xi \int_0^{r_b(\theta)} \sum_{i=1}^{3} M_i^* \left\{ \frac{[R_k\cos\phi_o-2R_k\cos\xi\cos(\phi_o+\xi)](r-R_k\cos\xi)dr}{[r^2+R_k^2-2rR_k\cos\xi+(z_i-z_o)^2]^{3/2}} \right.$$

$$- \frac{\cos(\phi_o+\xi)[r^2+R_k^2-2rR_k\cos\xi+(z_i-z_o)^2]dr}{[r^2+R_k^2-2rR_k\cos\xi+(z_i-z_o)^2]^{3/2}}$$

$$\left. + \frac{[R_k^2\cos\phi_o\cos\xi+\cos(\phi_o+\xi)[R_k^2-2rR_k\cos\xi+(z_i-z_o)^2+2R_k\cos\xi(r-R_k\cos\xi)]]dr}{[r^2+R_k^2-2rR_k\cos\xi+(z_i-z_o)^2]^{3/2}} \right\}$$

(2.3.6b)

Integrating with respect to r yields

$$P_{ok}^{(2)}(\phi_o,z_o) = \chi_t \int_0^{2\pi} d\theta \sum_{i=1}^{3} M_i^* \left[\frac{R_k\cos(2\theta-\phi_o)}{(r^2+R_k^2-2rR_k\cos(\theta-\phi_o)+(z_i-z_o)^2]^{1/2}} \right.$$

$$- \cos\theta\sinh^{-1}\left(\frac{r-R_k\cos(\theta-\phi_o)}{(R_k^2\sin^2(\theta-\phi_o)+(z_i-z_o)^2)^{1/2}} \right)$$

$$-\frac{(r-R_k\cos(\theta-\phi_o))(R_k^2[\cos\theta-\cos(3\theta-2\phi_o)]+(z_i-z_o)^2\cos\theta)}{(R_k^2\sin^2(\theta-\phi_o)+(z_i-z_o)^2)(r^2+R_k^2-2rR_k\cos(\theta-\phi_o)+(z_i-z_o)^2)^{1/2}}\Bigg]\Bigg|_{r=0}^{r=r_b(\theta)}$$

(2.3.6c)

The induced pole density distributions on the channel walls given by (2.3.c) are functions of the magnetic domain parameters $\{r_i\}$ and δ, and as these parameters change so do the induced pole densities.

It shall be shown that the gradients of the channel wall pole density distributions contribute to the pressure gradients, hence we shall derive expressions for them below. The density gradients with respect to the radial parameters is obtained by direct differentiation of (2.3.6c) with respect to r_i

$$\frac{\partial P_{ok}}{\partial r_i}(\phi_o,z_o) = \chi_t \int_0^{2\pi} d\theta \left(\frac{\partial r_b(\theta)}{\partial r_j}\right) \sum_{i=1}^{3} M_i^* \left\{\frac{-(r_b-R_k\cos(\theta-\phi_o))R_k\cos(2\theta-\phi_o)}{(r_b^2+R_k^2-2R_kr_b\cos(\theta-\phi_o)+(z_i-z_o)^2)^{3/2}}\right.$$

$$\left.-\frac{\cos\theta}{(r_b^2+R_k^2-2r_bR_k\cos(\theta-\phi_o)+(z_i-z_o)^2)^{1/2}}+\frac{(R_k^2(\cos\theta-\cos(3\theta-2\phi_o))+(z_i-z_o)2\cos\theta)}{(R_k^2\sin^2(\theta-\phi_o)+(z_i-z_o)^2)}\right\}$$

$$\times\left[\frac{R_k^2\sin^2(\theta-\phi_o)+(z_i-z_o)^2}{(r_b^2+R_k^2-2r_bR_k\cos(\theta-\phi_o)+(z_i-z_o)^2)^{3/2}}\right] \qquad (2.3.7)$$

The gradient with respect to the variable δ is given by

$$\frac{\partial P_{ok}}{\partial \delta}(\phi_o, z_o) = \chi_t \int_0^{2\pi} d\theta \sum_{i=1}^{3} M_i^* \frac{(2k-3)}{|\cos\phi_o|} \left\{ \cos(2\theta-\phi_o) \cdot \left(\frac{-1.0}{[R_k^2+(z_i-z_o)^2]^{1/2}} + \right.\right.$$

$$\left. \frac{1.0}{[R_k^2+r_b^2-2r_bR_k\cos(\theta-\phi_o)+(z_i-z_o)^2]^{1/2}} \right)$$

$$-R_k\cos(2\theta-\phi_o)\left(\frac{R_k-r_b\cos(\theta-\phi_o)}{[r_b^2+R_k^2-2r_bR_k\cos(\theta-\phi_o)+(z_i-z_o)^2]^{3/2}} - \frac{R_k}{[R_k^2+(z_i-z_o)^2]^{3/2}} \right)$$

$$-\cos\theta\left[\frac{-\cos(\theta-\phi_o)+\dfrac{(R_k-r_b\cos(\theta-\phi_o))}{[r_b^2+R_k^2-2r_bR_k\cos(\theta-\phi_o)+(z_i-z_o)^2]^{1/2}}}{r_b-R_k\cos(\theta-\phi_o)+[r_b^2+R_k^2-2r_bR_k\cos(\theta-\phi_o)+(z_i-z_o)^2]^{1/2}} \right.$$

$$\left. - \frac{-\cos(\theta-\phi_o)+\dfrac{R_k}{[R_k^2+(z_i-z_o)^2]^{1/2}}}{-R_k\cos(\theta-\phi_o)+[R_k^2+(z_i-z_o)^2]^{1/2}} \right]$$

$$-\left(\frac{R_k^2[\cos\theta-\cos(3\theta-2\phi_o)]+(z_i-z_o)^2\cos\theta}{R_k^2\sin^2(\theta-\phi_o)+(z_i-z_o)^2}\right)\left(\frac{\cos(\theta-\phi_o)(z_i-z_o)^2}{[R_k^2+(z_i-z_o)^2]^{3/2}}\right.$$

$$\left.-\frac{\cos(\theta-\phi_o)}{(r_b^2+R_k^2-2r_bR_k\cos(\theta-\phi_o)+(z_i-z_o)^2)^{1/2}}-\frac{(r_b-R_k\cos(\theta-\phi_o)(R_k-r_b\cos(\theta-\phi_o))}{(r_b^2+R_k^2-2r_bR_k\cos(\theta-\phi_o)+(z_i-z_o)^2)^{3/2}}\right)$$

$$-\left(\frac{(r_b-R_k\cos(\theta-\phi_o)}{(r_b^2+R_k^2-2r_bR_k\cos(\theta-\phi_o)+(z_i-z_o)^2)^{1/2}}+\frac{R_k\cos(\theta-\phi_o)}{(R_k^2+(z_i-z_o)^2)^{1/2}}\right)$$

$$\times\left(\frac{-2R_k\sin^2(\theta-\phi_o)(R_k^2\cos\theta-\cos(3\theta-2\phi_o)+(z_i-z_o)^2\cos\theta)}{[R_k^2\sin^2(\theta-\phi_o)+(z_i-z_o)^2]^2}\right.$$

$$\left.\left.+\frac{2R_k[\cos\theta-\cos(3\theta-2\phi_o)]}{[R_k^2\sin^2(\theta-\phi_o)+(z_i-z_o)^2]}\right)\right\} \qquad (2.3.8)$$

It is worth noting that the gradients (2.3.7) and (2.3.8) have many repeated terms, and although the expressions are large their computation

turns out to be reasonably simple.

It should be realized that the formulated induced pole density distribution gradients on the two channel walls 1 and 2 will further induce corrections on each other, and from Eqns. (2.1.5a),(2.1.5b), we have for the radial parameter gradients the identical set of equations

$$\left.\begin{aligned} \frac{\partial P_1(\phi_i,z_j)}{\partial r_m} &= \frac{\partial P_{o1}(\phi_i,z_j)}{\partial r_m} + \sum_{k,\ell} K^{(1)}_{ik,j\ell}\frac{\partial P_2(\phi_k,z_\ell)}{\partial r_m} \\ \frac{\partial P_2(\phi_i,z_j)}{\partial r_m} &= \frac{\partial P_{o2}(\phi_i,z_j)}{\partial r_m} + \sum_{k,\ell} K^{(2)}_{ik,j\ell}\frac{\partial P_1(\phi_k,z_\ell)}{\partial r_m} \end{aligned}\right\} \qquad (2.3.9)$$

For the gradients with respect to the bubble center parameter δ, we find from Eqn. (2.1.5b) that the discrete kernels $K^{(1)}$ and $K^{(2)}$ are functions of δ, and hence

$$\left.\begin{aligned} \frac{\partial P_1(\phi_i,z_j)}{\partial \delta} &= \frac{\partial P_{o1}(\phi_i,z_j)}{\partial \delta} + \sum_{k,\ell}\left[K^{(1)}_{ik,j\ell}\frac{\partial P_2(\phi_k,z_\ell)}{\partial \delta} + P_2(\phi_k,z_\ell)\frac{\partial K^{(1)}_{ik,j\ell}}{\partial \delta}\right] \\ \frac{\partial P_2(\phi_i,z_j)}{\partial \delta} &= \frac{\partial P_{o2}(\phi_i,z_j)}{\partial \delta} + \sum_{k,\ell}\left[K^{(2)}_{ik,j\ell}\frac{\partial P_1(\phi_k,z_\ell)}{\partial \delta} + P(\phi_k,z_\ell)\frac{\partial K^{(2)}_{ik,j\ell}}{\partial \delta}\right] \end{aligned}\right\} \qquad (2.3.10a)$$

where

$$\frac{\partial K^{(1,2)}_{ik,j\ell}}{\partial \delta} = -\chi_t 2w\sec^2\phi \left\{ \frac{\mp 1.0}{[((w\mp\delta)+\tan\phi_i-(w\mp\delta)\tan\phi_k)^2+4w^2+(z_\ell-z_j)^2]^{3/2}} \right.$$

$$\left. - \frac{3(w\pm\delta)[(w\mp\delta)\tan\phi_i-(w\pm\delta)\tan\phi_i][\mp\tan\phi_i \mp \tan\phi_k]}{[((w\mp\delta)\tan\phi_i-(w\pm\delta)\tan\phi_k)^2+4w^2+(z_\ell-z_j)^2]^{5/2}} \right\} \qquad (2.3.10b)$$

For reasons explained at the end of Sec. 2.1, (2.3.10) and (2.1.5) must be iteratively solved together.

It is obvious that the problem of formulating the expressions for the induced pole density and pole density gradient distributions even for the simplest case (straight channel) is a tedious task.

2.4 Pressures and Pressure Gradients

We are now in a position to formulate the expressions for the pressure contributions due to the various field contributions in Eqns. (2.2.18) and (2.2.19), and their gradients with respect to the variable parameters $\{r_m\}$ and δ. The various contributions are then added to give the total pressures and pressure gradients at the selected locations which we call the "pressure sampling points".

We shall start by formulating the demagnetizing pressures

due to a two layer bubble supporting material (implanted and non-implanted layers) with both layers of infinite extension (see Fig. 2.5a). We then superpose a correction to the demagnetizing pressures (see Fig. 2.5b) to account for the finite width of the implanted region (channel), which is aritificially called "channel bases demagnetizing pressure". The domain wall pressure, bias field pressure and the "induced pole channel pressures" then follow.

2.4.1 The Average Demagnetizing Pressures

In general, a sudden change in magnetization leads to an effective surface pole density equal to the change in magnetization. For a magnetic domain penetrating through a two layer material substrate, the z-component of the magnetic field at a point (x_o, y_o, z_o) due to the surface pole contributions at location (x,y) is expressed by

$$dH_{z_o} = k(r)\,dxdy\left[\frac{-M_1(z_o+z_1)}{[(x-x_o)^2+(y-y_o)^2+(z_1+z_o)^2]^{3/2}} + \frac{+(M_1-M_2)z_o}{[(x-x_o)^2+(y-y_o)^2+z_o^2]^{3/2}}\right.$$

$$\left. + \frac{M_2(z_o-z_2)}{[(x-x_o)^2+(y-y_o)^2+(z_o-z_2)^2]^{3/2}}\right] \qquad (2.4.1a)$$

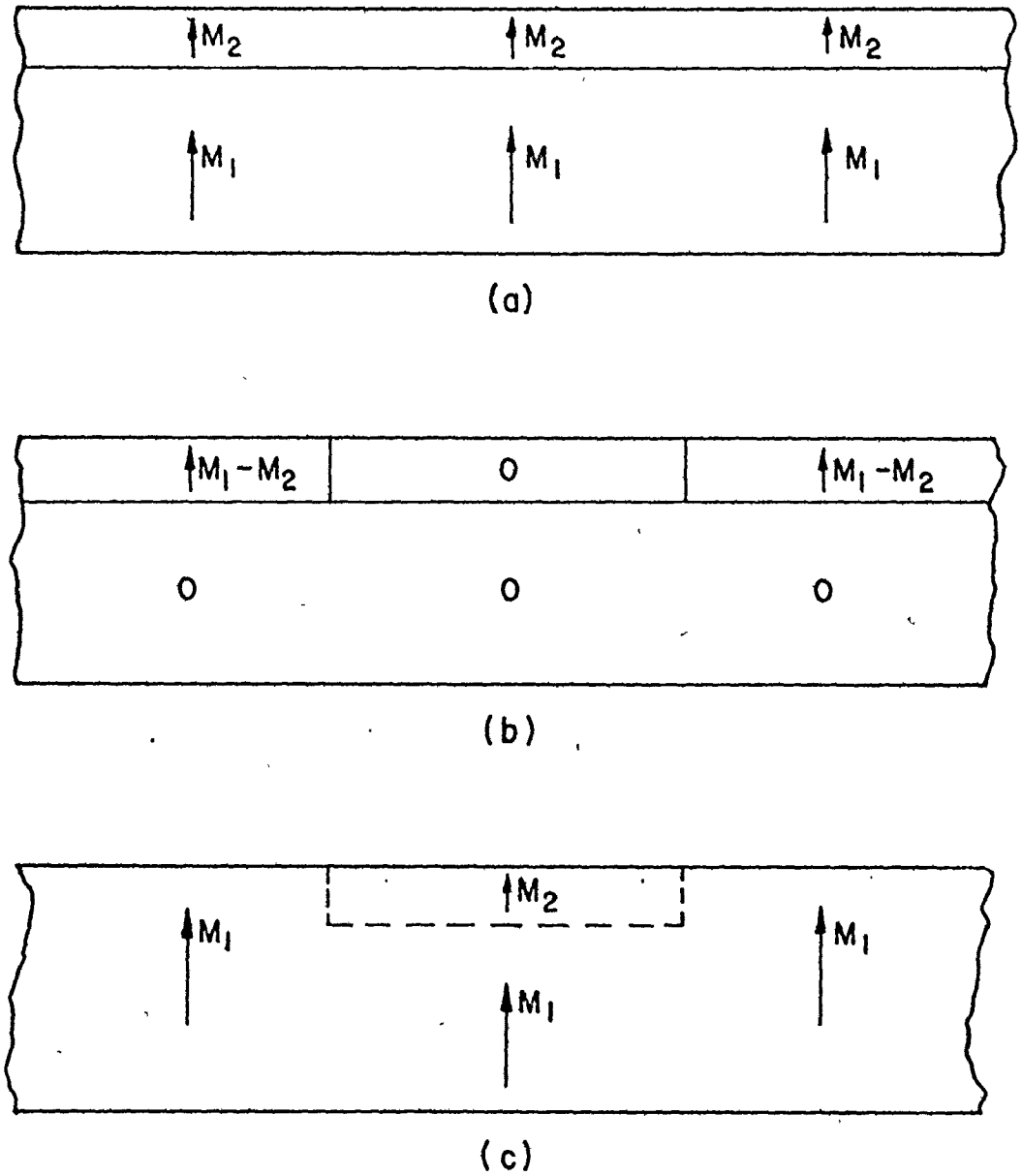

FIG. 2.5 Superposition of the magnetic configuration in (a) & (b) yields an ion implanted channel (c).

where

$$k(r) = 1-u(r_b(\theta)-r) \tag{2.4.1b}$$

and

$$u(x) = \begin{cases} 0 & x < 0 \\ 1 & x \geq 0 \end{cases} \tag{2.4.1c}$$

An extension of the approach of [14] leads to an average demagnetizing pressure

$$\bar{p}_{Do} = \frac{1}{T}\left[2\int_{-z_1}^{0} M_1\{\int_S dH_{z_o}\}dz_o + 2\int_0^{z_2} M_2\{\int_S dH_{z_o}\}\, dz_o\right] \tag{2.4.2}$$

where $\{\int_S dH_{z_o}\}$ denotes integration over the whole xy-plane, and

z_1, z_2 are the coordinates of the lower and the upper surfaces of the bubble material respectively (see Fig. 2.3).

By putting

$$\rho^2 = (x-x_o)^2+(y-y_o)^2 = r^2+r_o^2 - 2rr_o\cos(\theta-\theta_o) \tag{2.4.3}$$

and integrating Eqn. (2.4.2) with respect to z_o we directly obtain

$$\bar{p}_{Do} = -\frac{2}{T}\int_S dxdyk(r)\ \{M_1\Bigg[-\Bigg(\frac{M_2}{[\rho^2+(z_1+z_2)^2]^{1/2}} + \frac{(M_1-M_2)}{[\rho^2+z_1^2]^{1/2}} - \frac{M_1}{\rho}\Bigg)$$

$$+\Bigg(\frac{M_2}{[\rho^2+z_2^2]^{1/2}} + \frac{(M_1-M_2)}{\rho} - \frac{M_1}{[\rho^2+z_1^2]^{1/2}}\Bigg)\Bigg]$$

$$+M_2\Bigg[\Bigg(\frac{M_2}{\rho} + \frac{(M_1-M_2)}{[\rho^2+z_2^2]^{1/2}} - \frac{-M_1}{[\rho^2+(z_1+z_2)^2]^{1/2}}\Bigg) - \Bigg(\frac{M_2}{[\rho^2+z_2^2]^{1/2}} + \frac{(M_1-M_2)}{\rho}$$

$$-\frac{M_1}{[\rho^2+z_1^2]^{1/2}}\Bigg)\Bigg]\Bigg\}$$

$$= -\frac{2}{T}\int_S dxdyk(r)\ \Bigg\{\frac{-2M_1M_2}{[\rho^2+(z_1+z_2)^2]^{1/2}} + \frac{2(M_1^2+M_2^2-M_1M_2)}{\rho}$$

$$+\frac{2(M_1M_2-M_1^2)}{[\rho^2+z_1^2]^{1/2}} + \frac{2(M_1M_2-M_2^2)}{[\rho^2+z_2^2]^{1/2}}\Bigg\}$$

$$= -\frac{2}{T}\int_S dxdyk(r)\ \{-2M_1M_2\left(\frac{1}{[\rho^2+(z_1+z_2)^2]^{1/2}}-\frac{1}{\rho}\right)$$

$$+\ 2M_1(M_2-M_1)\left(\frac{1}{[\rho^2+z_1^2]^{1/2}}-\frac{1}{\rho}\right)+\ 2M_2(M_1-M_2)\left(\frac{1}{[\rho^2+z_2^2]^{1/2}}-\frac{1}{\rho}\right)\Big\}$$

(2.4.4)

If one defines

$$C_1 = 2M_1(M_1-M_2)\quad,\quad C_2=2M_2(M_2-M_1)\quad,\quad C_3 = 2M_1M_2$$

and $\qquad z_3 = z_1+z_2$

then the pressure at the 0th pressure sampling point can be expressed by

$$\bar{p}_{zo} = -\frac{2}{T}\int_0^{2\pi} d\theta \int_0^{\infty} rdr[1-2u(r_b(\theta)-r)]\ \sum_{i=1}^{3} C_i\left(\frac{1}{[\rho^2+z_i^2]^{1/2}}-\frac{1}{\rho}\right)$$

$$= -\frac{2}{T}\int_0^{2\pi} d\theta \sum_{i=1}^{3} C_i[\,|_{r=0}^{r=r_b(\theta)}\ \{(r^2+r_o^2-2rr_o\cos(\theta-\theta_o)+z_i^2)^{1/2}-(r^2+r_o^2-2r_orcos(\theta-\theta_o))^{1/2}$$

$$+r_o\cos(\theta-\theta_o)\left(\sinh^{-1}\left(\frac{r-r_o\cos(\theta-\theta_o)}{\sqrt{r_o^2\sin^2(\theta-\theta_o)+z_i^2}}\right)-\sinh^{-1}\left(\frac{r-r_o\cos(\theta-\theta_o)}{\sqrt{r_o^2\sin^2(\theta-\theta_o)}}\right)\right)$$

$$+\Bigg|_{r=\infty}^{r=r_b(\theta)}\Bigg\{(r^2+r_o^2-2rr_o\cos(\theta-\theta_o)+z_i^2)^{1/2}-(r^2+r_o^2-2r_orcos(\theta-\theta_o))^{1/2}$$

$$+r_o\cos(\theta-\theta_o)\left(\sinh^{-1}\left(\frac{r-r_o\cos(\theta-\theta_o)}{\sqrt{r_o^2\sin^2(\theta-\theta_o)+z_i^2}}\right)-\sinh^{-1}\left(\frac{r-r_o\cos(\theta-\theta_o)}{\sqrt{r_o^2\sin^2(\theta-\theta_o)}}\right)\right)\Bigg]\Bigg\}$$

(2.4.5a)

The limits can be changed [1] in (2.4.5) to yield the equivalent expression

$$\bar{p}_{zo} = -\frac{2}{T}\int_0^{2\pi} d\theta\Bigg[2\sum_{i=1}^{3}C_i\Bigg\{r_b^2+r_o^2-2r_br_o\cos(\theta-\theta_o)+z_i^2)^{1/2}-(r_o^2+z_i^2)^{1/2}$$

$$-(r_b^2+r_o^2-2r_br_o\cos(\theta-\theta_o))^{1/2}+r_o$$

$$+r_o\cos(\theta-\theta_o)\,\ell n\left(\frac{r_b-r_o\cos(\theta-\theta_o)+[r_b^2+r_o^2-2r_or_b\cos(\theta-\theta_o)+z_i^2]^{1/2}}{r_b-r_o\cos(\theta-\theta_o)+[r_b^2+r_o^2-2r_or_b\cos(\theta-\theta_o)]^{1/2}}\right.$$

$$\left.\times\frac{[r_o-r_o\cos(\theta-\theta_o)]}{[-r_o\cos(\theta-\theta_o)+r_o^2+z_i^2]^{1/2}]}\right)\Bigg\}$$

$$=\sum_{i=1}^{3}\frac{4\pi C_i z_i}{T}\Bigg] \qquad (2.4.5b)$$

where (r_o, θ_o) are the polar co-ordinates of the pressure sampling point at which we compute the pressure. Equation (2.4.5b) can be recast in a form whose integrand behaves smoothly. This is done by removing an apparent singularity by integrating analytically a part of the above integrand. Thus we obtain the final convenient form for $\bar{p}_{zo}$

$$\bar{p}_{zo} = -\frac{2}{T}\int_0^{2\pi} d\theta \left[\sum_{i=1}^{3} 2C_i \left\{ (r_b^2+r_o^2-2r_b r_o \cos(\theta-\theta_o)+z_i^2)^{1/2} - (r_o^2+z_i^2)^{1/2} \right.\right.$$

$$- (r_o^2+r_b^2-2r_b r_o \cos(\theta-\theta_o))^{1/2} + r_o$$

$$+ r_o \cos(\theta-\theta_o) \ln\left(\frac{r_b - r_o\cos(\theta-\theta_o) + [r_b^2+r_o^2-2r_o\cos(\theta-\theta_o)+z_i^2]^{1/2}}{r_b - r_o\cos(\theta-\theta_o) + [r_b^2+r_b^2 r_o \cos(\theta-\theta_o)]^{1/2}} \right.$$

$$\left.\left.\left. \times \frac{r_o(1-\cos(\theta-\theta_o))^{1/2}}{[(r_o^2+z_i^2)^{1/2} - r_o\cos(\theta-\theta_o)]} \right)\right\}\right] - \sum_{i=1}^{3} \frac{4\pi C_i (z_i - r_o)}{T}$$

(2.4.6)

The gradients of the demagnetizing pressures with respect to the radial parameters $\{r_j\}$ are directly given by

$$\frac{\partial \bar{p}_{zo}}{\partial r_j} = \left[\sum_{i=1}^{3} \frac{4\pi C_i}{T} \left(\frac{\partial r_o}{\partial r_j}\right)\right] - \frac{2}{T}\int_0^{2\pi} d\theta \left[2 \sum_{i=1}^{3} C_i \left\{\frac{\partial r_o}{\partial r_j}\left(1 - \frac{r_o}{[r_o^2+z_i^2]^{1/2}}\right)\right.\right.$$

$$\overbrace{+\left(r_b \frac{\partial r_b}{\partial r_j} + r_o \frac{\partial r_o}{\partial r_j} - \cos(\theta-\theta_o)\left[r_b \frac{\partial r_o}{\partial r_j} + r_o \frac{\partial r_o}{\partial r_j}\right]\right)}^{F1}$$

$$\times\left([r_b^2+r_o^2-2r_o r_b \cos(\theta-\theta_o)+z_i^2]^{-1/2} - [r_b^2+r_o^2-2r_b r_o \cos(\theta-\theta_o)]^{-1/2}\right)$$

$$+\left(\frac{\partial r_o}{\partial r_j}\right)\cos(\theta-\theta_o)\,\ell n\left[\frac{(r_b-r_o\cos(\theta-\theta_o)+[r_b^2+r_o^2-2r_b r_o\cos(\theta-\theta_o)+z_i^2]^{1/2})}{(r_b-r_o\cos(\theta-\theta_o)+[r_b^2+r_o^2-2r_b r_o\cos(\theta-\theta_o)]^{1/2})}\right.$$

$$\left.\times \frac{r_o[1-\cos(\theta-\theta_o)]^{1/2}}{([r_o^2+z_i^2]^{1/2}-r_o\cos(\theta-\theta_o))}\right]$$

$$+r_o\cos(\theta-\theta_o)\left[\left(\frac{\partial r_b/\partial r_j - \cos(\theta-\theta_o)\partial r_o/\partial r_j + F1[r_b^2+r_o^2-2r_b r_o\cos(\theta-\theta_o)+z_i^2]^{-1/2}}{r_b-r_o\cos(\theta-\theta_o)+[r_b^2+r_o^2-2r_b r_o\cos(\theta-\theta_o)+z_i^2]^{1/2}}\right)\right.$$

$$-\left(\frac{\partial r_b/\partial r_j-\cos(\theta-\theta_o)\partial r_o/\partial r_j+F1[r_b^2+r_o^2-2r_b r_o\cos(\theta-\theta_o)]^{-1/2}}{r_b-r_o\cos(\theta-\theta_o)+[r_b^2+r_o^2-2r_b r_o\cos(\theta-\theta_o)]^{1/2}}\right)$$

$$+\frac{\partial r_o}{\partial r_j}\left(1-\frac{\left[r_o[r_o^2+z_i^2]^{-1/2}-\cos(\theta-\theta_o)\right]}{[r_o^2+z_i^2]^{1/2}-r_o\cos(\theta-\theta_o)}\right)\Bigg)\Bigg\}\Bigg] \qquad (2.4.7)$$

It is seen that the demagnetizing pressures at the sampling points are independent of the variable δ.

2.4.2 Channel Bases Demagnetization Pressures

In computing the demagnetization pressure we have effectively assumed a channel of infinite width, since the channel does have a finite width we should add a correcting factor to take this into account. A successful application of this superposition principle has been demonstrated in [14]. Since we have assumed that the magnetization of layer 1 (the nonimplanted region) is M_1 and that of layer 2 (from the upper surface to a depth D) is M_2 (see Fig. 2.5a), we should further superpose a magnetization (M_1-M_2) on the entire layer 2 except at the channel (see Fig. 2.5b). In this way, the channel becomes the only part of the bubble material, which has magnetization M_1 with a net magnetization M_2 as shown in Fig. 2.5c. This superposed demagnetization will add

an extra demagnetizing field due to its corresponding effecti surface pole density. The extra so called "channel base demagnetizin field" component along the z-direction at a point (x_o, y_o, z_o) due to an area element at $(x,y,0)$ and (x,y,z_2) is given by

$$dH_z = -(M_1-M_2)\left[\frac{z_o dxdy}{[x^2+(y-y_o)^2+z_o^2]^{3/2}} + \frac{(z_2-z_o)dxdy}{[x^2+(y-y_o)^2+(z_2-z_o)^2]^{3/2}}\right] \tag{2.4.8}$$

The average "channel base demagnetizing" pressure at the sampling point (x_o, y_o) is given by

$$\bar{p}_{zo} = -2\frac{(M_1-M_2)}{T}\left\{\int_{-z_1}^{0}\int_{-\infty}^{\infty}\int_{w}^{\infty} M_1\left[\frac{z_o dz_o dxdy}{[x^2+(y-y_o)^2+z_o^2]^{3/2}} - \frac{(z_o-z_2)dz_o dxdy}{[x^2+(y-y_o)^2+(z_o-z_2)^2]^{3/2}}\right]\right.$$

$$+\int_{0}^{z_2}\int_{-\infty}^{\infty}\int_{+w}^{+\infty} M_2\left[\frac{z_o dz_o dxdy}{[x^2+(y-y_o)^2+z_o^2]^{3/2}} - \frac{(z_o-z_2)dz_o dxdy}{[x^2+(y-y_o)^2+(z_o-z_2)^2]^{3/2}}\right]$$

$$-\int_{-z_1}^{0}\int_{-\infty}^{\infty}\int_{-w}^{-\infty} M_1\left[\frac{z_o dz_o dxdy}{[x^2+(y-y_o)^2+z_o^2]^{3/2}} - \frac{(z_o-z_2)dz_o dxdy}{[x^2+(y-y_o)^2+(z_o-z_2)^2]^{3/2}}\right]$$

$$-\int_{0}^{z_2}\int_{-\infty}^{\infty}\int_{-w}^{-\infty} M_2\left[\frac{z_o dz_o dxdy}{[x^2+(y-y_o)^2+z_o^2]^{3/2}} - \frac{(z_o-z_2)dz_o dxdy}{[x^2+(y-y_o)^2+(z_o-z_2)^2]^{3/2}}\right]\Bigg\} \tag{2.4.9}$$

It can be shown that, by integrating (2.4.9) with respect to the variable x and then y, it reduces to the form

$$\bar{p}_{co} = -4\frac{(M_1-M_2)}{T}\Bigg\{\int_{-z_1}^{0} M_1 dz_o\Bigg[\tan^{-1}\left(\frac{y-y_o}{z_o}\right)\Bigg|_{w}^{\infty} - \tan^{-1}\left(\frac{y-y_o}{z_o}\right)\Bigg|_{-w}^{-\infty}$$

$$-\tan^{-1}\left(\frac{y-y_o}{z_o-z_2}\right)\Bigg|_{w}^{\infty} + \tan^{-1}\left(\frac{y-y_o}{z_o-z_2}\right)\Bigg|_{-w}^{-\infty}\Bigg]$$

$$+\int_{0}^{z_2} M_2 dz_o\Bigg[\tan^{-1}\left(\frac{y-y_o}{z_o}\right)\Bigg|_{w}^{\infty} - \tan^{-1}\left(\frac{y-y_o}{z_o}\right)\Bigg|_{-w}^{-\infty}$$

$$-\tan^{-1}\left(\frac{y-y_o}{z_o-z_2}\right)\Bigg|_{w}^{\infty} + \tan^{-1}\left(\frac{y-y_o}{z_o-z_2}\right)\Bigg|_{-w}^{-\infty}\Bigg]\Bigg\} \tag{2.4.10}$$

By taking the limits and integrating by parts, Eqn. (2.4.10) reduces to

$$\tilde{p}_{co} = -4\frac{(M_1-M_2)}{T}\Bigg\{M_1\Bigg(z_o\left[-\tan^{-1}\left(\frac{w-y_o}{z_o}\right)-\tan^{-1}\left(\frac{w+y_o}{z_o}\right)\right]\Bigg|_{-z_1}^{0}$$

$$+(z_o-z_2)\left[\tan^{-1}\left(\frac{w-y_o}{z_o-z_2}\right)+\tan^{-1}\left(\frac{w+y_o}{z_o-z_2}\right)\right]\Bigg|_{z_1}^{0}$$

$$-\int_{-z_1}^{0}\left[\frac{(w-y_o)z_o}{[z_o^2+(w-y_o)^2]}+\frac{(w+y_o)z_o}{[z_o^2+(w+y_o)^2]}-\frac{(z_o-z_2)(w-y_o)}{[(z_o-z_2)^2+(w-y_o)^2]}-\frac{(w+y_o)(z_o-z_2)}{[(w+y_o)^2+(z_o-z_2)^2]}\right]dz_o\Bigg)$$

$$+M_2\Bigg(z_o\left[-\tan^{-1}\left(\frac{w-y_o}{z_o}\right)-\tan^{-1}\left(\frac{w+y_o}{z_o}\right)\right]_0^{z_2}$$

$$+(z_o-z_2)\left[\tan^{-1}\left(\frac{w-y_o}{z_o-z_2}\right)+\tan^{-1}\left(\frac{w+y_o}{z_o-z_2}\right)\right]_0^{z_2}$$

$$-\int_0^{z_2}dz_o\left[\frac{z_o(w-y_o)}{[z_o^2+(w-y_o)^2]}+\frac{z_o(w+y_o)}{[z_o^2+(w+y_o)^2]}-\frac{(w+y_o)(z_o-z_2)}{[(z_o-z_2)^2+(w-y_o)^2]}-\frac{(w+y_o)(z_o-z_2)}{[(w+y_o)^2+(z_o-z_2)^2]}\right]\Bigg)$$

$$+2\pi(M_1z_1+M_2z_2)\Bigg\} \qquad (2.4.11)$$

By performing the direct integrations in (2.4.11) we arrive at the final equation for the channel base demagnetization pressure given by

$$\bar{p}_{co} = -4\frac{(M_1-M_2)}{T}\Bigg\{2\pi(M_1z_1+M_2z_2)$$

$$+M_1\Big[-z_1\Big(\tan^{-1}\Big(\frac{w-y_o}{z_1}\Big)+\tan^{-1}\Big(\frac{w+y_o}{z_1}\Big)\Big)$$

$$+z_2\Big(\tan^{-1}\Big(\frac{w-y_o}{z_2}\Big)+\tan^{-1}\Big(\frac{w+y_o}{z_2}\Big)\Big)$$

$$-(z_1+z_2)\Big(\tan^{-1}\Big(\frac{w-y_o}{z_1+z_2}\Big)+\tan^{-1}\Big(\frac{w-y_o}{z_1+z_2}\Big)\Big)$$

$$-\Big(\frac{w-y_o}{2}\Big)\Bigg\{\ln\Big(1+\frac{z_1^2}{(w-y_o)^2}\Big)-\ln\Big(1+\frac{z_2^2}{(w-y_o)^2}\Big)+\ln\Big(1+\Big(\frac{z_1+z_2}{w-y_o}\Big)^2\Big)\Bigg\}$$

$$-\Big(\frac{w+y_o}{2}\Big)\Bigg\{\ln\Big(1+\frac{z_1^2}{(w+y_o)^2}\Big)-\ln\Big(1+\frac{z_2^2}{(w+y_o)^2}\Big)+\ln\Big(1+\frac{z_1+z_2}{(w+y_o)^2}\Big)^2\Big)\Bigg\}\Bigg]$$

$$+2M_2\Big[-z_2\Big(\tan^{-1}\Big(\frac{w-y_o}{z_2}\Big)+\tan^{-1}\Big(\frac{w+y_o}{z_2}\Big)\Big)$$

$$-\Big\{\frac{(w-y_o)}{2}\ln\Big(1+\frac{z_2^2}{(w-y_o)^2}\Big)+\frac{(w+y_o)}{2}\ln\Big(1+\frac{z_2^2}{(w+y_o)^2}\Big)\Big\}\Big]\Bigg\} \qquad (2.4.12)$$

The channel base demagnetizing pressure gradients with respect to the variable x_j are obtained by direct differentiation of (2.4.12) to give

$$\frac{\partial \bar{p}_{co}}{\partial x_j} = -2\frac{(M_1-M_2)}{T}\left(\frac{\partial y_o}{\partial x_j}\right)\left\{ M_1\left[\ln\left(1+\frac{z_1^2}{(w-y_o)^2}\right)-\ln\left(1+\frac{z_1^2}{(w+y_o)^2}\right)\right.\right.$$

$$\left.-\ln\left(1+\frac{z_2^2}{(w-y_o)^2}\right)+\ln\left(1+\frac{z_2^2}{(w+y_o)^2}\right)+\ln\left(1+\left(\frac{z_1+z_2}{w-y_o}\right)^2\right)-\ln\left(1+\left(\frac{z_1+z_2}{w+y_o}\right)^2\right)\right]$$

$$\left.+2M_2\left[\ln\left(1+\frac{z_2^2}{(w-y_o)^2}\right)-\ln\left(1+\frac{z_2^2}{(w+y_o)^2}\right)\right]\right\} \qquad (2.4.13)$$

Since $y_o=\delta+r_o\cos\theta_o$,

$$\frac{\partial y_o}{\partial \delta} = 1, \quad \text{and} \quad \frac{\partial y_o}{\partial r_j} = \cos\theta_o\left(\frac{\partial r_o}{\partial r_j}\right) \qquad (2.4.14)$$

hence we can obtain the gradients $\frac{\partial \bar{p}_{co}}{\partial r_j}$ and $\frac{\partial \bar{p}_{co}}{\partial \delta}$ by substituting the appropriate term for $\left(\frac{\partial y_o}{\partial x}\right)$ in (2.4.14) into (2.4.13).

An inspection of equations (2.4.12) and (2.4.13) shows that the channel base pressures decrease as we go away from the channel center towards the side wall, while the gradients increase negatively very quickly.

2.4.3 Domain Wall Pressures

It has been shown [1] that the domain wall contributes an effective magnetic pressure at a point on the wall given by

$$p_w = \frac{-\sigma_w}{R} \tag{2.4.15a}$$

where σ_w is the wall energy density and R is the radius of curvature of the wall at this point. For a domain wall penetrating into two regions, the average domain wall pressure is given by

$$\bar{p}_{\sigma o} = -\frac{1}{T}(\sigma_1 z_1 + \sigma_2 z_2) \times \frac{1}{R_o}\bigg|_{r=r_o} \tag{2.4.15b}$$

where R_o is the "radius of curvature" of the wall at the sampling point (r_o, θ_o), and R^{-1} is given by [24]

$$R^{-1} = \frac{\left[1+2\left(\frac{1}{r}\frac{dr}{d\theta}\right)^2 + \frac{1}{r}\frac{d^2r}{d\theta^2}\right]}{r\left[1+\left(\frac{1}{r}\frac{dr}{d\theta}\right)^2\right]^{3/2}} \tag{2.4.15c}$$

For the domain wall pressure, only the gradients with respect to the radial parameters exist and are given by

$$\frac{\partial \bar{p}_{\sigma o}}{\partial r_j} = -\frac{(\sigma_1 z_1 + \sigma_2 z_2)}{T} \left\{ \left[\frac{\partial r_o}{\partial r_j}\left(-\frac{1}{r^2} - \frac{6}{r^2}\left(\frac{1}{r}\frac{dr}{d\theta}\right)^2 - \frac{2}{r^3}\frac{d^2r}{d\theta^2}\right)\right.\right.$$

$$+ \frac{4}{r^3}\left(\frac{dr}{d\theta}\right) \frac{\partial}{\partial r_j}\left(\frac{dr}{d\theta}\right) + \frac{1}{r^2} \frac{\partial}{\partial r_j}\left(\frac{d^2r}{d\theta^2}\right)\Big]\Big[1+\left(\frac{1}{r}\frac{dr}{d\theta}\right)^2\Big]^{-3/2}$$

$$- \frac{3}{r}\left(\frac{1}{r}\frac{dr}{d\theta}\right)\Big[1+\left(\frac{1}{r}\frac{dr}{d\theta}\right)^2\Big]^{-5/2}\Big[1+2\left(\frac{1}{r}\frac{dr}{d\theta}\right)^2 + \frac{1}{r}\frac{d^2r}{d\theta^2}\Big]\Big[-\frac{1}{r^2}\frac{dr}{d\theta}\Big(\quad\Big)_j$$

$$+ \frac{1}{r}\frac{\partial}{\partial r_j}\left(\frac{dr}{d\theta}\right)\Big]\Big\} \qquad (2.4.16)$$

The various partial derivatives appearing in Eqn. (2.4.16) have been explicitly derived in (2.2.13) and (2.2.14).

2.4.4 External Bias Field Pressure

The stable magnetic domain can only be sustained by an external bias field H_B (Fig. 2.1). This external bias field contributes a "bias field pressure" given by the expression

$$\bar{P}_{Bo} = -\frac{1}{T}[2M_1z_1+2M_2z_2]H_B \qquad (2.4.17)$$

where H_B is the z-component of an external uniform magnetic field. The bias field pressure gradients are all zero.

2.4.5 Channel Wall Induced Pole Pressure

The pole density distributions induced on the channel walls

(Sec. 2.1) will in turn contribute to the z-component of the magnetic field at the magnetic domain wall, and hence to the pressures on it. The z-component of the magnetic field at (r_o,θ_o,z_o) due to the induced pole density $P_k\ (\phi_i,z_i)$ at (ϕ_i,z_i) is given by

$$dH_z = \frac{dz_i d\phi_i \sec^2\phi_i (w+(2k-3)\delta) P_k\ (\phi_i,z_i)(z_o-z_i)}{[r_o^2+R_k^2-2r_oR_k\cos(\theta_o-\phi_i)+(z_o-z_i)^2]^{3/2}} \tag{2.4.18}$$

where $R_k = (w+(2k-3)\delta)/|\cos\phi_i|$, and w, δ are shown in Fig. 2.2.

This gives an average pressure contribution at the sampling point (r_o,θ_o) expressed by

$$\bar{p}_{cwo} = \frac{1}{T}\sum_{k=1}^{2}\int_0^D dz_i \int_0^{\pi/2} d\phi_i \sec^2\phi_i (w+(2k-3)\delta) P_k\ (\phi_i,z_i)$$

$$\left\{\int_0^{z_2} 2M_2(z_o-z_i)dz_o\left[\frac{1}{[\rho_1^2+(z_o-z_i)^2]^{3/2}}+\frac{1}{[\rho_2^2+(z_o-z_i)^2]^{3/2}}\right]\right.$$

$$\left.+\int_{-z_1}^{0} 2M_1(z_o-z_i)dz_o\left[\frac{1}{[\rho_1^2+(z_o-z_i)^2]^{3/2}}+\frac{1}{[\rho_2^2+(z_o-z_i)^2]^{3/2}}\right]\right\} \tag{2.4.19a}$$

where

$$\left.\begin{aligned} \rho_1^2 &= r_o^2+R_k^2-2r_oR_k\cos(\theta_o-\phi_i) \\ \text{and} \\ \rho_2^2 &= r_o^2+R_k^2-2r_oR_k\cos(\theta_o+\phi_i) \end{aligned}\right\} \qquad (2.4.19b)$$

We can express (2.4.19a) in a more convenient form, namely,

$$\bar{p}_{cwo} = \frac{1}{T}\sum_{k=1}^{2}\int_0^D dz_i \int_0^{\pi/2} d\phi_i \sec^2\phi_i (w+(2k-3)\delta)B_k(\phi_i,z_i)P_k\ (\phi_i,z_i) \quad (2.4.20a)$$

where B_k could be obtained by straightforward integration of (2.4.19a) with respect to the variable z_o, that is,

$$B_k(\phi_i,z_i) =$$

$$2M_1\left[\frac{-1}{[\rho_1^2+z_i^2]^{1/2}}+\frac{1}{[\rho_1^2+(z_i-z_1)2]^{1/2}}+\frac{1}{[\rho_2^2+(z_1+z_i)^2]^{1/2}}-\frac{1}{[\rho_2^2+z_i^2]^{1/2}}\right]$$

$$+2M_2\left[\frac{1}{[\rho_1^2+z_i^2]^{1/2}}-\frac{1}{[\rho_1^2+(z_i-z_2)^2]^{1/2}}+\frac{1}{[\rho_2^2+z_i^2]^{1/2}}-\frac{1}{[\rho_2^2+(z_i-z_2)^2]^{1/2}}\right].$$

(2.4.20b)

The gradients of the channel wall induced pole density with respect to the radial parameters $\{r_j\}$ are given by

$$\frac{\partial \bar{p}_{cwo}}{\partial r_j} = \frac{1}{T}\int_0^D dz_i \int_0^{\pi/2} d\phi_i \sec^2\phi_i\,(w+(2k-3)\delta) \sum_{k=1}^{2} \{P_k(\phi_i,z_i)\frac{\partial B_k(\phi_i,z_i)}{\partial r_j}$$

$$+B_k(\phi_i,z_i)\frac{\partial P_k(\phi_i,z_i)}{\partial r_j} \qquad (2.4.21a)$$

where $\frac{\partial P_k(\phi_i,z_i)}{\partial r_j}$ was given in (2.3.7) and $\frac{\partial B_k(\phi_i,z_i)}{\partial r_j}$ is obtained by differentiating (2.4.20b)

$$\frac{\partial B_k(\phi_i,z_i)}{\partial r_j} = -2\left[\frac{\partial r_o}{\partial r_j}\right]\Bigg\{[r_o-R_k\cos(\theta_o-\phi_i)]$$

$$\times\left(M_1\left[\frac{1}{[\rho_1^2+(z_1+z_i)^2]^{3/2}}-\frac{1}{[\rho_1^2+z_i^2]^{3/2}}\right]+M_2\left[\frac{1}{[\rho_1^2+z_i^2]^{3/2}}-\frac{1}{[\rho_1^2+(z_i-z_2)^2]^{3/2}}\right]\right)$$

$$+[r_o-R_k\cos(\theta_o+\phi_i)]$$

$$\times\left(M_1\left[\frac{1}{[\rho_2^2+(z_1+z_i)^2]^{3/2}}-\frac{1}{[\rho_2^2+z_i^2]^{3/2}}\right]+M_2\left[\frac{1}{[\rho_2^2+z_i^2]^{3/2}}-\frac{1}{[\rho_2^2+(z_i-z_2)^2]^{3/2}}\right]\right)\Bigg\}$$

(2.4.21b)

The gradient with respect to the variable parameter δ is given by

$$\frac{\partial \bar{p}_{cwo}}{\partial \delta} = \frac{1}{T}\int_0^D dz_i \int_0^{\pi/2} d\phi_i \sec^2\phi_i \sum_{i=1}^{2} \{(2k-3)P_k(\phi_i,z_i)B_k(\phi_i,z_i)$$

$$+(w+(2k-3)\delta)\left(P_k(\phi_i,z_i)\frac{\partial B_k(\phi_i,z_i)}{\partial \delta} + B_k(\phi_i,z_i)\frac{\partial P_k(\phi_i,z_i)}{\partial \delta}\right)\Bigg\} \quad (2.4.22a)$$

where $\frac{\partial P_k(\phi_i,z_i)}{\partial \delta}$ is given by (2.3.10) and (2.3.8) and $\frac{\partial B_k(\phi_i,z_i)}{\partial \delta}$

is expressed by

$$\frac{\partial B_k(\phi_i,z_i)}{\partial \delta} = -2\frac{(2k-3)}{|\cos\phi_i|}\{(R_k-r_o\cos(\theta_o-\phi_i))$$

$$\times\left(M_1\left[\frac{1}{[\rho_1^2+(z_1+z_i)^2]^{3/2}} - \frac{1}{[\rho_1^2+z_i^2]^{3/2}}\right]+M_2\left[\frac{1}{[\rho_1^2+z_i^2]^{3/2}} + \frac{1}{[\rho_1^2+(z_i-z_2)^2]^{3/2}}\right]\right)$$

$$+ (R_k-r_o\cos(\theta_o+\phi_i))\}$$

$$\times \left(M_1 \left[\frac{1}{[\rho_2^2+(z_1+z_i)^2]^{3/2}} + \frac{1}{[\rho_2^2+z_i^2]^{3/2}} \right] + M_2 \left[\frac{1}{[\rho_2^2+z_i^2]^{3/2}} - \frac{1}{[\rho_2^2+(z_i-z_2)^2]^{3/2}} \right] \right) \Bigg\}$$

(2.4.22b)

Once again it is obvious that though the formula appear to be complicated, many terms are repetative and this greatly simplifies the computation procedures.

2.5 Model Adaptation

It has been reported [11] that ion implantation changes the magnetization and "quality factor" of the implanted region of the bubble material, while other workers [4,5] report the almost complete disappearance of the fixed magnetization in the implanted region and the appearance of a large in-plane susceptibility. Both mechanisms are found to supress hard bubbles, but in the latter case the bubble is believed to penetrate only through the unimplanted region and is capped by a 90° domain wall, at the implanted-nonimplanted boundary. Although the formulation presented in this chapter directly applies to the first case, it readily accommodates the second situation where the 90°

domain wall cap has the effect of an equivalent uniform bias field [22] which can be expressed as

$$H_{Bequiv} = \frac{[\sigma_{wcap}]}{2[M_1 z_1 + M_2 z_2]} \tag{2.5.1}$$

where σ_{wcap} is the 90° domain wall energy of the bubble cap.

The proceeding formulation has been programmed and successfully tested and the results are discussed in Chapter 4.

CHAPTER 3

CIRCULAR DOMAIN OF VARIABLE PENETRATION IN AN ION IMPLANTED CHANNEL

In this chapter, the proposed model for the ion implantation mechanism will be applied to study the stability of a circular magnetic domain of variable penetrations in both the implanted and the non-implanted regions. The bubble domain is again assumed to be wholly situated inside the ion implanted channel.

We shall again assume that the magnetic domain configuration can be expressed by the single valued function $r_b(\theta)$ [Ch.2, Sec. 2.2] expandable in the form

$$r_b(\theta) = \sum_{n=0}^{\infty} r_n \cos[(\theta-\theta_n)n]$$

Expressions for the energy of the bubble domain, as well as for the domain energy gradients with respect to the variables are derived for the case of a straight channel. The domain variables are: the bubble radius r_o the bubble domain penetration z_1 and z_2 into the nonimplanted and implanted regions respectively, and the bubble axis shift δ from the channel symmetry plane as shown in Figs. 3.1 to 3.3.

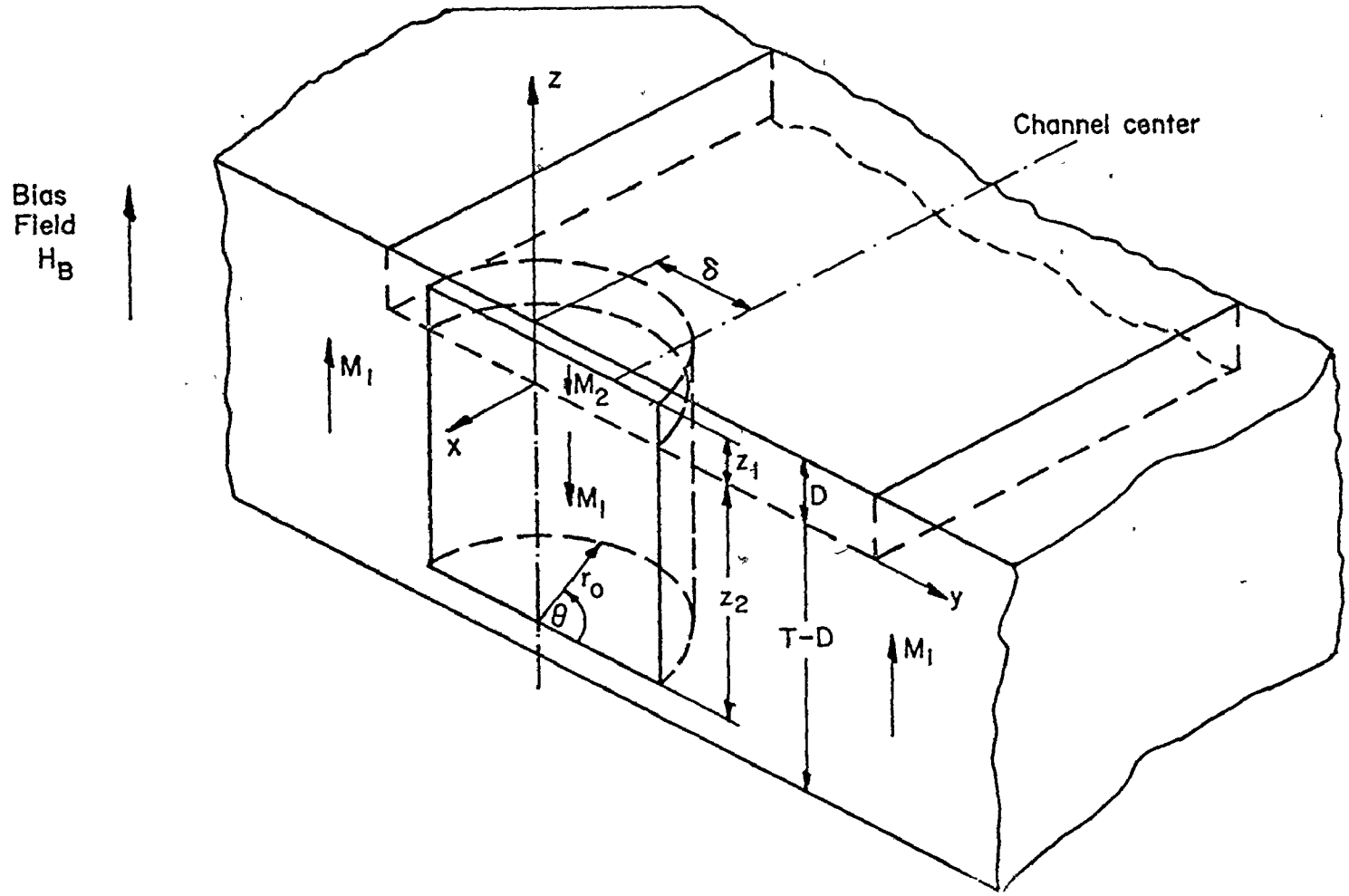

FIG. 3.1 The circular domain of variable penetration in ion implanted channel

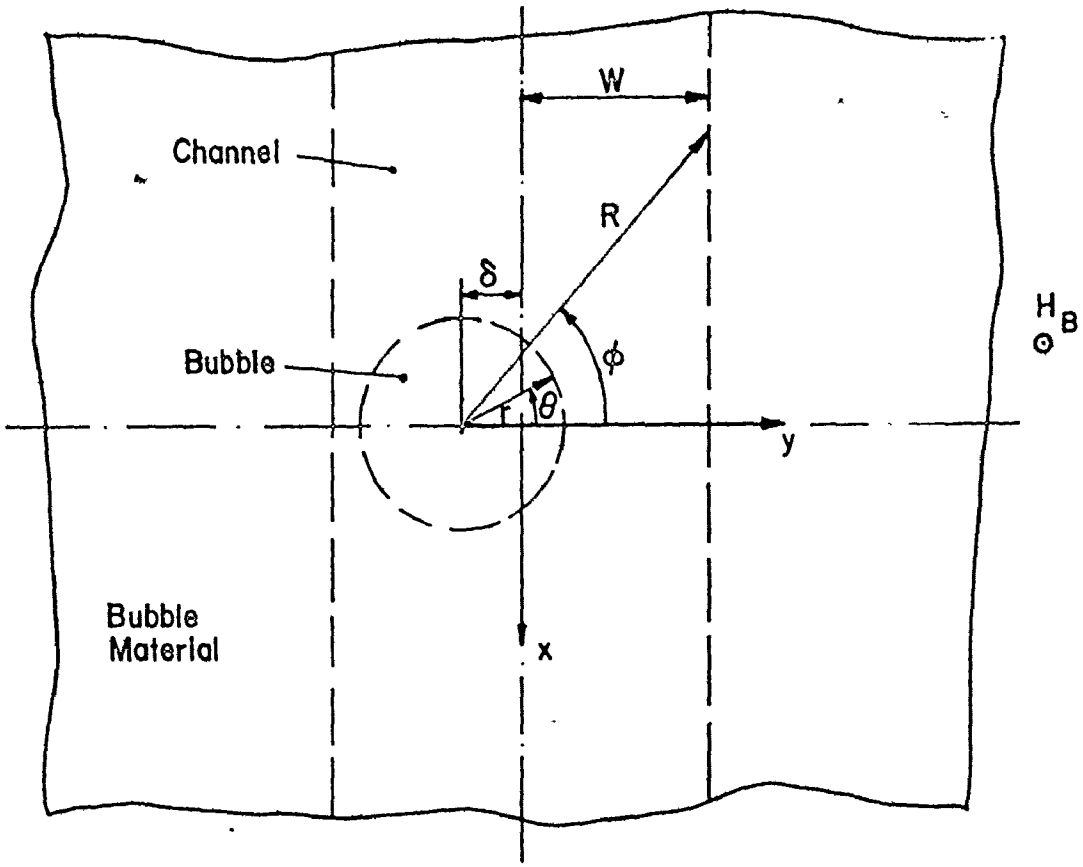

FIG. 3.2 Top view of circular cylindrical bubble in implanted channel

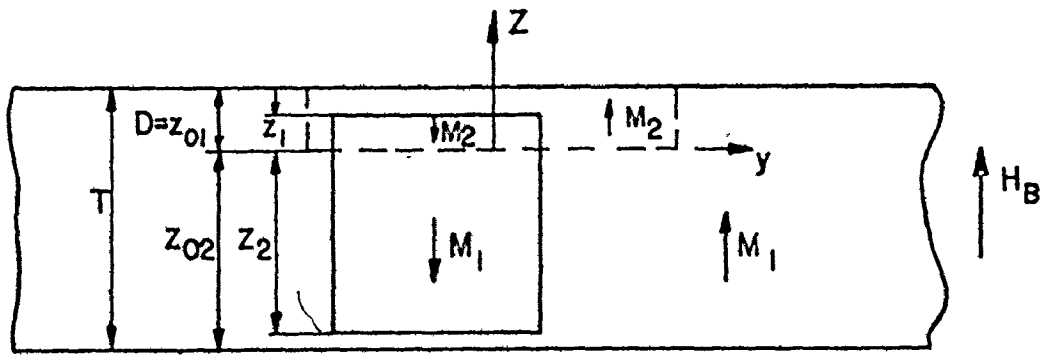

FIG. 3.3 Cross-section of circular cylindrical bubble in symmetry plane y z.

The formulation will be presented in a concise form with many intermediate steps omitted.

3.1 The Energy and Energy Gradients

The total energy of the domain is expressed as a sum of several energy contributions

$$E_T = E_w + E_H + E_D + E_{CB} + E_{cw} \tag{3.1.1}$$

where E_w is the domain wall energy, E_H is the external bias field energy, E_D is the demagnetization energy, E_{CB} is the channel width demagnetization energy and, E_{cw} is the channel wall induced pole energy.

The following subsection will present derivations of the mathematical expressions for the various energies and energy gradients.

3.1.1 Domain Wall Energy

The domain wall energy is given by [1]

$$E_w = (\sigma_1 z_1 + \sigma_2 z_2) \int_0^{2\pi} \left[r_b^2(\theta) + \left(\frac{\partial r_b(\theta)}{\partial \theta}\right)^2\right]^{1/2} d\theta$$

$$+ \left\{\left[\sigma_1' g\left(\frac{z_1}{z_{o1}}\right) + \sigma_2' g\left(\frac{z_2}{z_{o2}}\right)\right] \int_0^{2\pi} r_b^2(\theta) d\theta\right\} \tag{3.1.2a}$$

where

$$z_{o1} = D, \; z_{o2} = T-D$$

where σ_i and σ_i' are the wall energy densities of the cylindrical side wall and the cap walls of the bubble respectively, the subscripts refer to the nonimplanted (1) and implanted (2) regions, z_1 and z_2 are the co-ordinates of the upper and lower bubble cap respectively, z_{o1} and z_{o2} are the co-ordinates of the upper and lower surfaces of the bubble material (Fig. 3.3), g(u) is the unit step-like function

$$g(u) = \begin{cases} 1 & , \quad 0 < u < 1 \\ 0 & , \quad u \geq 1 \end{cases} \tag{3.1.2b}$$

The term in brackets in Fqn. (3.1.2a), accounts for the wall energy of the upper and lower caps of the bubble.

Since for a circular domain $r_b(\theta)=r_o$, we obtain

$$E_w = 2\pi r_o(\sigma_1 z_1+\sigma_2 z_2)+\pi r_o^2[\sigma_1' g(\frac{z_1}{z_{o1}})+\sigma_2' g(\frac{z_2}{z_{o2}})] \tag{3.1.2c}$$

It is noted that at the unit step-like function $g(\frac{z_i}{z_{oi}})$ assume a non-zero value of the last term in Eqns. (3.1.2a) and (3.1.2b), only within the ranges $0 \leq z_1 < z_{o1}$ and $0 \leq z_2 < z_{o2}$; that is, the bubble has two, one or no cap. If the bubble has no cap, then it is an ordinary bubble, penetrating throughout the thickness of its host material, and the cap energy term promptly vanishes.

In order to avoid numerical difficulties encountered in the gradient expressions for such an abrupt function g( ) we replace it by a smooth approximating function f(u) of the form

$$f\left(\frac{z_i}{z_{i_o}}\right) = \left[1 - \left(\frac{z}{z_{i_o}}\right)^{2p}\right]^{1/2p} \qquad 0 < z \leq z_{oi} \tag{3.1.2d}$$

where p is a large positive integer. Within the bubble material this approximate function seems to be more realistic than the pulse function g(u).

The gradients are found by direct differentiation of (3.1.2c) after substituting f(u) for g(u),

$$\frac{\partial E_w}{\partial r_o} = (\sigma_1 z_1 + \sigma_2 z_2)2\pi + 2\pi r_o\left[\sigma_1' f\left(\frac{z_1}{z_{01}}\right) + \sigma_2' f\left(\frac{z_2}{z_{02}}\right)\right] \tag{3.1.3a}$$

$$\frac{\partial E_w}{\partial z_1} = 2\pi r_o \sigma_1 + \frac{\pi r_o^2 \sigma_1'}{z_{01}}\left[-\left(\frac{z_1}{z_{01}}\right)^{2p-1}\right]\left[1-\left(\frac{z_1}{z_{01}}\right)^{2p}\right]^{(1/2p-1)} \tag{3.1.3b}$$

$$\frac{\partial E_w}{\partial z_2} = 2\pi r_o \sigma_2 + \frac{\pi r_o^2 \sigma_2'}{z_{02}}\left[-\left(\frac{z_2}{z_{02}}\right)^{2p-1}\right]\left[1-\left(\frac{z_1}{z_{01}}\right)^{2p}\right]^{(1/2p-1)} \tag{3.1.3c}$$

$$\frac{\partial E_w}{\partial \delta} = 0 \tag{3.1.3d}$$

3.1.2 The External Bias Field Energy

The bias field energy difference due to a uniform external bias field H_B is given by [1]

$$E_H = 2H_B[M_1Z_1 + M_2Z_2] \int_0^{2\pi} \frac{1}{2} r_b^2(\theta)\, d\theta \tag{3.1.4a}$$

and for the case of a circular domain this reduces to

$$E_H = 2H_B[M_1Z_1 + M_2Z_2]\pi r_o^2 \tag{3.1.4b}$$

The gradients are given by

$$\frac{\partial E_H}{\partial r_o} = 4\pi r_o[M_1Z_1 + M_2Z_2]H_B \tag{3.1.5a}$$

$$\frac{\partial E_H}{\partial Z_1} = 2\pi r_o^2 M_1 H_B \tag{3.1.5b}$$

$$\frac{\partial E_H}{\partial Z_2} = 2\pi r_o^2 M_2 H_B \tag{3.1.5c}$$

$$\frac{\partial E_H}{\partial \delta} = 0 \tag{3.1.5d}$$

3.1.3 The Demagnetization Energy

This is the demagnetization energy of the bubble in a two-layer material of infinite extention.

The magnetization of an ion implanted material supporting a magnetic bubble domain is given by [1],

$$\vec{M}_s = \vec{1}_z[1-2u(r_b(\theta)-r)][M_1u(z)u(z_1-z)+M_2u(-z)u(z_2+z)] \tag{3.1.6}$$

where z is measured from the interface between the ion implanted and nonimplanted regions (Fig. 3.3), and u(x) is the unit step function defined in Eqn. (2.4.1c).

The magnetic pole density is given by

$$\vec{\nabla}\cdot\vec{M}_2 = [1-2u(r_b(\theta)-r)][-M_1u(z)\delta(z_1-z)+M_1\delta(z)u(z_1-z)-M_2\delta(z)u(z_2+z)$$

$$+M_2\delta(z_2+z)u(-z)]$$

$$= k(r_b(\theta);r)[\vec{\nabla}.\vec{M}_s(z)] \tag{3.1.7}$$

where $k(r_b(\theta);r) = 1-2u(r_b(\theta)-r)$ (3.1.8)

The total demagnetization energy is now given by [1].

$$E_D = \frac{1}{2}\int dV \int dV' \frac{(\vec{\nabla}.\vec{M})(\vec{\nabla}.\vec{M}')}{|\vec{r}-\vec{r}'|}$$

$$= \frac{1}{2}\int dV \int dV' \left\{\frac{k(r_b(\theta);r)k(r_b(\theta);r')[\vec{\nabla}.M_s(z)][\vec{\nabla}.\vec{M}_s'(z')]}{|\vec{r}-\vec{r}'|}\right. \tag{3.1.9}$$

where

$$\rho^2 = r^2+r'^2-2rr'\cos(\theta-\theta')$$

$$\text{and} \quad |\vec{r}-\vec{r}'| = \rho^2+(z-z')^2 \tag{3.1.10}$$

The change in demagnetization energy due to the magnetic domain is given by

$$E_D = \frac{1}{2}\int_0^{2\pi} d\theta \int_0^{\infty} rdr \int_0^{2\pi} d\theta' \int_0^{\infty} r'dr'[k(r_b(\theta);r)k(r_b(\theta);r')-1]$$

$$\times \int_{-\infty}^{\infty} dz \int_{-\infty}^{\infty} dz' \left\{\frac{[\vec{\nabla}.\vec{M}_s(z)][\vec{\nabla}.\vec{M}_s'(z')]}{|\vec{r}-\vec{r}'|}\right. \tag{3.1.11a}$$

$$E_D = \frac{1}{2}\int_0^{2\pi} d\theta \int_0^{2\pi} d\theta' \int_0^{\infty} rdr \int_0^{\infty} r'dr'[kk'-1]\left\{\frac{[M_1^2+M_2^2+(M_1-M_2)^2]}{\rho}\right.$$

$$- \frac{2M_1(M_1-M_2)}{[\rho^2+z_1^2]^{1/2}} + \frac{2M_2(M_1-M_2)}{[\rho^2+z_2^2]^{1/2}} - \frac{2M_1M_2}{[\rho^2+(z_1+z_2)^2]^{1/2}} \}$$

$$= \int_0^{2\pi} d\theta \int_0^{2\pi} d\theta' \int_0^{\infty} rdr \int_0^{\infty} r'dr' [kk'-1] \{-M_1(M_1-M_2)[\frac{1}{[\rho^2+z_1^2]^{1/2}} - \frac{1}{\rho}]$$

$$+M_2(M_1-M_2)[\frac{1}{[\rho^2+z_2^2]^{1/2}} - \frac{1}{\rho}]-M_1M_2[\frac{1}{[\rho^2+(z_1+z_2)^2]^{1/2}} - \frac{1}{\rho}]\} \qquad (3.1.11b)$$

By following the steps of Thiele [1], we obtain the final expression for the demagnetization energy

$$E_D = -(2\pi)^2[z_1^3M_1(M_1-M_2)I(\frac{2r_o}{z_1})+z_2^3M_2(M_2-M_1)I(\frac{2r_o}{z_2})$$

$$+(z_1+z_2)^3M_1M_2I(\frac{2r_o}{z_1+z_2})] \qquad (3.1.12a)$$

where $I(x)$ is given by [1]

$$I(x) = -\frac{2x}{3\pi}[x^2+(1+\frac{1}{x^2})^{1/2}\{(1-x^2)E\ell^{(1)}(\frac{x^2}{1-x^2})-E\ell^{(2)}(\frac{x^2}{1-x^2})\}] \qquad (3.1.12b)$$

and $E\ell^{(1)}$ and $E\ell^{(2)}$ are the elliptic integrals of the first and second kinds, respectively.

The demagnetization energy gradients are given by

$$\frac{\partial E_D}{\partial r_o} = -8\pi^2\left[z_1^2 M_1(M_1-M_2)F\left(\frac{2r_o}{z_1}\right)+z_2^2 M_2(M_2-M_1)F\left(\frac{2r_o}{z_2}\right)+(z_1+z_2)^2 M_1 M_2 F\left(\frac{2r_o}{z_1+z_2}\right)\right] \tag{3.1.13a}$$

$$\frac{\partial E_D}{\partial z_1} = -4\pi^2\left[M_1(M_1-M_2)\left\{3z_1^2 I\left(\frac{2r_o}{z_1}\right)-2z_1 r_o F\left(\frac{2r_o}{z_1}\right)\right\}\right.$$
$$\left.+M_1 M_2\left\{3(z_1+z_2)^2 I\left(\frac{2r_o}{z_1+z_2}\right)-2(z_1+z_2)r_o F\left(\frac{2r_o}{z_1+z_2}\right)\right\}\right] \tag{3.1.13b}$$

$$\frac{\partial E_D}{\partial z_2} = -4\pi^2\left[M_2(M_2-M_1)\left\{3z_2^2 I\left(\frac{2r_o}{z_2}\right)-2z_2 r_o F\left(\frac{2r_o}{z_2}\right)\right\}\right.$$
$$\left.+M_1 M_2\left\{3(z_1+z_2)^2 I\left(\frac{2r_o}{z_1+z_2}\right)-2(z_1+z_2)r_o F\left(\frac{2r_o}{z_1+z_2}\right)\right\}\right] \tag{3.1.13c}$$

and

$$\frac{\partial E_D}{\partial \delta} = 0 \tag{3.1.13d}$$

where

$$F(x) = \frac{2x^2}{\pi}\left\{\int_0^{\pi/2}\left[x^{-2}+\sin^2\phi\right]^{1/2}d\phi-1\right\} \tag{3.1.13e}$$

3.1.4 The Channel Width Demagnetization Energies

As in Ch. 2 (Sec. 2.4.1) in formulating the demagnetization energy we effectively assumed that the whole surface of the substrate was ion bombarded giving us a two-layer material, but actually only a strip of width 2w is ion implanted to a depth D, and so we must add a contribution as in (Ch. 2. Sec. 2.4.2) to correct for the finite width of the ion implanted channel. The channel width demagnetizing energy is expressed in the form

$$E_{CH} = -2(M_1-M_2)\left[M_2G(w;D-z_2)+(M_1-M_2)G(w;D)-M_1G(w;z_1+D)\right.$$

$$\left.-M_2G(w;z_2)+(M_1-M_2)G(w;0)+M_1G(w;z_1)\right] \qquad (3.1.14)$$

where

$$G(w;z_i) = \int_{-\infty}^{\infty} dx\left\{\int_{w}^{\infty} dy \int_{S} dx_o dy_o\left[\frac{1}{\rho}-\frac{1}{[\rho^2+z_i^2]^{1/2}}\right]\right.$$

$$\left.+\int_{-\infty}^{-w} dy \int_{S} dx_o dy_o\left[\frac{1}{\rho}-\frac{1}{[\rho^2+z_i^2]^{1/2}}\right]\right\} \qquad (3.1.15a)$$

and (x_o,y_o) are the coordinates of a point in the domain, (x,y) are the coordinates of a point outside the channel, and

$$\rho^2 = (x-x_o)^2+(y-y_o)^2 \qquad (3.1.15b)$$

For a circular magnetic domain (3.1.15a) reduces to

$$G(w,z_i) = \int_0^{2\pi} d\theta \int_0^{r_o} rdr \left\{ \int_w^{\infty} dy \left[\ln\left(\frac{(x+[x^2+(y-y_o)^2+z_i^2]^{1/2})(|y-y_o|)}{(x+[x^2+(y-y_o)^2]^{1/2})([z_i^2+(y-y_o)^2]^{1/2})} \right) \right|_{-\infty}^{\infty} \right.$$

$$\left. + \int_{-\infty}^{w} dy \left[\ln\left(\frac{(x+[x^2+(y-y_o)^2+z_i^2]^{1/2})(|y-y_o|)}{(x+[x^2+(y-y_o)^2]^{1/2})([z_i^2+(y-y_o)^2]^{1/2})} \right) \right|_{-\infty}^{\infty} \right\}$$

$$= \int_0^{2\pi} d\theta \int_0^{r_o} rdr \{ (w-y_o)\ln(1+\frac{z_i^2}{(w-y_o)^2}) + (w+y_o)\ln(1+\frac{z_i^2}{(w+y_o)^2})$$

$$+2z_i[\tan^{-1}(\frac{w-y_o}{z_i}) + \tan^{-1}(\frac{w+y_o}{z_i})] - 2\pi z_i \} \qquad (3.1.16)$$

where

$$y_o = \delta + r_o\cos\theta \qquad (3.1.17)$$

We now make the following substitutions

$$\left.\begin{aligned} \xi &= w-y_o = w-\delta-r_o\cos\theta \quad ; \quad c_1 = -w+\delta \\ \eta &= w+y_o = w+\delta+r_o\cos\theta \quad ; \quad c_2 = -w-\delta \end{aligned}\right\} \tag{3.1.18}$$

Substituting (3.1.18) into (3.1.16) gives

$$G(w;z_i) = \int_0^{2\pi} d\theta \left\{ \int_{r=0}^{r=r_o} (c_1+\xi)\,d\xi\left[\xi\ln\left(\frac{z_i^2}{\xi^2}\right)+2z_i\tan^{-1}\left(\frac{\xi}{z_i}\right)-\pi z_i\right]\right.$$

$$\left. + \int_{r=0}^{r=r_o} (c_2+\eta)\,d\eta\left[\eta\ln\left(1+\frac{z_i^2}{\eta^2}\right)+2z_i\tan^{-1}\left(\frac{\eta}{z_i}\right)-\pi z_i\right]\right\}/\cos^2\theta$$

$$= \int_0^{2\pi} d\theta\sec^2\theta\left(\left\{\left(\frac{\xi^3}{3}+\frac{c_1\xi^2}{2}\right)\ln\left(1+\frac{z_i^2}{\xi^2}\right)+2z_i\left(\frac{\xi^2}{2}+c_1\xi\right)\tan^{-1}\left(\frac{\xi}{z_i}\right)\right.\right.$$

$$\left. - 2z_i^2\left[\frac{\xi}{6}+\frac{c_1}{4}\ln\left(1+\frac{\xi^2}{z_i^2}\right)-\frac{z_i}{6}\tan^{-1}\left(\frac{\xi}{z_i}\right)\right]-\frac{\pi z_i}{2}(\xi+c_1)^2\right\}\Bigg|_{r=0}^{r=r_o}$$

$$+\left\{\left(\frac{\eta^3}{3}+c_2\frac{\eta^2}{2}\right)\ln\left(1+\frac{z_i^2}{\eta^2}\right)+2z_i\left(\frac{\eta^2}{2}+c_2\eta\right)\tan^{-1}\left(\frac{\eta}{z_i}\right)\right.$$

$$\left.\left. -2z_i^2\left[\frac{\eta}{6}+\frac{c_2}{4}\ln\left(1+\frac{\eta^2}{z_i^2}\right)-\frac{z_i}{6}\tan^{-1}\left(\frac{\eta}{z_i}\right)\right]-\frac{\pi z_i}{2}(\eta+c_2)^2\right\}\Bigg|_{r=0}^{r=r_o}\right) \tag{3.1.19}$$

Combining (3.1.14) and (3.1.19) gives the channel width demagnetization energy.

The gradients of the channel width demagnetization energy with respect to a variable v_i are given by

$$\frac{\partial E_{CH}}{\partial v_i} = -2(M_1-M_2)\Big[M_2 \frac{\partial G}{\partial v_i}(w,D-z_2)+(M_1-M_2)\frac{\partial G}{\partial v_i}(w,D)$$

$$-M_1 \frac{\partial G}{\partial v_i}(w,z_1+D)-M_2 \frac{\partial}{\partial v_i}G(w,z_2)+(M_1-M_2)\frac{\partial G}{\partial v_i}(w;0)+M_1 \frac{\partial}{\partial v_i} G(w;z_1)\Big] \tag{3.1.20}$$

The gradients $\frac{\partial G}{\partial v_i}(w,z_i)$ are given by

$$\frac{\partial G}{\partial r_o}(w,z_i) = \int_0^{2\pi} d\theta\Big[-r_o\{(w-\delta-r_o\cos\theta)\ln\Big(1+\frac{z_i^2}{(w-\delta-r_o\cos\theta)^2}\Big)$$

$$+2z_i\tan^{-1}\Big(\frac{w-\delta-r_o\cos\theta}{z_i}\Big)-\pi z_i\}$$

$$-r_o\{(w+\delta+r_o\cos\theta)\ln\Big(1+\frac{z_i^2}{(w+\delta+r_o\cos\theta)^2}\Big)+2z_i\tan^{-1}\Big(\frac{w+\delta+r_o\cos\theta}{z_i}\Big)$$

$$-\pi z_i\}\Big] \tag{3.1.21a}$$

$$\frac{\partial G}{\partial z_j}(w;z_i) = \left(\frac{\partial z_i}{\partial z_j}\right) \int_0^{2\pi} d\theta \sec^2\theta \left\{ \int_0^{r_o} (\xi+c_1)\, d\xi \left[2\tan^{-1}\left(\frac{\xi}{z_i}\right)-\pi\right] \right.$$

$$\left. + \int_0^{r_o} (\eta+c_2)\, d\eta \left[2\tan^{-1}\left(\frac{\eta}{z_i}\right)-\pi\right] \right\}$$

$$= \left(\frac{\partial z_i}{\partial z_j}\right) \int_0^{2\pi} d\theta \sec^2\theta \left(\left|_{r=0}^{r=r_o} \left\{ (\xi^2+2c_1\xi)\left(2\tan^{-1}\left(\frac{\xi}{z_i}\right)-\pi\right) - z_i\left(\xi+c_1 \ln\left(1+\frac{\xi^2}{z_i^2}\right)\right.\right.\right.$$

$$\left. - z_i \tan^{-1}\left(\frac{\xi}{z_i}\right) \right\}$$

$$\left. + \left|_{r=0}^{r=r_o} \left\{ (\eta^2+2c_2\eta)\left(2\tan^{-1}\left(\frac{\eta}{z_i}\right)-\pi\right) - z_i\left(\eta+c_2 \ln\left(1+\frac{\eta^2}{z_i^2}\right) - z_i \tan^{-1}\left(\frac{\eta}{z_i}\right)\right.\right\} \right)$$

(3.1.21b)

where δ_{ij} is the Kronecker delta symbol

$$\frac{\partial G}{\partial \delta}(w;z_i) = \int_0^{2\pi} d\theta \sec^2\theta \left(\left\{ (\xi+c_1)\left[\xi \ln\left(1+\frac{z_i^2}{\xi^2}\right)+2z_i \tan^{-1}\left(\frac{\xi}{z_i}\right)\right]\right.\right.$$

$$\left. + \left[\frac{\xi^2}{2}\ln\left(1+\frac{z_i^2}{\xi^2}\right)+2z_i\,\xi \tan^{-1}\left(\frac{\xi}{z_i}\right) - \frac{z_i^2}{2}\ln\left(1+\frac{\xi^2}{z_i^2}\right)\right]\right\} \Bigg|_{r=0}^{r=r_o}$$

$$+ \left\{ (\eta+c_2)\left[\eta \ln\left(1+\frac{z_i^2}{\eta^2}\right)+2z_i \tan^{-1}\left(\frac{\eta}{z_i}\right)\right]\right.$$

$$+\left[\frac{\eta^2}{2}\ln\left(1+\frac{z_i^2}{\eta^2}\right)+2z_i\eta\tan^{-1}\left(\frac{\eta}{z_i}\right)-\frac{z_i^2}{2}\ln\left(1+\frac{\eta^2}{z_i^2}\right)\right]\Bigg\}\Bigg|_{r=0}^{r=r_o}\Bigg) \qquad (3.1.21c)$$

Combining (3.1.20) and (3.1.21) yields the channel-width demagnetization energy gradients.

3.1.5 Channel Wall Induced Pole Energy

This is the energy due to the interaction between the circular domain and the poles on the channel walls, induced by the empty channel and the bubble domain.

The channel wall energy is given by $E_{cw}=E_{cw1}+E_{cw2}$, where E_{cwk} is the channel wall induced pole energy contribution of the kth wall (k=1,2).

Let us define $R_k = (w+(2k-3)\delta)/|\cos\phi|$, and $x_k=(w+(2k-3)\delta)\tan\phi$, where ϕ is the angle of the location of a point on the channel wall with respect to the cylindrical co-ordinates of the domain (Fig. 3.2), and

$$\left.\begin{aligned}\rho_1^2 &= r^2+R_k^2 - 2rR_k\cos(\theta-\phi)\\ \rho_2^2 &= r^2+R_k^2 - 2rR_k\cos(\theta+\phi)\end{aligned}\right\} \qquad (3.1.22)$$

where (r,θ) is a point inside the bubble domain.

The channel wall induced pole energy of the kth wall is given by

$$E_{cwk} = \int_0^{\pi/2} d\phi \sec^2\phi \int_0^D dz(w+(2k-3)\delta)P_k(\phi,z) \int_0^{2\pi} d\theta \int_0^{r_o} r dr$$

$$\times\ 2\Bigg[(M_1-M_2)\left\{\frac{1}{[\rho_1^2+z^2]^{1/2}} + \frac{1}{[\rho_2^2+z^2]^{1/2}}\right\} - M_1\left\{\frac{1}{[\rho_1^2+(z_1-z)^2]^{1/2}}\right.$$

$$\left. - \frac{1}{[\rho_2^2+(z_1-z)^2]^{1/2}}\right\} + M_2\left\{\frac{1}{[\rho_1^2+(z_2-z)^2]^{1/2}} - \frac{1}{[\rho_2^2+(z_2-z)^2]^{1/2}}\right\}\Bigg]$$

$$= \int_0^{\pi/2} d\phi \sec^2\phi \int_0^D dz\ 2(w+(2k-3)\delta)P_k(\phi,z)Q_k(\phi,z) \qquad (3.1.23)$$

where

$$Q_k(\phi,z) = 2\int_0^{2\pi} d\theta \sum_{i=1}^{3} M_i^*\{(r_o^2+R_k^2-2r_oR_k\cos(\theta-\phi)+(z-z_i)^2)^{1/2}$$

$$-(R_k^2+(z-z_i)^2)^{1/2}+(r_o^2+R_k^2-2r_oR_k\cos(\theta+\phi)+(z-z_i)^2)^{1/2}-(R_k^2+(z-z_i)^2)^{1/2}$$

$$-R_k\cos(\theta-\phi)\,\ell n\left(\frac{r_o-R_k\cos(\theta-\phi)+[r_o^2+R_k^2-2r_oR_k\cos(\theta-\phi)+(z-z_i)^2]^{1/2}}{-R_k\cos(\theta-\phi)+[R_k^2+(z-z_i)^2]^{1/2}}\right)$$

$$-R_k\cos(\theta+\phi)\,\ell n\left(\frac{r_o-R_k\cos(\theta+\phi)+[r_o^2+R_k^2-2r_oR_k\cos(\theta+\phi)+(z-z_1)^2]^{1/2}}{-R_k\cos(\theta+\phi)+[R_k^2+(z-z_i)^2]^{1/2}}\right)\Bigg\} \qquad (3.1.24)$$

where $M_1^*=M_1$, $M_2^*=M_2$, $M_3^*=M_1-M_2$, $z_3=0$

By differentiating (3.1.23), the channel wall induced pole energy gradients are found to be

$$\frac{\partial E_{cwk}}{\partial r_o} = \int_0^{\pi/2} d\phi \sec^2\phi \int_0^D dz\,(w+(2k-3)\delta)\left[P_k(\phi,z)\frac{\partial Q_k(\phi,z)}{\partial r_o} + Q_k(\phi,z)\frac{\partial P_k(\phi,z)}{\partial z_j}\right] \tag{3.1.25a}$$

$$\frac{\partial E_{cwk}}{\partial z_j} = \int_0^{\pi/2} d\phi \sec^2\phi \int_0^D dz\,(w+(2k-3)\delta)\left[P_k(\phi,z)\frac{\partial Q_k(\phi,z)}{\partial z_j} + Q_k(\phi,z)\frac{\partial P_k(\phi,z)}{\partial z_j}\right] \tag{3.1.25b}$$

$$\frac{\partial E_{cwk}}{\partial \delta} = \int_0^{\pi/2} d\phi \sec^2\phi \int_0^D dz\{(2k-3)P_k(\phi,z)Q_k(\phi,z)+(w+(2k-3)\delta)\left[P_k(\phi,z)\frac{\partial Q_k(\phi,z)}{\partial \delta}\right.$$

$$\left. + Q_k(\phi,z)\frac{\partial}{\partial \delta} P_k(\phi,z)\right]\} \tag{3.1.25c}$$

While the gradients $\frac{\partial P_k(\phi,z)}{\partial r_o}$ and $\frac{\partial P_k(\phi,z)}{\partial \delta}$ have already been worked out in (2.3.7), (2.3.8), (2.3.10), $\frac{\partial P_k(\phi,z)}{\partial z}$ can be worked out easily by direct differentiation of (2.3.6).

The gradients $\frac{\partial Q_k(\phi,z)}{\partial v_i}$ are given by

$$\frac{\partial Q_k(\phi,z)}{\partial r_o} = 2\int_0^{2\pi} d\theta \sum_{i=1}^{3} M_i^*\{(r_o^2+R_k^2-2r_oR_k\cos(\theta-\phi)+(z-z_i)^2)^{-1/2}$$

$$+(r_o^2+R_k^2-2r_oR_k\cos(\theta+\phi)+(z-z_i)^2)^{-1/2}\} \qquad (3.1.26a)$$

$$\frac{\partial Q_k(\phi,z)}{\partial \delta} = 2\int_0^{2\pi} d\theta \sum_{i=1}^{3} M_i^*\left(\frac{\partial R_k}{\partial \delta}\right)\{\frac{R_k-r_o\cos(\theta-\phi)}{[r_o^2+R_k^2-2r_oR_k\cos(\theta-\phi)+(z-z_i)^2]^{1/2}}$$

$$+\frac{R_k-r_o\cos(\theta+\phi)}{[r_o^2+R_k^2-2r_oR_k\cos(\theta+\phi)+(z-z_i)^2]^{1/2}} - \frac{2R_k}{[R_k^2+(z-z_i)^2]^{1/2}}$$

$$-\cos(\theta-\phi)\,\ell n\left(\frac{r_o-R_k\cos(\theta-\phi)+[r_o^2+R_k^2-2r_oR_k\cos(\theta-\phi)+(z-z_i)^2]^{1/2}}{-R_k\cos(\theta-\phi)+[R^2{}_k+(z-z_i)^2]^{1/2}}\right)$$

$$-\cos(\theta+\phi)\,\ell n\left(\frac{r_o-R_k\cos(\theta+\phi)+[r_o^2+R_k^2-2r_oR_k\cos(\theta+\phi)+(z_i-z)^2]^{1/2}}{-R_k\cos(\theta+\phi)+[R_k^2+(z-z_i)^2]^{1/2}}\right)$$

$$-R_k\cos(\theta-\phi)\left[\frac{-\cos(\theta-\phi)+\dfrac{R_k-r_o\cos(\theta-\phi)}{[r_o^2+R_k^2-2r_oR_k\cos(\theta-\phi)+(z-z_i)^2]^{1/2}}}{r_o-R_k\cos(\theta-\phi)+[r_o^2+R_k^2-2r_oR_k\cos(\theta-\phi)+(z-z_i)^2]^{1/2}}\right.$$

$$- \frac{-\cos(\theta-\phi) + \dfrac{R_k}{[R_k^2+(z-z_i)^2]^{1/2}}}{-R_k\cos(\theta-\phi)+[R_k^2+(z-z_i)^2]^{1/2}} \Bigg]$$

$$-R_k\cos(\theta+\phi)\Bigg[\frac{-\cos(\theta+\phi) + \dfrac{R_k-r_o\cos(\theta+\phi)}{[r_o^2+R_k^2-2r_oR_k\cos(\theta+\phi)+(z-z_i)^2]^{1/2}}}{r_o-R_k\cos(\theta+\phi)+[r_o^2R_k^2-2r_oR_k\cos(\theta+\phi)+(z-z_i)^2]^{1/2}}$$

$$- \frac{-\cos(\theta+\phi) + \dfrac{R_k}{[R_k^2+(z-z_i)^2]^{1/2}}}{-R_k\cos(\theta+\phi)+[R_k^2+(z-z_i)^2]^{1/2}} \Bigg]\Bigg\} \qquad (3.1.26b)$$

$$\frac{\partial Q_k(\phi,z)}{\partial z_j} = 2\int_0^{2\pi} d\theta \sum_{i=1}^{3} M_i^*(z_i-z)\delta_{ij}\{+[r_o^2+R_k^2-2r_oR_k\cos(\theta-\phi)+(z-z_i)^2]^{-1/2}$$

$$-2[R_k^2+(z_i-z)^2]^{-1/2}+[r_o^2+R_k^2-2r_oR_k\cos(\theta+\phi)+(z-z_i)^2]^{-1/2}$$

$$+\frac{R_k\cos(\theta-\phi)}{[R_k^2\sin^2(\theta-\phi)+(z-z_i)^2]}\Bigg(\frac{r_o-R_k\cos(\theta-\phi)}{[r_o^2+R_k^2-2r_oR_k\cos(\theta-\phi)+(z-z_i)^2]^{1/2}}$$

$$+ \frac{R_k \cos(\theta-\phi)}{[R_k^2+(z-z_i)^2]^{1/2}} \Bigg)$$

$$+ \frac{R_k \cos(\theta+\phi)}{[R_k^2 \sin^2(\theta+\phi)+(z-z_i)^2]} \Bigg(\frac{r_o - R_k \cos(\theta+\phi)}{[r_o^2+R_k^2-2r_o R_k \cos(\theta+\phi)+(z-z_i)^2]^{1/2}}$$

$$+ \frac{R_k \cos(\theta+\phi)}{[R_k^2+(z-z_i)^2]^{1/2}} \Bigg) \Bigg\} \qquad (3.1.26c)$$

Combining (3.1.25) and (3.1.26) leads to the channel wall induced pole gradients.

3.2 Problem Solution

Once again we have the nonlinear bubble domain energy functional (3.1.1) and its gradients with respect to the assumed variables and we want to minimize E_T subject to the constraints that r_o, z_1, $|z_2|$ and δ are all positive real numbers and that

$$|\delta+r_o| \leq w \qquad (3.2.1)$$

$$z_2 < T-D \qquad (3.2.2)$$

$$z_1 < D \qquad (3.2.3)$$

The same numerical techniques used to solve for the deformable domain wholly situated inside an ion implanted could be used here. The problem presented in this chapter has not been, however, implemented and tested and is given here only for the sake of completeness of the theoretical investigation.

3.3. Remarks

Although there is an apparent similarity between the problem of Ch. 2 and Ch. 3, a transition from the equations of Ch. 2 to the equations of Ch. 3 is not obvious. This argument was borne in mind when making the decision on the inclusion of this chapter in the thesis.

Futhermore, the material of Ch. 2 and Ch. 3 outlines the approach to an even more general and more practical problem, that is, the stability of a noncircular, noncylindrical magnetic bubble of variable penetration (in both the implanted and the nonimplanted regions), and located within a channel of any geometry.

As an extension of the approach presented here, one could attempt to model the nonlinear functionals, thus arriving at a second level of approximation in order to obtain faster solutions.

CHAPTER 4

NUMERICAL RESULTS FOR A STRAIGHT ION IMPLANTED CHANNEL

The formulation for the generally deformable magnetic domain wholly situated inside an ion implanted channel, derived in Chapter 2, has been programmed for the special case of the straight channel with parallel channel-walls. The reasons for such a choice are two-fold. First, the straight channel, being the simplest possible, should clearly show the expected stable location and geometry of the domain due to the basic physical mechanisms incorporated in the proposed model in the clearest possible way, without introducing the extra geometric effects arising from a channel-width modulation. Second comes the fact that a thorough and exhaustive set of high-cost computer runs is justifiable only if the complete problem of the actual width modulated channel and the driving fields are combined together for the investigation of a real device such as the "channel bar propagating circuit" proposed by E. Della Torre and W. Kinsner [15]. A brief description of the actual program is given in Appendix 2, with the complete program listing.

4.1 Parameters

To test the proposed model, the material chosen for investigation was assumed to have the following parameters before ion implantation: the saturation magnetization M_1=18.0emu, the wall energy density σ_1=0.36 erg/cm^2, and the quality factor q_1=6.0. After ion implantation, the material parameters were assumed to change to M_2=17.8 emu, σ_2=0.36, erg/cm^2, and q_2=5.0.

The thickness of the material substrate, T, was 6 microns, the implanted channel depth, D, was taken as 0.6 microns and the external uniform bias field, H_B, was 100.0 Oe.

Although the chosen parameters do not belong to a specific material, the values are within the range of typical values for garnets. The changes in parameters are consistent with some experimental data [23].

4.2 Numerical Results

The diameter of a stable circular domain within a channel of infinite width was found to be $2R_o$=5.9, (R_o=2.9590429) microns.

The channels of the finite width investigated had half-widths (w) of 0.6T, T, 1.5T, and 2.0T. In all the program runs the total number of variables was five: four radial parameters and the bubble center location (δ) with respect to the channel center. The pressures and pressure gradients were computed at ten sampling points taken at

equal angular intervals. Due to the mirror symmetry about the plane passing through the domain center and normal to the channel axis, sampling points were taken for half the domain only. The induced channel wall pole densities and pole density gradients were computed at the mid-depth of the channel ($z=D/2$) and at ten points along each channel wall, the points being spread from the mirror symmetry plane to infinity with unequal intervals. All numerical integrations were done using Simpson's technique, after assuring the smooth continuity of the integrand functions.

Although the program has the facility of computing the pressures and pressure gradients for any number of radial parameters and at any number of sampling points, as well as the induced pole densities and pole density gradients at a larger number of points along the channel and at various depths, the results obtained are sufficiently representative. Increasing the number of points and variables greatly increases the already large computation time. Intermediate printouts have been obtained to study the evolution of the solution with some interesting observations that will be discussed in the next section.

The change in the magnetic domain geometry with the channel width is shown through the four Fourier coefficients (C_o, C_1, C_2 and C_3) in Table 1. The coefficients describe the approximate radial function, as well as their percentage with respect to the basic coefficient C_o which represents the average domain radius. The stable locations

TABLE 1

CHANNEL WIDTH [μm] / FOURIER COEFFICIENTS c_i[μm] c_i/c_o[%]	7.2	12.0	18.0	24.0
c_o	2.89	2.91	2.91	2.91
c_1	-7.10×10^{-2}	-11.50x10-2	-12.86×10^{-2}	-13.15×10^{-2}
c_1/c_o	-2.46	-3.95	-4.41	4.51
c_2	-9.39×10^{-3}	-6.23×10^{-3}	-6.04×10^{-3}	-6.01×10^{-3}
c_2/c_o	-0.342	-0.213	-0.207	-0.206
c_3	-1.16×10^{-4}	-2.89×10^{-4}	-3.12×10^{-4}	-3.15×10^{-4}
c_3/c_o	-0.0039	-0.0099	-0.011	-0.011
Domain Center* δ[μm]	0.504	2.86	5.92	8.92
Clearance from Channel Wall ≈ [μm]	0.28	0.36	0.32	0.30

* Obtained according to a stopping criterion when changes are less than 10^{-6} microns

of the bubble center as estimated according to the specified stopping criteria are also given in Table 1.

The relations C_1/C_o, C_2/C_o and C_3/C_o versus channel width are shown in Fig. 4.1. It is interesting to notice that all the coefficients C_1, C_2 and C_3 are negative as opposed to C_o. This is explained by the fact that as the domain approaches one of the channel walls, the pressure contribution, due to the channel width demagnetization, decreases very rapidly; this is partly balanced by a decrease in the negative domain wall pressures for the points nearest to the channel wall, this requires that the curvature of the domain should decrease for those sampling points nearest to the channel wall, and this in turn implies that the coefficients should be negative as observed.

Figure 4.1 shows an increase in the normalized odd harmonics (C_1/C_o, C_3/C_o) and a decrease in the normalized even harmonic (C_2/C_o) as the channel width increases, and they approach steady values as the width becomes very large. This behaviour is due to the fact that for a very narrow channel, although the domain may tend to be attracted by one wall or the other, due to the balance between the channel width demagnetization pressure and channel wall induced pole pressures, the other wall is still near enough to exert a counter attraction. While the odd harmonics would tend to decrease the curvature for that part of the domain nearest to the preferred channel wall at the expense of increasing it on that part of the domain

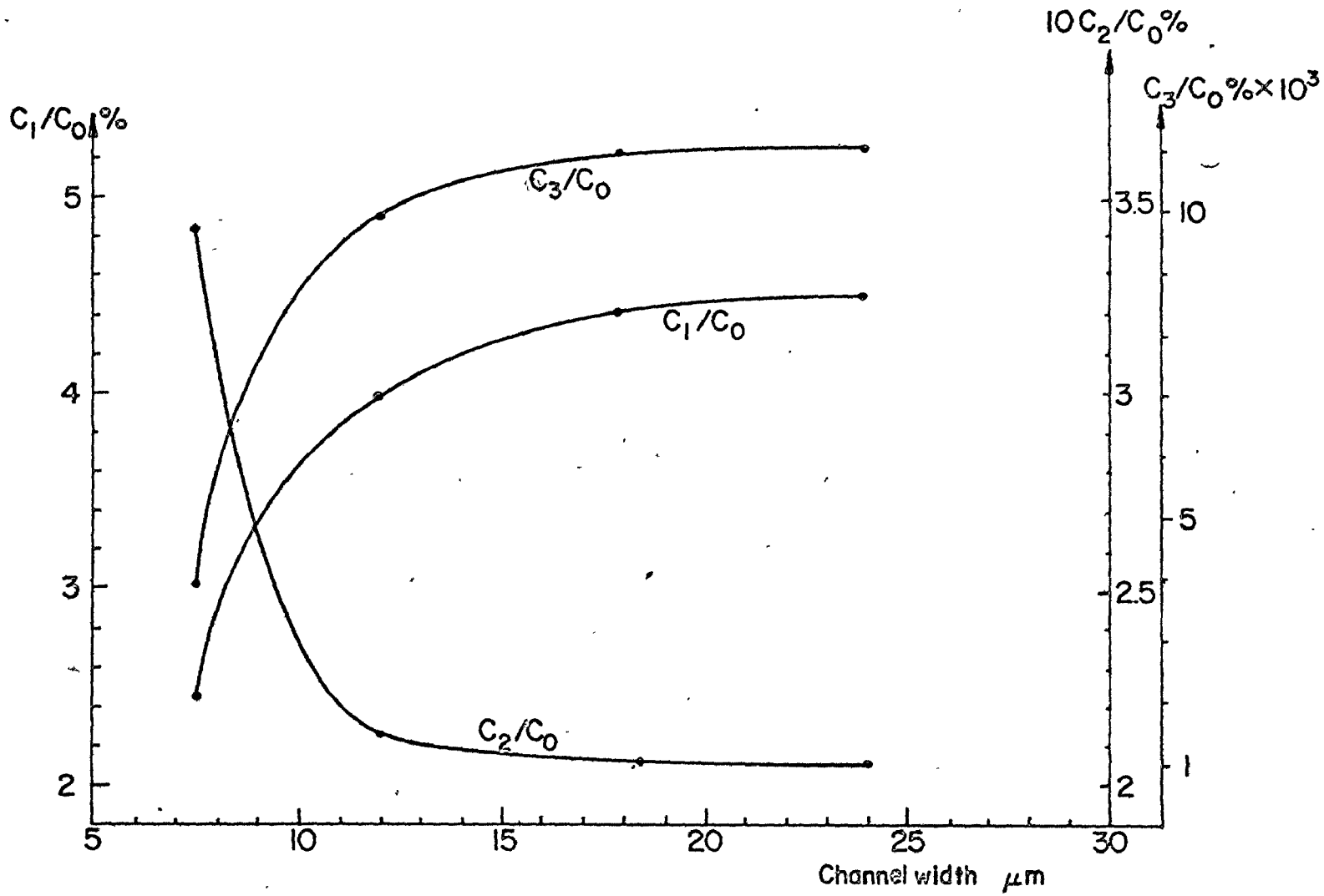

FIG. 4.1 Normalized harmonics

facing the less preferred channel wall, the even harmonics would tend to decrease the curvature of both parts of the domain walls facing the channel walls. As the channel width increases the symmetry of the pressure contributions decrease about a plane passing through the bubble axis and parallel to the xz plane, hence the compensation from the wall curvature requires that the odd harmonics increase and the even harmonics decrease to compensate more effectively for the deficient pressure contributions next to the preferred channel wall. The normalized harmonics tend to attain steady values for large channel widths as the effect of the less preferred channel wall decreases quickly and eventually becomes negligible leaving only the effect of the wall nearest to the domain to dominate

The conclusions of the above discussion are summarized in Fig. 4.2. Figure 4.2a shows three function representations of the effect of three harmonics given by

$$R''_n(\theta) = 2-\cos(n\theta) \ , \quad n = 1,2,3,... \tag{4.1a}$$

Figure 4.2b shows superposition of the contributions due to three harmonics C_1, C_2 and C_3 and $C_o/10$ taken from Table 1, for 2w=12.0 μm. This means that the figure is a polar plot of the function

$$r''_b(\theta) = r_b(\theta) - 0.9\ C_o \tag{4.1b}$$

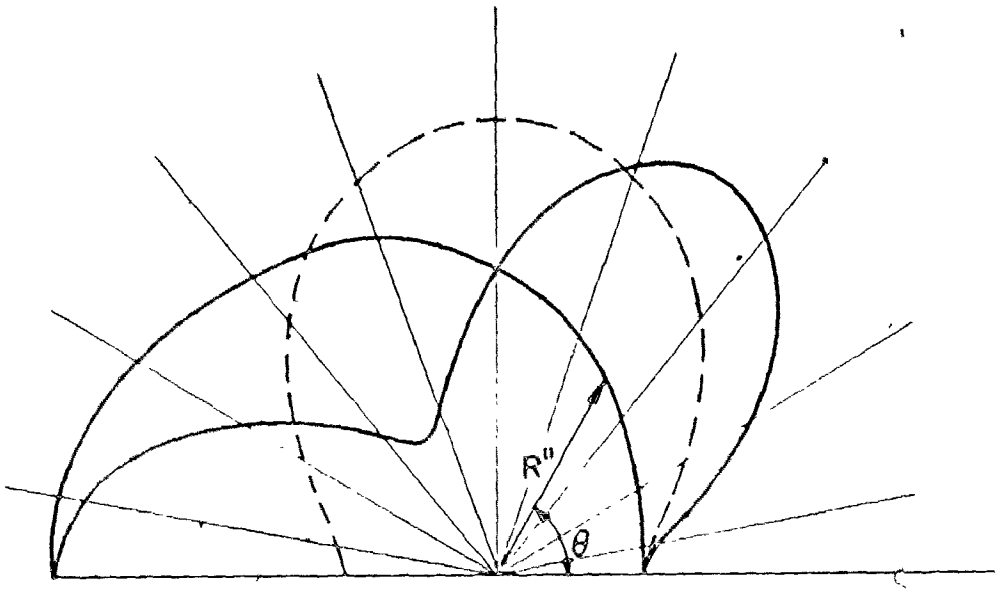

(a)

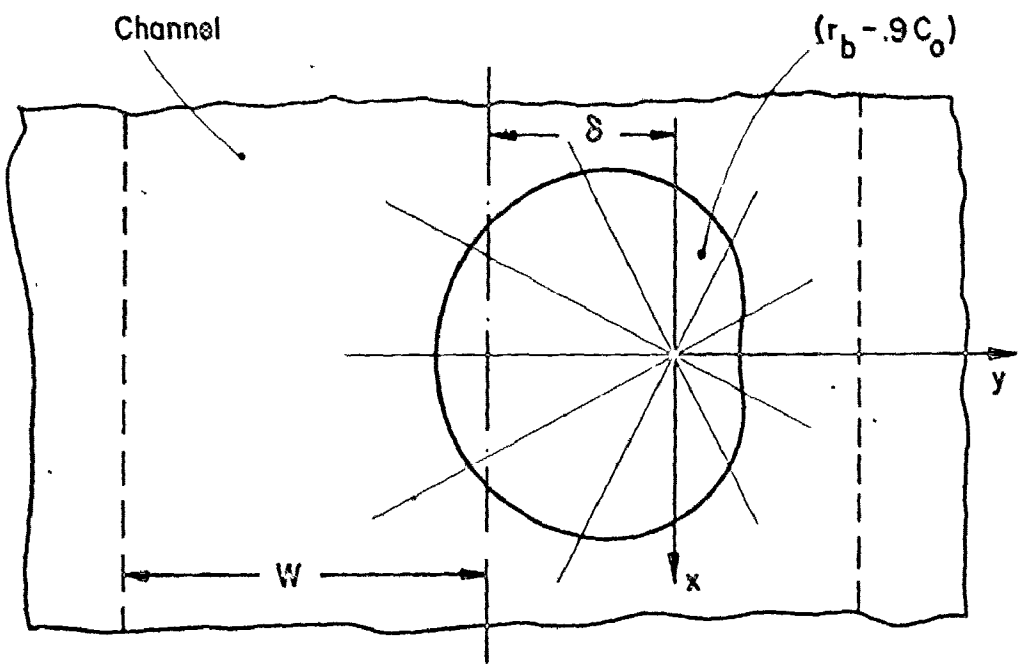

(b)

FIG. 4.2 (a) Three cylindrical harmonics and
(b) their superposition according to table 1.

This has been done to demonstrate the effect of the harmonics by effectively promoting the harmonics with respect to C_o. Notice that the radial function $r_b''(\theta)$ in Fig. 4.2b is slightly flattened on its side near the right channel wall, which is the channel wall nearest to the domain. This is consistent with the physical considerations of a bubble within a straight wall channel. It should be noticed that the deformation has been neither mentioned nor revealed by the published experimental and theoretical results. Thus, our analysis is capable of providing a deeper insight into the problem.

The channel wall induced pole densities for the channel of width 2w=12.0μm are shown in Fig. 4.3. The character of the curves is similar for all the channel widths considered. For that channel wall nearest to the bubble, the figure shows a sharp peak for the induced pole density. The induced pole density reaches its maximum where the bubble wall is closest to the channel wall and quickly falls off as one moves away from the bubble along the channel wall, then it decreases at a slower rate. The induced pole density distribution, for the channel wall further from the domain, is a smoothly decreasing function.

One can understand this behaviour, by imagining that the bubble's pole inducing field is due to some equivalent effective poles p_{il}

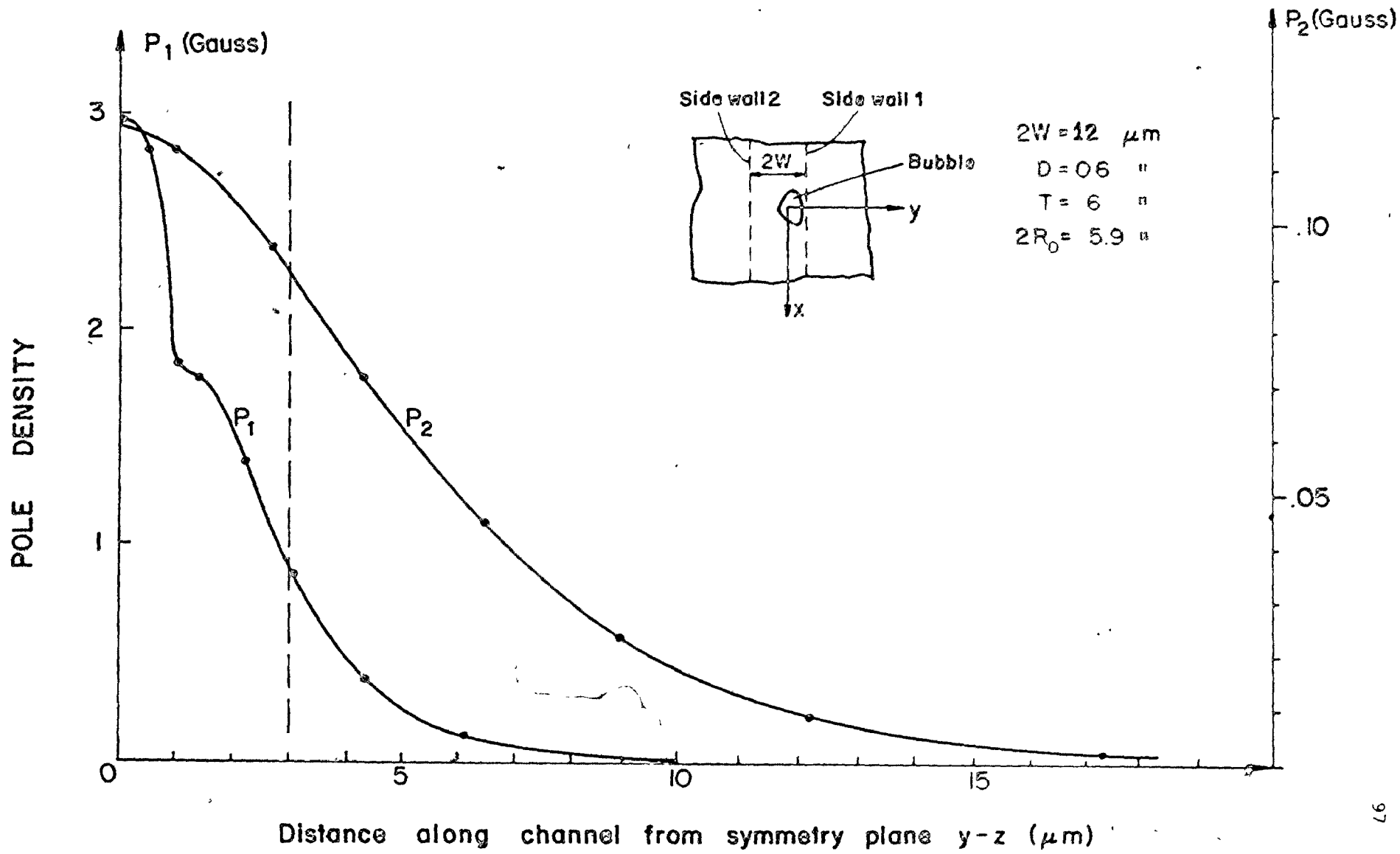

FIG. 4.3 Induced pole densities on side channel walls

localized on the bubble co-ordinate z-axis as shown in Fig. 4.4a at $-z_2, 0$, and z_1, and another set of equivalent localized poles p_{i2} in the zy plane with the same z-co-ordinates as p_{i1}. The equivalent poles p_{i2} are there to simulate the large inducing fields contributed by the bubble domain elements nearest to the wall, while the poles p_{i1} simulate the average inducing fields due to the rest of the bubble. The simulated pole inducing field contributions are shown in Fig. 4.4b, and they clearly explain the sharp peak in Fig. 4.3.

It is worth mentioning that since the sum of p_{i1} and p_{i2} is equal to the total bubble poles at the ith level, it is almost a constant, and as the bubble approaches a channel wall p_{i2} increases in magnitude and is shifted in position nearer to the channel wall, hence its inducing field contribution becomes of a larger value but if a smaller width along the channel wall length, p_{i1} on the other hand decreases. While this pole distribution should always be expected, the changes in the domain geometry may have some mild smoothing effect on the induced pole density distribution if the number of harmonics considered is large.

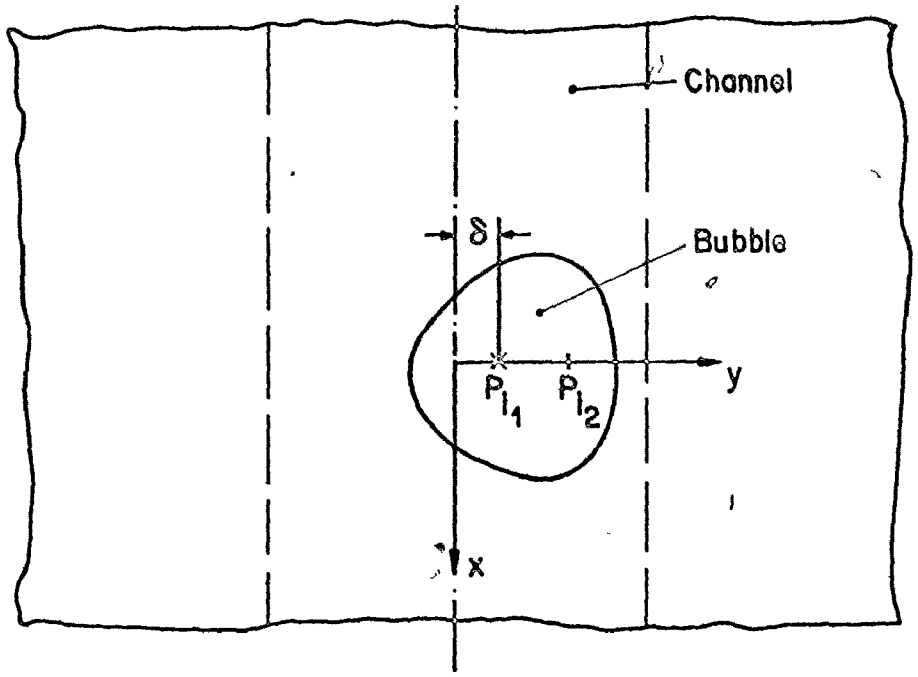

(a)

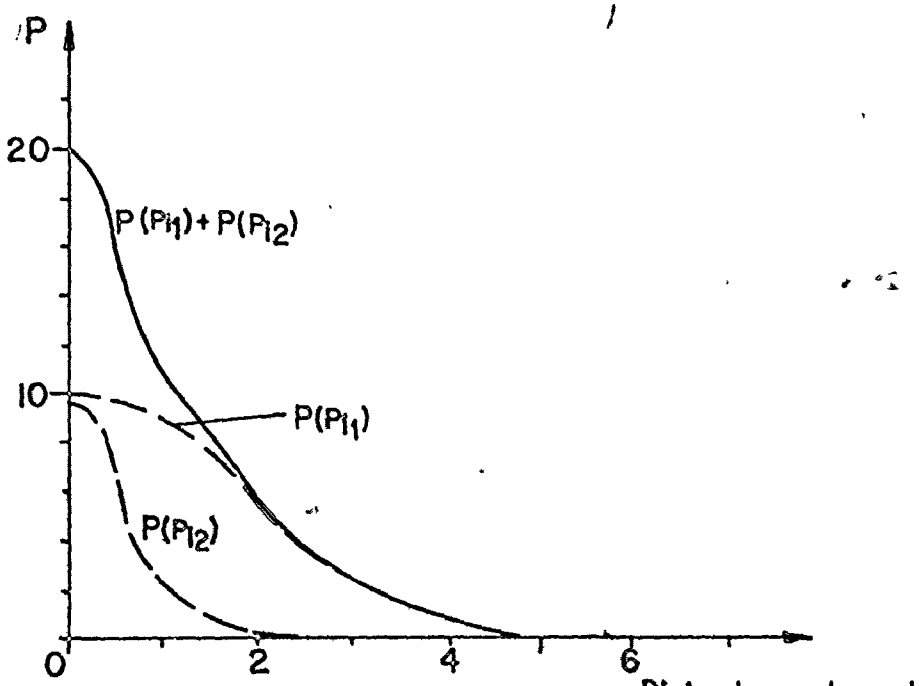

(b)

FIG.4.4 Equivalent poles within a bubble and their pole distribution on the channel side wall.

4.3 Numerical Considerations

In the course of computer runs of the program several interesting aspects were observed. A primary analysis indicates the great importance of selecting a proper starting point for a quick approach to the solution. There is the possibility of existence of either one local minimum, that would tend to settle the domain at the center of the channel, or two local minima each of which tends to attract the domain next to the channel walls. There still is the third possibility of having all three local minima simultaneously, the one at the channel center being in astable equilibrium. The minima next to the channel walls are probably very sharp and strongly localized as compared to the one at the channel center.

Since there are in general three local minima the selection of the proper starting values becomes of genuine importance since, especially for the stable strongly localized minima next to the walls, there will be a numerical tendency towards the astable minimum at the channel center.

If one assumes that all the radial parameters of the domain are lumped into one effective parameter R_{eff}, expressed as a norm, then sketches for Σp_i^2 versus the deviation of the bubble center from channel center (δ) could be drawn for various values of R_{eff} (Fig. 4.5).

To approach the required minimum next to one of the channel

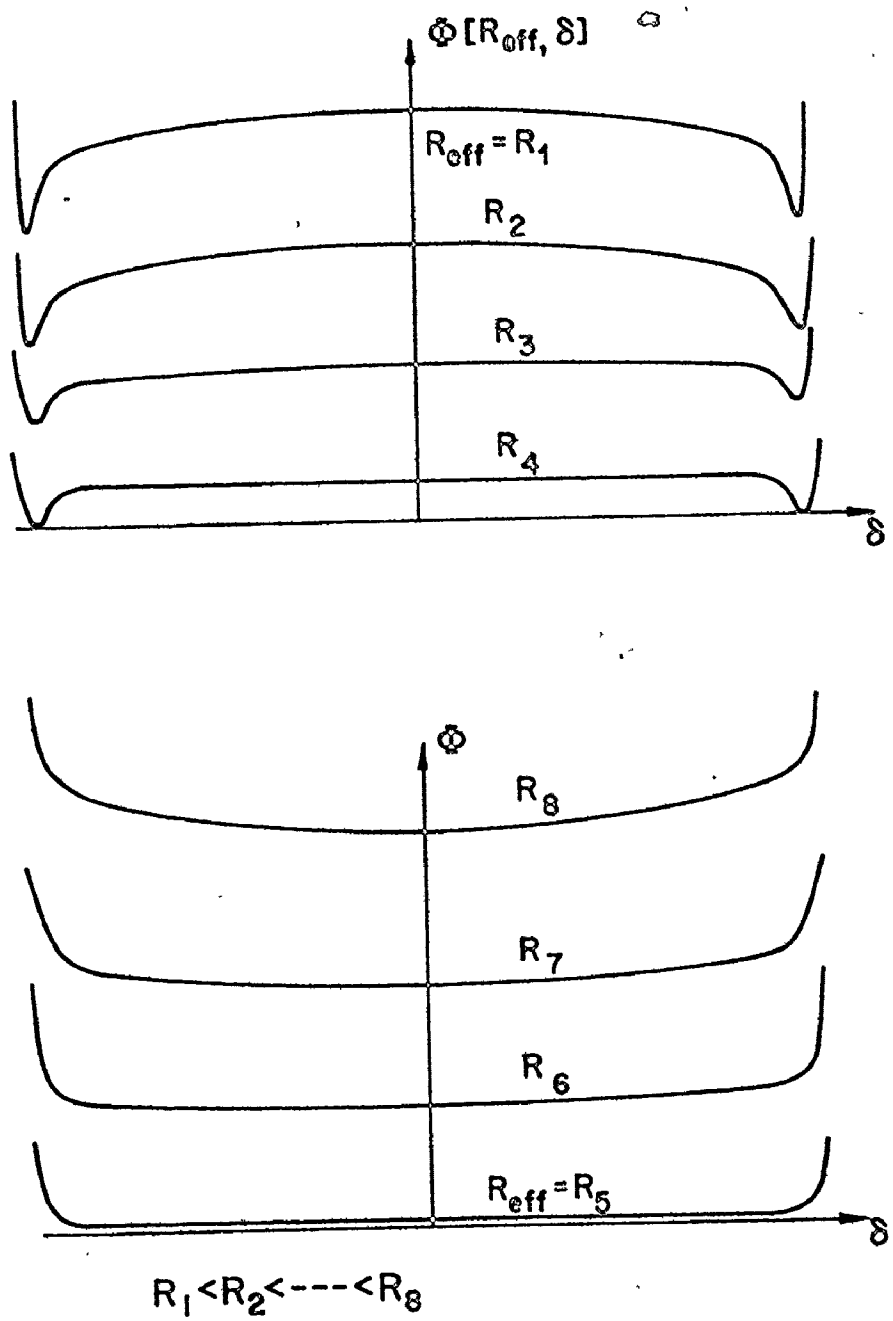

FIG. 4.5 Schematic behaviour of objective functional

walls one has to carefully select the starting point such that if a minimum exists, the gradients approach the proper minimum. This implies taking an initial radius smaller than the expected optimum c_o (e.g., $C_o \cong 0.8R_o$ the free circular domain radius), and the center of the domain as near to the channel wall as possible.

In all the program runs there was an indication that only one minimum exists, the one at the channel center, although the channel of finite width contributes a larger demagnetizing pressure (at its center) which sharply decreases as we approach the channel walls. Physically, one would expect the bubble to have a stable position next to channel wall, and indeed such is the position experimentally observed [5]. This apparent contradiction could be explained as follows: to minimize the objective Σp_i^2, the pressures should decrease (theoretically they should be zero) such that at some sampling points the pressures are positive while at others they are negative so that we obtain sort of a least squares fit about the zero pressure value. The pressures should alternate between positive and negative values with highest possible frequency (i.e., if p_i is positive, then p_{i+1} should be negative. In the case studied, the pressures near the channel wall are all negative though fluctuating, but as we move away from the wall the pressures at the sampling points turn positive and fluctuate. Since in this model, the bubble center gradients are negatively increasing as we approach the channel walls, we find that

the net objective functional gradients with respect to the bubble center location tends to push the domain towards the center rather than towards the wall. This behaviour is attributed to the insufficient number of the radial variables and consequently the number of harmonics used to describe the geometry; this makes the geometry too stiff to properly adjust to the pressures, hence the existing correlation of the pressure signs and magnitudes obtained. One may remedy this problem by creasing the number of radial variables (or harmonics) to the number of sampling points N_s or larger. A possibly more efficient way is to take the first few harmonics up to the second and then taking the rth harmonic such that N_s/r=integer, and a few such that r/N_s=integer, since these would probably be the most effective fine controls on the geometry. None of these however guarantee improved results.

When enough harmonics are taken into consideration, those large negative pressures at the points nearest to the wall, which sharply increase on its approach, would be strongly compensated with some of them turning positive.

Another observation confirming the above reasoning came when one started with a symmetric bubble situated exactly at the channel center, the domain tends to move towards the channel wall, even though the tendency is again weak due to the geometric stiffness. This confirms that the domain physically tends towards the channel wall but is deterred midway due to the geometric stiffness .

CHAPTER 5

CONCLUSIONS AND RECOMMENDATIONS

This thesis adds two new contributions to the theory of magnetic domains in thin films, as well as an endeavour to qualitatively understand the underlying physical mechanism of change of the magnetic properties as a result of ion implantation.

This is the first mathematical model describing the mutual interaction between an ion implanted channel and a magnetic domain wholly situated inside this channel. The model incorporates the resulting effects due to the change of saturation magnetization, domain wall energy density and in-plane susceptibility with the exception of the susceptibility normal to the plane.

The second contribution is a variational formulation for an approximate functional Σp_i^2 which allows for the general deformation of the magnetic domain to attain its minimum energy state. In this formulation, the pressures p_i at several sampling points on the domain boundary are calculated rather than the energy of the whole domain; the sensitivity of the former approach to the changes in parameters is greater than the latter. This is an extension of the functional approach, applied to magnetic strip domains [14], and has

been applied to magnetic bubbles.

From the formulation and numerical results presented in this thesis several conclusions can be drawn.

It can be seen that the number of harmonics required to describe the geometry of the magnetic domain should be equal or greater than the number of sampling points at which we compute the pressures; this would give the facility of altering the geometry at the various sampling points in a finer way without undesired changes at the remaining sampling points. A deficient number of harmonics would lead to a geometrically stiff function with strong correlations between the various sampling points. Increasing the number of harmonics (radial parameters) implies an increase in computation time.

The abrupt change in physical parameters from the non-implanted to the ion-implanted region incorporated in the model, lead to gradients of infinite values at the interface surfaces. This problem appeared in the cases of "channel width demagnetization" and "empty channel bases induced pole density on the channel walls". The simplest remedy is to assume a small transition region, where the parameters change smoothly (e.g., linearly), to simulate the true physical situation in which the abrupt change is not allowed thermodynamically and does not occur. In Chapter 2 the treatment of the former case is given. It is to be observed that additional parameters for the widths of the transition regions will appear.

The induced pole density distribution on the channel walls with the selected parameters do not contribute in any significant fashion to the bubble domain deformation as compared to the finite channel width demagnetization field, and could possibly be dropped if one seeks a quick estimate, since an appreciable duration of the total computation time goes to computing these pole distributions, their gradients, and their mutual corrections.

The problem of a magnetic domain wholly situated inside the ion implanted channel is slightly artificial in the sense that we have to constrain the domain to the channel by applying mathematical constraints. However, the domain should be allowed to move freely with the possibility of penetrating into the non-implanted region if it finds it more favourable. To incorporate such a possibility, the demagnetizing pressure corrections, due to the bubble penetration, and their gradients have been formulated (Appendix 1) since it is the only complicated extra factor; the remaining changes are merely changes in the parameters of the formulae in Chapter 2, with the exception of the channel wall induced poles which have a correction, similarly worked out as in Appendix 1. The new modified formulation would then lead to an unconstrained obejctive functional which is again solved as before.

It can be said that the formulation of the proposed model of a generally deformable magnetic domain inside an ion implanted (or physical) channel has been presented and tested with success, possibly for the first time where the domain is allowed to freely deform.

The channels of practical interest are those with a modulated width (or depth), this would require the modification of the "finite width demagnetization" pressure and pressure gradient contributions. The remaining pressure and gradient contributions would remain unaltered, except for the wall induced pole densities and their gradients which would have to take into account the projection of the pole inducing field projections along the normal to the channel wall which vary along the channel.

If one assumes a semi-infinite width modulated channel (neglecting end effects), a proposed way of describing the channel geometry is to expand the channel width in a harmonic series along the channel length, same as the domain. This would give the extra facility for an optimization of the channel geometry. A further extension might be a combination of the modulated channel with the driving fields and examining the propagation and deformation of the domain

It is my belief and hope that this investigation would be the base for further theoretical and experimental investigation of the problem and a possible guide to the methods of its analysis.

REFERENCES

1. A.A. Thiele, "Theory of Static Stability of Cylindrical Domains in Uniaxial Platelets", J. Appl. Phys., Vol. 41, No. 3, 1970, pp. 1139-1145.
2. W.J. Tabor, A.H. Bobeck, G.P. Vella-Coleiro and A. Rosencwaig, "A New Type of Cylindrical Magnetic Domain (Bubble Isomers)", BSTJ , Vol. 51, No. 6, 1972, pp. 1427-1431.
3. A.H. Bobeck, S.L. Blank and H.J. Levinstein, "Multilayer Garnet Films for Hard Bubble Supression", AIP Conf. Proc., No. 10, Vol. 1, 1972, pp. 498-503.
4. A. Rosencwaig, "The Effect of a Second Magnetic Layer on Hard Bubbles", BSTJ, Vol. 51, No. 6, 1972, pp. 1440-1444.
5. R. Wolfe and J.C. North, "Supression of Hard Bubbles in Magnetic Garnet Films by Ion Implantation", BSTJ, Vol. 51, No. 6, 1972, pp. 1436-1440.
6. P. Chaudhari, J.J. Cuomo, R.J. Gambino, "Amorphous Metallic Films for Bubble Domain Applications", IBM Journal Res. & Dev., Vol. 17, 1972, pp. 66-68.
7. H. Callen, "Growth Induced Anisotropy by Preferential Site Ordering in Garnet Crystals", Appl. Phys. Lett., Vol. 18, No. 7, 1971, pp. 931-938.

8. G.S. Almasi, E.A. Giess, R.J. Hendel, G.E. Keefe, Y.S. Lin, and M. Slusarczuk, "Bubble domain Propagation Mechanism in Ion Implanted Structures", AIP Conf. Proc., Vol. 24, 1974, pp. 630-634.

9. G.S. Almasi, G.E. Keefe and Y.S. Lin, "Design Rules and Alternate Mechanisms for Bubble Domain Propagation in Contiguous Disk Devices", Intermag Conf. (London), Paper 21.8 (April 1975).

10. A.R. MacIntosh, "Mechanisms of Magnetic Anisotropy in Rare Earth Metals", AIP Conf. Prof., Vol. 1, No. 10, 1972, pp. 1256-1259.

11. H.L. Hu, E.A. Giess, "Hard Bubble Supression and Controlled State Generation of One Micron Bubbles in Ion Implanted Garnet Films", AIP Conf. Proc., Vol. MAG-11, No. 5, 1975, pp. 1085-1087.

12. Tai-Lin Hsu, "Stability of Bubble States in a Capped Garnet Film", Intermag Conf. (London), Paper 1.9, 1975.

13. W.J. DeBonte, "Stability of Half Bubbles in Double Layer Films", AIP Conf. Proc.,Vol. 1, No. 10, 1972, pp. 349-353.

14. W. Kinsner, E. Della Torre and R. Hutton, "Bubble Cutting Circuits", IEEE Trans. Magn., Vol. MAG-10, No. 4, 1974, pp. 1071-1079.

15. E. Della Torre, W. Kinsner, "Channel-Bar Propagate Circuit", Intermag Conf. (London), Paper 21.9, 1975.

16. W.Y. Chu, "Extrapolation in Least pth Approximation and Nonlinear Programming", Inter. Rep. No. SOC-71, 1974.

17. J.W. Bandler, C. Charalambous, "Nonlinear Programming using Minimax Techniques", J. Optim. Theor. Appl., Vol. 13, 1974, pp. 607-619.

18. W. Jones, N.H. March, "Theoretical Solid State Physics", Vol. 1, (New York: John Wiley, 1973).

19. A.H. Bobeck, E. Della Torre, "Magnetic Bubbles" (Amsterdam: North Holland, 1975).

20. S. Chikazumi, "Physics of Magnetism", (New York: John Wiley, 1964).

21. R.C. Sherwood, P.H. Schmidt, D.H. Smith and E.M. Walters, "Uniaxial Magnetic Garnets For Domain Wall Bubble Devices", Appl. Phys. Lett., Vol. 17, No. 3, 1970, pp. 328-331.

22. A.B. Smith, M. Kestigan, W.R. Bekebrede, "LPE Garnet Film, Without Hard Bubbles", AIP Conf. Proc., No. 18, 1973, pp. 167-171.

23. R. Wolfe, J.C. North, W.A. Johnson, R.R. Spiwak, L.J. Varnerin, and R.F. Fischer, "Ion Implanted Patterns for Magnetic Bubble Propagation", AIP Conf. Proc., No. 10, 1973, pp. 339-343.

24. E. Della Torre, "Pressures on Cylindrical Magnetic Domain Walls", IEEE Trans. Magn., Vol. MAG-6, No. 4, 1970, pp. 822-827.

APPENDIX 1

DEMAGNETIZATION PRESSURE FOR A DOMAIN PENETRATION OUTSIDE THE CHANNEL

Instead of artifically constraining the domain to stay inside the channel the possibility of the domain penetrating into the unimplanted region should be considered, and the domain should be completely free to select its most favourable geometric configuration and location. While the formulations for the various pressure contributions in Chapter 2 apply equally well for the case of a domain penetrating outside the channel with changes in the parameters, new terms appear in the demagnetization pressure contributions of 2.4.1 and will be formulated in what follows.

Let us assume that the channel wall k(k=1,2) is modulated and given in the cylindrical co-ordinates of the domain by the single valued function $r_k=r_c^k(\theta)$, while the domain geometry is given by $r=r_b(\theta)$.

The z-component of the demagnetizing field at (x_o,y_o,z_o) due to an incremental area dxdy at (x,y,z_i) (Fig. A.1) is expressed as

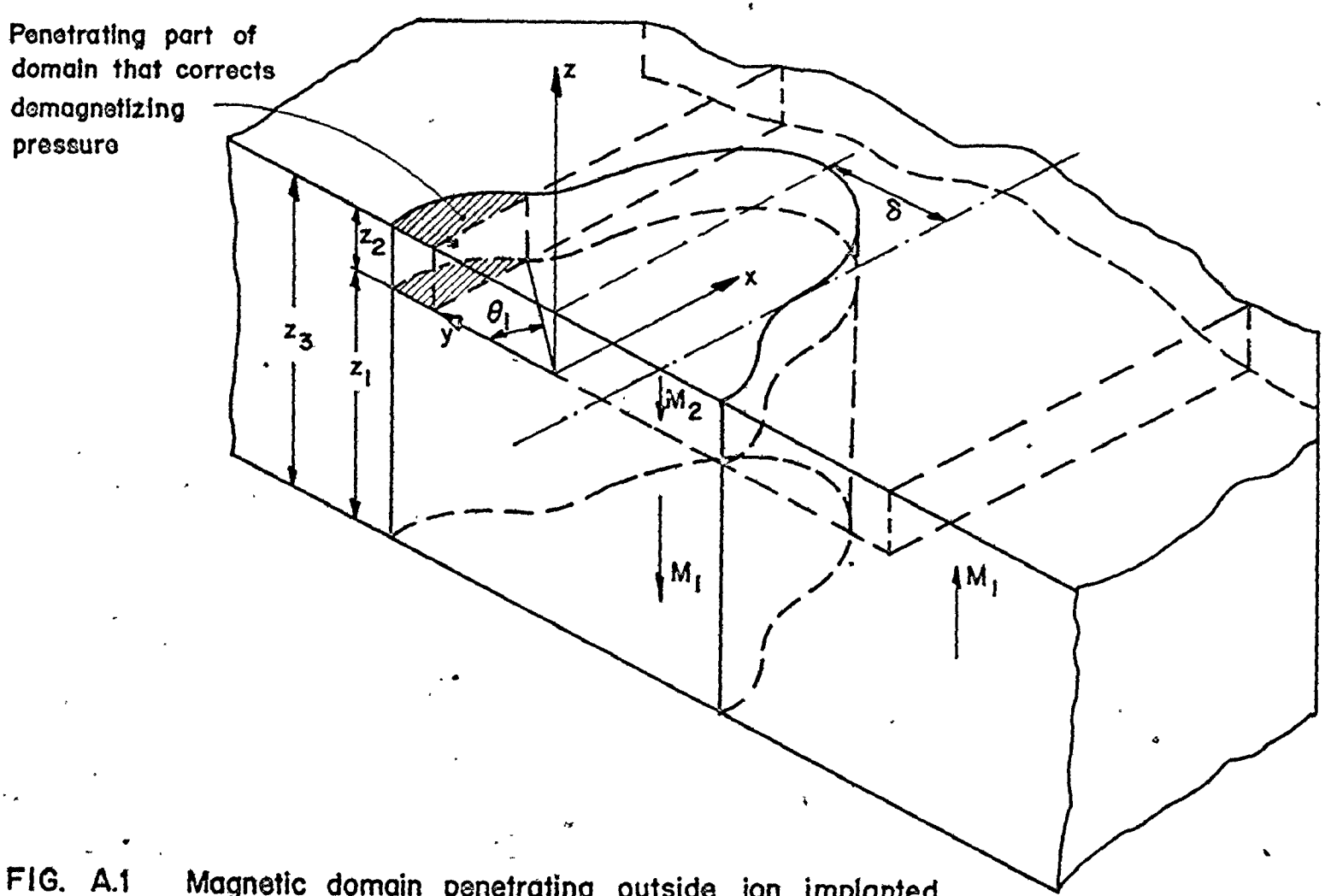

FIG. A.1 Magnetic domain penetrating outside ion implanted channel

$$dH_{z_o} = k(r)\left[\frac{-M_1(z_o+z_1)}{[\rho^2+(z_o+z_k)^2]^{3/2}} + \frac{\{(M_1-M_2)[(1-f(r_b,r_c,\rho)]\}z_o}{[\rho^2+z_o^2]^{3/2}}\right.$$

$$\left. + \frac{\{M_2+(M_1-M_2)f(r_b,r_c,\rho)\}\ (z_o-z_2)}{[\rho^2+(z_o-z_2)^2]^{3/2}}\right] dxdy \qquad (A.1.1)$$

where

$$\rho^2=r^2+r_o^2-2rr_o\cos(\theta-\theta_o) \qquad (A.1.2)$$

$$\Delta = M_1-M_2 \qquad (A.1.3)$$

and $f(r_b,r_c,\rho)$ is the unit pulse starting at $r_c(\theta)$ and ending at $r_b(\theta)$ if both regions intersect, unity if the domain completely penetrates outside the channel and zero if the domain is wholly inside the channel, and $k(r)$ is as defined in (2.4.1b & c).

The pressure at (r_o,θ_o) is given by

$$\bar{p}_{DO} = \frac{1}{T}\left[\int_{-z_1}^{0} 2M_1\{\int_S dH_{z_o}\}dz_o+2(M_2+\Delta u(r_o-r_c))\int_0^{z_2}\{\int_S dH_{z_o}\}dz_o\right]$$

$$= -\frac{2}{T}\left(\int_S dxdy\ k(r)\left\{M_1\left[\frac{-(M_2+\Delta\cdot f)}{[\rho^2+(z_1+z_2)^2]^{1/2}} - \frac{\Delta(1-f)}{[\rho^2+z_1^2]^{1/2}} + \frac{M_1}{\rho}\right.\right.\right.$$

$$+\frac{(M_2+\Delta\cdot f)}{[\rho^2+z_2^2]^{1/2}}+\frac{\Delta(1-f)}{\rho}-\frac{-M_1}{[\rho^2+z_1^2]^{1/2}}\Bigg]+(M_2+\Delta u(r_o-r_c))\Bigg[\frac{(M_2+\Delta\cdot f)}{\rho}+$$

$$\frac{\Delta(1-f)}{[\rho^2+z_2^2]^{1/2}}-\frac{M_1}{[\rho^2+(z_1+z_2)^2]^{1/2}}-\frac{(M_2+\Delta f)}{[\rho^2+z_2^2]^{1/2}}-\frac{\Delta(1-f)}{\rho}+\frac{M_1}{[\rho^2+z_1^2]^{1/2}}\Bigg]\Bigg\}\Bigg) \tag{A.1.4}$$

By collecting terms and comparing with Eqn. (2.4.4) we can write (A.1.4) in the form

$$\bar{p}_{DO}=\bar{p}^0_{DO}-\frac{2}{T}\Bigg(\int_S dxdyk(r)\Bigg\{\Delta\cdot f\Bigg[\frac{-1}{[\rho^2+(z_1+z_2)^2]^{1/2}}-\frac{1}{\rho}$$

$$+\frac{1}{[\rho^2+z_1^2]^{1/2}}+\frac{1}{[\rho^2+z_2^2]^{1/2}}\Bigg]+(M_2+\Delta u(r_o-r_c)\Bigg[\frac{2}{\rho}-\frac{2}{[\rho^2+z_2^2]^{1/2}}\Bigg]$$

$$+\Delta\cdot u(r_o-r_c)\Bigg[\frac{M_2}{\rho}+\frac{\Delta}{[\rho^2+z_2^2]^{1/2}}-\frac{M_1}{[\rho^2+(z_1+z_2)^2]^{1/2}}-\frac{M_2}{[\rho^2+z_2^2]^{1/2}}$$

$$-\frac{\Delta}{\rho}+\frac{M_1}{[\rho^2+z_1^2]^{1/2}}\Bigg]\Bigg\}\Bigg)=\bar{p}^0_{DO}+\bar{p}^p_{DO} \tag{A.1.5}$$

where $\bar{p}^p_{DO}$ is the correction due to the bubble penetration outside the channel.

$\bar{p}^{0}_{DO}$ is the demagnetization presure for a domain inside the channel, as derived in Sec. 2.4 .

The terms with the expression $u(r_o-r_c)$ in (A.1.5) are for those sampling points taken in the penetration zone, that is, outside the channel. The "penetration demagnetizing pressures" is expressed as

$$\bar{p}^{p}_{DO} = p^{p}_{1} + p^{p}_{2} \tag{A.1.6}$$

where

$$p^{p}_{1} = -\frac{2}{T}u(r_o-r_c(\theta))\ \Delta\int_0^{2\pi} d\theta \int_0^{\infty} rdrk(r) \sum_{i=1}^{3} M_i^{*}\left[-\frac{1}{\rho} + \frac{1}{[\rho^2+z_i^2]^{1/2}}\right] \tag{A.1.7}$$

and $M_1^{*}=M_1,\ M_2^{*}=M_1-2M_2,\ M_3^{*}=M_1,\ z_3=z_1+z_2$ (A.1.8)

and the second term in (A.1.6) is given by

$$p^{p}_{2} = -\frac{2}{T}\Delta\int_S dxdyk(r)f(r_c,r_b,\rho)\sum_{i=1}^{3} J_i\left[-\frac{1}{\rho} + \frac{1}{[\rho^2+z_i^2]^{1/2}}\right] \tag{A.1.9}$$

with $J_1=M_1$, $J_2=M_1-2(M_2+\Delta u(r_o-r_c)$, $J_3=-M_1$ (A.1.10)

and z_i is the same as in (A.1.8).

A close comparison of the terms in Eqn. (2.4.4) and those in (A.1.7) shows that p_1^p can be directly accommodated in the expressions derived in Sec. 2.4 by merely replacing M_2 in eqn. (2.4.2) by $(M_2+\Delta u(r_o-r_c))$. Thus we avoid repeating for p_1^p all the previous formulations in sec. 2.4.

The second term p_2^p given by Eqn. (A.1.9) cannot be accommodated like p_1^p into those equations of Sec. 2.4 but should be explicitly worked out.

We shall define θ_1 and θ_2 as the two solutions of the equation

$$r_b(r_i,\theta_i)=r_c(\delta,\theta_i) \quad (i=1,2) \tag{A.1.11}$$

(although in general 2N(N is an integer) solutions may exist we assume the simplest case).

Then p_2^p can be expressed by

$$p_2^p = \frac{2}{T}\Delta\int_{\theta_1}^{\theta_2} d\theta \sum_{i=1}^{3} J_i \Big\{ r_b^2+r_o^2-2r_br_o\cos(\theta-\theta_o)+z_i^2)^{1/2}$$

$$-(r_c^2+r_o^2-2r_cr_b\cos(\theta-\theta_o)+z_i^2)^{1/2}-(r_b^2+r_o^2-2r_br_o\cos(\theta-\theta_o))^{1/2}$$

$$+(r_c^2+r_o^2-2r_or_c\cos(\theta-\theta_o)^{1/2}$$

$$+r_o\cos(\theta-\theta_o)\,\ln\left[\left(\frac{r_b-r_o\cos(\theta-\theta_o)+[r_o^2+r_b^2-2r_or_b\cos(\theta-\theta_o)+z_i^2]^{1/2}}{r_c-r_o\cos(\theta-\theta_o)+[r_c^2+r_o^2-2r_or_c\cos(\theta-\theta_o)+z_i^2]^{1/2}}\right)\right.$$

$$\left.\left.\times\left(\frac{r_c-r_o\cos(\theta-\theta_o)+[r_o^2+r_c^2-2r_or_c\cos(\theta-\theta_o)]^{1/2}}{r_b-r_o\cos(\theta-\theta_o)+[r_o^2+r_b^2-2r_or_b\cos(\theta-\theta_o)]^{1/2}}\right)\right]\right\} \qquad \text{(A.1.12)}$$

The gradient with respect to the bubble center parameter δ is given by

$$\frac{\partial p_2^p}{\partial\delta}=\frac{2\Delta}{T}\int_{\theta_1}^{\theta_2}d\theta\sum_{i=1}^{3}J_i\left\{\overbrace{\left[r_c\frac{\partial r_c}{\partial\delta}-\cos(\theta-\theta_o)r_o\frac{\partial r_c}{\partial\delta}\right]}^{F3}\right.$$

$$\times\left[(r_c^2+r_o^2-2r_or_c\cos(\theta-\theta_o))^{-1/2}-(r_c^2+r_o^2-2r_or_c\cos(\theta-\theta_o)+z_i^2)^{-1/2}\right]$$

$$+r_o\cos(\theta-\theta_o)\left[\left(\frac{\frac{\partial r_c}{\partial\delta}+\frac{F3}{[r_o^2+r_c^2-2r_or_c\cos(\theta-\theta_o)]^{1/2}}}{r_c-r_o\cos(\theta-\theta_o)+[r_c^2+r_o^2-2r_or_c\cos(\theta-\theta_o)]^{1/2}}\right)\right.$$

$$\left.\left.-\left(\frac{\frac{\partial r_c}{\partial\delta}+\frac{F3}{[r_c^2+r_o^2-2r_or_c\cos(\theta-\theta_o)+z_i^2]^{1/2}}}{r_c-r_o\cos(\theta-\theta_o)+[r_c^2+r_o^2-2r_or_c\cos(\theta-\theta_o)+z_i^2]^{1/2}}\right)\right]\right\} \qquad \text{(A.1.13)}$$

The gradients with respect to the radial parameters are given by

$$\frac{\partial p_2^P}{\partial r_j} = \left(\frac{2}{T} \Delta \int_{\theta_1}^{\theta_2} d\theta \sum_{i=1}^{3} J_i \overbrace{\left\{ \left[r_o \frac{\partial r_o}{\partial r_j} - r_c \frac{\partial r_o}{\partial r_j} \cos(\theta-\theta_o) \right] \right.}^{F2} \right]$$

$$\times \left[(r_c^2+r_o^2-2r_o r_c \cos(\theta-\theta_o)+z_i^2)^{-1/2} - (r_c^2+r_o^2-2r_o r_c \cos(\theta-\theta_o))^{-1/2} \right]$$

$$\overbrace{+\left[r_b \frac{\partial r_b}{\partial r_j} + r_o \frac{\partial r_o}{\partial r_j} - \cos(\theta-\theta_o)\left(r_b \frac{\partial r_o}{\partial r_j} + r_o \frac{\partial r_b}{\partial r_j} \right) \right]}^{F1}$$

$$\times \left[(r_b^2+r_o^2-2r_o r_c \cos(\theta-\theta_o)+z_i^2)^{-1/2} - (r_b^2+r_o^2-2r_b r_o \cos(\theta-\theta_o))^{1/2} \right]$$

$$+ \frac{\partial r_o}{\partial r_j} \cos(\theta-\theta_o) \ln \left[\left(\frac{r_b - r_o \cos(\theta-\theta_o) + [r_b^2+r_o^2-2r_o r_b \cos(\theta-\theta_o)+z_i^2]^{1/2}}{r_b - r_o \cos(\theta-\theta_o) + [r_b^2+r_o^2-2r_o r_b \cos(\theta-\theta_o)]^{1/2}} \right) \right.$$

$$\left. \times \left(\frac{r_c - r_o \cos(\theta-\theta_o) + [r_c^2+r_o^2-2r_o r_c \cos(\theta-\theta_o)]^{1/2}}{r_c - r_o \cos(\theta-\theta_o) + [r_c^2+r_o^2-2r_o r_c \cos(\theta-\theta_o)+z_i^2]^{1/2}} \right) \right]$$

$$+r_o\cos(\theta-\theta_o)\left[\frac{\dfrac{\partial r_b}{\partial r_j}-\cos(\theta-\theta_o)\dfrac{\partial r_o}{\partial r_j}+\dfrac{F1}{[r_b^2+r_o^2-2r_or_b\cos(\theta-\theta_o)+z_i^2]^{1/2}}}{r_b-r_o\cos(\theta-\theta_o)+[r_o^2+r_b^2-2r_or_b\cos(\theta-\theta_o)+z_i^2]^{1/2}}\right.$$

$$-\frac{\dfrac{\partial r_b}{\partial r_j}-\cos(\theta-\theta_o)\dfrac{\partial r_o}{\partial r_j}+\dfrac{F1}{[r_o^2+r_b^2-2r_or_b\cos(\theta-\theta_o)]^{1/2}}}{r_b-r_o\cos(\theta-\theta_o)+[r_o^2+r_b^2-2r_br_o\cos(\theta-\theta_o)]^{1/2}}$$

$$-\frac{-\cos(\theta-\theta_o)\dfrac{\partial r_o}{\partial r_j}+\dfrac{F2}{[r_o^2+r_c^2-2r_or_c\cos(\theta-\theta_o)+z_i^2]^{1/2}}}{r_c-r_o\cos(\theta-\theta_o)+[r_o^2+r_c^2-2r_or_c\cos(\theta-\theta_o)+z_i^2]^{1/2}}$$

$$\left.+\frac{-\cos(\theta-\theta_o)\dfrac{\partial r_o}{\partial r_j}+\dfrac{F2}{[r_o^2+r_c^2-2r_or_c\cos(\theta-\theta_o)]^{1/2}}}{r_c-r_o\cos(\theta-\theta_o)+[r_o^2+r_c^2-2r_or_c\cos(\theta-\theta_o)]^{1/2}}\right]\Bigg\}\Bigg)$$

$$+\frac{2}{T}\Delta\sum_{i=1}^{3}J_i\left\{I(r_b(\theta_2),\ r_c(\theta_2),\ r_o)\frac{\partial\theta}{\partial r_j}\bigg|_{\theta=\theta_2}-I(r_b(\theta_1),r_c(\theta_1),r_o)\frac{\partial\theta}{\partial r_j}\bigg|_{\theta=\theta_2}\right\}$$

(A.1.14)

The last term is identically zero and $I(r_b(\theta)), r_c(\theta), r_o)$ is the integrand of Eqn. (A.1.12).

These expressions for p and their gradients should be incorporated in the solution method of chapters 2 and 4. It is expected that the solution of the generalized problem will be identical to that of Ch. 4 only if the channel walls are straight along the x direction. If the channel is modulated in width, it is conceivable that a bubble domain could penetrate <u>outside</u> the channel. This behaviour of the bubble should be particularly pronounced for a channel with sharp reentrant protrusions.

APPENDIX 2

PROGRAM DESCRIPTION

The problem of a deformable magnetic domain wholly situated in a straight ion implanted channel, formulated in Ch. 2, has been programmed. This is a nonlinear variational problem subject to constraints to keep the domain inside the channel.

An important part of the program, called CHAB1, is the program package FLNLP2 [16]. In this package, the Bandler-Charalambous technique is used to transform the nonlinear constrained problem to an equivalent unconstrained minimax problem [17]. The least pth approximation is then employed to solve the resulting minimax problem. Although the program package includes an extrapolation facility to extrapolate to $p \to \infty$, this has not been used.

A block diagram for the main structure of the complete computer program is shown in Fig. A.2. The program is broken up into the following basic units:

(1) Main Program: Reads input data, calls FLNLP2 to solve nonlinear constrained problem.

(2) Subroutine FLNLP2: Reads optimization data, calls GRDCHK if required to check analytic gradients, calls QUASIN to perform optimization and calls FINAL to print final output.

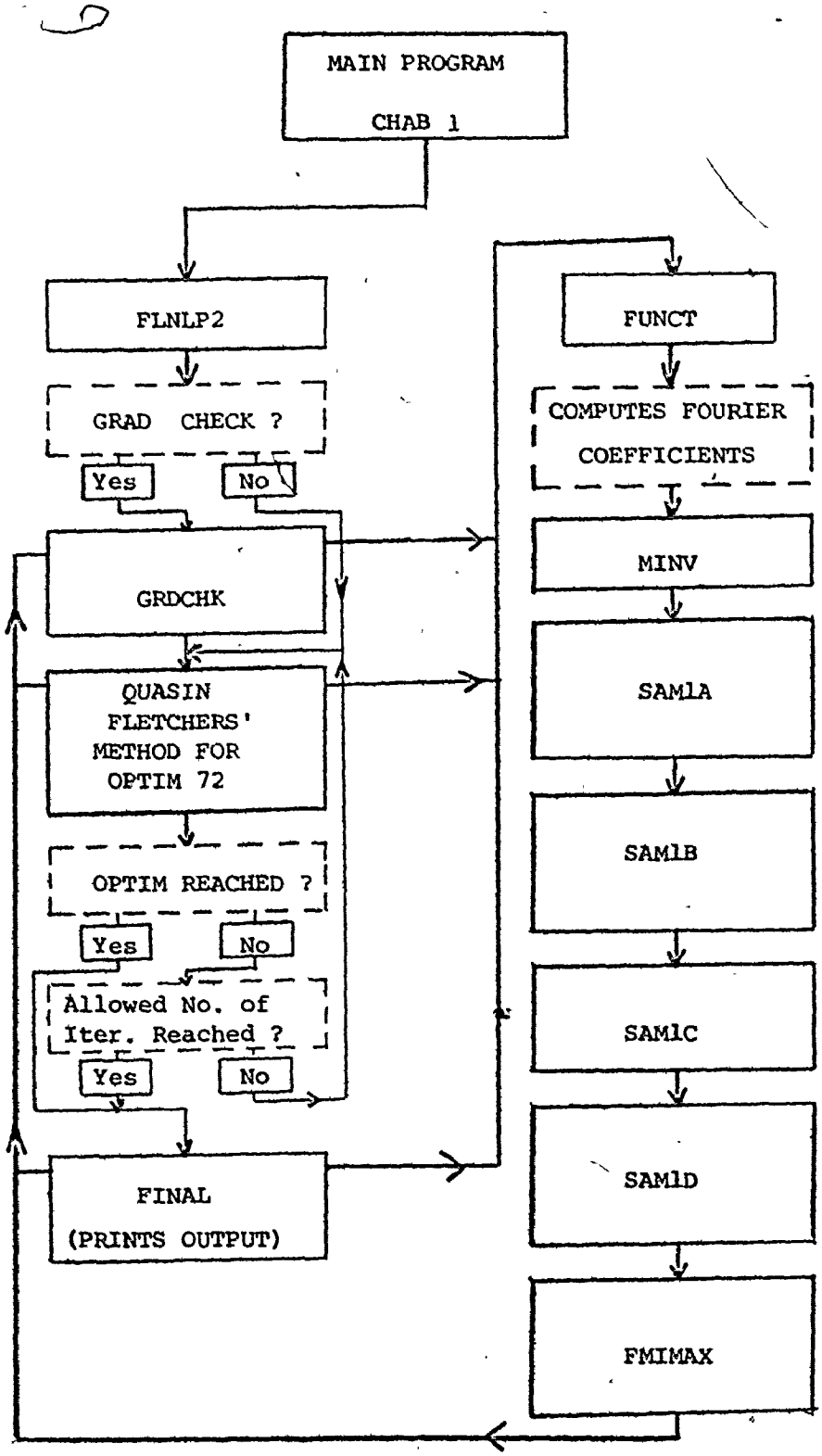

Fig. A.2 Block Diagram of CHAB1.

(3) Subroutine FMIMAX: Transforms constrained problem to an unconstrained objective minimax problem using the Bandler-Charalambous technique.

(4) Subroutine GRDCHK: Checks the supplied analytical gradients by comparing with numerical gradients obtained by perturbation.

(5) Subroutine QUASIN: Optimization program using Fletcher's quasi-Newton method.

(6) Subroutine FUNCT: Calculates Fourier coefficients, computes objective functional and functional gradients, computes constraints and constraint gradients.

(7) Subroutine SAM1A: Computes the initial induced pole density and initial pole density gradients on channel wall 1.

(8) Subroutine SAM1B: Computes the initial induced pole density and initial pole density gradients on channel wall 2.

(9) Subroutine SAM1C: Computes the mutual correction of the induced pole density and pole density gradients by iteration.

(10) Subroutine SAM1D: Computes the pressures and pressure gradients at the pressure sampling points.

The solution was obtained after 40 function evaluations on the average, each function evaluation takes approximately 4 seconds of computation time on a CDC 6400 computer, for an accuracy of 10^{-6}.

```
C       PROGRAM CHAB1,TO COMPUTE THE STABLE BUBBLE GEOMETRY AND
C       LOCATION IN AN ION IMPLANTED CHANNEL ACCORDING TO THE
C       ANALYSIS AND MODEL BY SAMI HAKIM MIKHAIL.
C       PROGRAM BUBBLE DOMAIN DEFORMATION
        DIMENSION X(7),G(7),H(28),W(28),EPS(7),XE(7,8,10),XB(7)
        COMMON/SS2/SM(2),WE1,WE2,HAP,T,DEP,AS,NV,NS,NXO,NZO,
       *NIN,HPI,A1,A2,A3,A4,D(3),Z(3),CS(3),CZR(3),SUSP,
       *T1,T2,T3
        COMMON/SS5/WID
        COMMON/SS15/DMC,DMF
C       PROGRAM CONSTANTS
C       ***********************************************
C       DATA INPUT (MODEL PARAMETERS)
C       ***********************************************
C       SATURATION MAGNETIZATION(NONIMPLANTED MATERIAL)
        SM(1)=18.0
C       SATURATION MAGNETIZATION (IMPLLANTED MATERIAL)
        SM(2)=17.8
C       WALL ENERGY DENSITY(NONIMPLANTED MATERIAL)
        WE1=0.36
C       WALL ENERGY DENSITY(IMPLANTED MATERIALS)
        WE2=0.36
C       EXTERNAL UNIFORM BIAS MAGNETIC FIELD
        HAP=100.0
C       THICKNESS OF BUBBLE SUPPORTING CRYSTAL FILM
        T=6.0E-4
C       DEPTH OF ION IMPLANTED CHANNEL
        DEP=T/10.0
C       HALF-WIDTH OF A STRAIGHT ION IMPLANTED CHANNEL
        WID=T
C       NUMBER OF RADIAL PARAMETERS AND FOURIER COEFS.
        NV=6
C       NUMBER OF SAMPLING POINTS AT WHICH PRESSURES ARE COMPUTED
        NS=11
C       NUMBER OF DEPTHS AT WHICH INDUCED POLE DENSITY IS COMPUTED
        NZO=1
C       NUMBER OF POINTS ALONG CHANNEL SEMI-INFINITE HALF LENGTHS
C       AT WHICH INDUCED POLE DENSITY IS COMPUTED
        NXO=10
C       NUMBER OF EVEN DIVISIONS DIVIDING THE RANGE FROM 0 TO 2PI
C       USED IN NUMERICAL INTIGRATION BY SIMPSONS RULE
        NIN=2.0*NS
        HPI=2.0*ATAN(1.0)
        F1=2.0*HPI
        A1=HPI/NV
        A2=HPI/NXC
        A3=HPI/NS
        A4=4.0*HPI/NIN
        D(1)=2.0*SM(1)
        D(2)=-2.0*SM(2)
        D(3)=-D(1)-D(2)
        Z(1)=T-DEP
        Z(2)=DEP
        Z(3)=T
        F2=2.0/T
        CS(1)=-F2*D(3)*D(1)
        CS(2)=-F2*D(3)*D(2)
        CS(3)=-F2*D(1)*D(2)
        T1=-(WE1*Z(1)+WE2*Z(2))/T
        T2=2.0*(SM(1)*Z(1)+SM(2)*Z(2))/T
```

```
      F4=F4+CC(L)*F8
      F6=F6+A(L,J)*F8
  220 CONTINUE
      F7=F4*F4
      F8=RDS(I)*RDS(I)
      F9=-F3*RDS(I)
      F10=F7+F8+2.0*F4*F9
      F10=ABS(F10)
      F10=SQRT(F10)
      DO 210 L=1,3
      F11=Z(L)*Z(L)
      F12=SQRT(F11+F8)
      F13=F11+F10*F10
      F14=SQRT(F13)
      CY1=F14-F12-F10+RDS(I)
      F15=F4+F9
      F5=ABS(1.0-F3)
      F5=SQRT(F5)
      F16=(F15+F14)/(F15+F10)
      CY2=F16*RDS(I)*F5/(F12+F9)
      CY3=F3*RDS(I)*ALOG(CY2)
      IF(J.NE.1) GO TO 280
      PRST=PRST+FVS*CS(L)*(CY1+CY3)
  280 F18=RDS(I)*F6+F4*DRS(I,J)
      F19=F4*F6+RDS(I)*DRS(I,J)-F3*F18
      F20=F19*(1.0/F14-1.0/F10)
      F21=-DRS(I,J)*(RDS(I)/F12-1.0)
      CY6=F20+F21
      CY7=DRS(I,J)*CY3/RDS(I)
      F22=F6-F3*DRS(I,J)
      F23=(F22+F19/F14)/(F15+F14)
      F24=-(F22+F19/F10)/(F15+F10)
      F25=DRS(I,J)*(1.0/RDS(I)-(RDS(I)/F12-F3)/(F12-RDS(I)*F3))
      CY8=RDS(I)*F3*(F23+F24+F25)
      PRSG=PRSG+FVS*CS(L)*(CY6+CY7+CY8)
  210 CONTINUE
      IF(J.NE.1) GO TO 310
      PRES(I)=PRES(I)+PRST+CMF-DMC*RDS(I)
  310 PRG(I,J)=PRG(I,J)+PRSG-DMC*DRS(I,J)
  200 CONTINUE
      RETURN
      END
      SUBROUTINE MINV(A,N,D,L,M)
      DIMENSION A(1),L(1),M(1)
C
C        SEARCH FOR LARGEST ELEMENT
      D=1.0
      NK=-N
      DO 80 K=1,N
      NK=NK+N
      L(K)=K
      M(K)=K
      KK=NK+K
      BIGA=A(KK)
      DO 20 J=K,N
      IZ=N*(J-1)
      DO 20 I=K,N
      IJ=IZ+I
   10 IF( ABS(BIGA)- ABS(A(IJ))) 15,20,20
   15 BIGA=A(IJ)
```

```
      F5=Z(1)/B2
      F6=Z(2)/B1
      F7=Z(2)/B2
      F8=Z(3)/B1
      F9=Z(3)/B2
      F4=ALOG(1.0+F4*F4)
      F5=ALOG(1.0+F5*F5)
      F6=ALOG(1.0+F6*F6)
      F7=ALOG(1.0+F7*F7)
      F8=ALOG(1.0+F8*F8)
      F9=ALOG(1.0+F9*F9)
      F10=-Z(1)*F1+Z(2)*F2-Z(3)*F3
      F11=-B1*(F4-F6+F8)-B2*(F5-F7+F9)
      F12=SM(1)*(F10+F11)
      F13=2.0*SM(2)*(-Z(2)*F2-B1*F6-B2*F7)
      PRES(I)=PRES(I)+T3*(F12+F13)
      F1=SM(1)*(F4-F5-F6+F7+F8-F9)/2.0
      F2=SM(2)*(F6-F7)
      PRG(I,NMS)=PRG(I,NMS)+T3*(F1+F2)
      DO 140 J=1,NV
      PRG(I,J)=PRG(I,J)+T3*Y2*DRS(I,J)*(F1+F2)
  140 CONTINUE
      WRITE(6,600) (PRES(I),I=1,NS)
      WRITE(6,700) ((PRG(I,J),J=1,NMS),I=1,NS)
C     CHANNEL WALL ENERGIES AND ENERGY-GRADIENTS
      B1=WID-AS
      B2=WID+AS
      DO 160 I=1,NS
      Q1=(2.0*I-1)*A3
      DO 160 M=1,NZO
      DO 160 N=1,NXO
      F1=2.0*DEP*B1/3.0
      F2=2.0*DEP*B2/3.0
      IF(MOD(N,2).EQ.0) F1=2.0*F1
      IF(MOD(N,2).EQ.0) F2=2.0*F2
      IF(N.EQ.1) F1=F1/2.0
      IF(N.EQ.1) F2=F2/2.0
      Q2=(N-1)*A2
      F3=COS(Q2)
      F4=COS(Q1-Q2)
      F5=COS(Q1+Q2)
      F6=ABS(B1/F3)
      F7=ABS(B2/F3)
      DIFR1=-1.0/F3
      DIFR2=1.0/F3
      ZZ(1)=DEP*(M-0.5)/NZO
      ZZ(2)=DEP-ZZ(1)
      ZZ(3)=T-ZZ(2)
      F8=RDS(I)*RDS(I)
      F9=F6*F6+F8-2.0*F6*RDS(I)*F4
      F10=F6*F6+F8-2.0*F6*RDS(I)*F5
      F11=F7*F7+F8+2.0*F7*RDS(I)*F4
      F12=F7*F7+F8+2.0*F7*RDS(I)*F5
      S1=RDS(I)-F6*F4
      S2=RDS(I)-F6*F5
      S3=RDS(I)+F7*F4
      S4=RDS(I)+F7*F5
      SQ1=F6-RDS(I)*F4
      SQ2=F6-RDS(I)*F5
      SQ3=F7+RDS(I)*F4
```

```
      SQ4=F7+RDS(I)*F5
      BG3=0.0
      BG4=0.0
      BV1=0.0
      BV2=0.0
      DO 162 J=1,NV
      BG1(J)=0.0
      BG2(J)=0.0
  162 CONTINUE
      DO 170 K=1,3
      F13=ZZ(K)*ZZ(K)
      F14=F9+F13
      F15=F10+F13
      F16=F11+F13
      F17=F12+F13
      F18=SQRT(F14)
      F19=SQRT(F15)
      F20=SQRT(F16)
      F21=SQRT(F17)
      BV1=BV1+CZR(K)*(1.0/F18+1.0/F19)
      BV2=BV2+CZR(K)*(1.0/F20+1.0/F21)
      BG3=BG3-DIFR1*CZR(K)*(SQ1/(F14*F18)+SQ2/(F15*F19))
      BG4=BG4-DIFR2*CZR(K)*(SQ3/(F16*F20)+SQ4/(F21*F17))
      DO 180 J=1,NV
      BG1(J)=BG1(J)-CZR(K)*(S1/(F14*F18)+S2/(F15*F19))*DRS(I,J)
      BG2(J)=BG2(J)-CZR(K)*(S3/(F16*F20)+S4/(F21*F17))*DRS(I,J)
  180 CONTINUE
  170 CONTINUE
      CY1=(PD1(M,N)*BV1*F1+PD2(M,N)*BV2*F2)/(F3*F3)
      PRES(I)=PRES(I)-CY1
      CY2=(-PD1(M,N)*BV1*F1/B1+PD2(M,N)*BV2*F2/B2)/(F3*F3)
      CY3=PD1(M,N)*BG3+PG1(NMS,M,N)*BV1
      CY4=PD2(M,N)*BG4+PG2(NMS,M,N)*BV2
      PRG(I,NMS)=PRG(I,NMS)-CY2-(F1*CY3+F2*CY4)/(F3*F3)
      DO 160 J=1,NV
      CY1=PD1(M,N)*BG1(J)+PG1(J,M,N)*BV1
      CY2=PD2(M,N)*BG2(J)+PG2(J,M,N)*BV2
      PRG(I,J)=PRG(I,J)-(CY1*F1+CY2*F2)/(F3*F3)
  160 CONTINUE
      WRITE(6,600) (PRES(I),I=1,NS)
      WRITE(6,700) ((PRG(I,J),J=1,NMS),I=1,NS)
C     DEMAGNETIZATION PRESSURES AND PRESSURE-GRADIENTS.
      DO 200 I=1,NS
      DO 200 J=1,NV
      Q1=(2.0*I-1)*A3
      PRST=0.0
      PRSG=0.0
      DO 210 K=1,NIN
      FVS=A4/3.0
      FVS=2.0*FVS
      IF(MOD(K,2).EQ.0) FVS=2.0*FVS
      Q2=(K-1)*A4
      F1=Q2-Q1
      F2=SIN(F1)
      F3=COS(F1)
      F4=0.0
      F6=0.0
      DO 220 L=1,NV
      F7=SIN((L-1)*Q2)
      F8=COS((L-1)*Q2)
```

```
      RDS(I)=0.0
      DX(I)=0.0
      DDX(I)=0.0
      DO 40 J=1,NV
      DRS(I,J)=0.0
      DR1(I,J)=0.0
      DR2(I,J)=0.0
   40 CONTINUE
C     WALL PRESSURES AND GRADIENTS
      DO 110 K=1,NV
      DO 110 I=1,NS
      Q1=(2.0*I-1)*A3
      F1=COS((K-1)*Q1)
      F2=SIN((K-1)*Q1)
      RDS(I)=RDS(I)+CC(K)*F1
      DX(I)=DX(I)-(K-1)*CC(K)*F2
      DDX(I)=DDX(I)-(K-1)*(K-1)*CC(K)*F1
      DO 110 J=1,NV
      DRS(I,J)=DRS(I,J)+A(K,J)*F1
      DR1(I,J)=DR1(I,J)-(K-1)*A(K,J)*F2
      DR2(I,J)=DR2(I,J)-(K-1)*(K-1)*A(K,J)*F1
  110 CONTINUE
      WRITE(6,61) (RDS(I),I=1,NS)
   61 FORMAT(/,2X,*RADII AT NS SAMPLING POINTS*,/,4(E14.6))
      WRITE(6,62) ((DRS(I,J),J=1,NV),I=1,NS)
   62 FORMAT(/,2X,*RADIAL GRADIENTS*,/,4(E14.6))
      DO 120 I=1,NS
      F1=DX(I)/RDS(I)
      F2=RDS(I)*RDS(I)
      CY1=1.0+F1*F1
      CY2=1.0+2.0*F1*F1-DDX(I)/RDS(I)
      CURV=CY2/(RDS(I)*(CY1**1.5))
      PRES(I)=PRES(I)+T1*CURV
      DO 120 J=1,NV
      F3=-DRS(I,J)*(1.0-2.0*DDX(I)/RDS(I)+6.0*DX(I)*F1)/F2
      F4=(-DR2(I,J)+4.0*F1*DR1(I,J))/F2
      CY3=F3+F4
      CY4=-3.0*F1*(-DRS(I,J)*F1+DR1(I,J))/F2
      PRG(I,J)=PRG(I,J)+T1*(CY3*CY1+CY4*CY2)/(CY1**2.5)
  120 CONTINUE
      WRITE(6,600) (PRES(I),I=1,NS)
  600 FORMAT(/,2X,*PRESSURE CHECK*,/,-(E14.6))
      WRITE(6,700) ((PRG(I,J),J=1,NNS),I=1,NS)
  700 FORMAT(/,2X,*PRESSURE GRADIENTS CHECK*,/,5(E14.6))
C     EXTERNAL BIAS FIELD PRESSURES
      DO 130 I=1,NS
      PRES(I)=PRES(I)+T2*HAP
  130 CONTINUE
      WRITE(6,800) (PRES(I),I=1,NS)
C     CHANNEL WIDTH PRESSURES AND PRESSURE-GRADIENTS
      DO 140 I=1,NS
       Q1=(2.0*I-1)*A3
      Y2=COS(Q1)
      Y1=AS+RDS(I)*Y2
      B1=WID-Y1
      B2=WID+Y1
      F1=ATAN(B1/Z(1))+ATAN(B2/Z(1))
      F2=ATAN(B1/Z(2))+ATAN(B2/Z(2))
      F3=ATAN(B1/Z(3))+ATAN(B2/Z(3))
      F4=Z(1)/B1
```

```
      DCZ2=-TAN(PHI)
      F20=COS(PHI)
      F2=(WID-AS)*TAN(PHI)
      CY2=DEP*(M-0.5)/NZO
      F3=F1-F2
      F4=F1+F2
      F5=CY1-CY2
      F6=4.0*WID*WID
      F7=F5*F5+F6
      F8=F7+F3*F3
      F9=F7+F4*F4
      B1=1.0/(F8**1.5)
      B2=1.0/(F9**1.5)
      QF=B1+B2
      QF=QF*2.0*WID*FVS/(F20*F20)
      QA=QF*PD1(M,N)
      CF=CF+QA
      SIC1=3.0*B1*F3*(DCZ1-DCZ2)/F8
      SIC2=3.0*B2*F4*(DCZ1+DCZ2)/F9
      SIC3=2.0*(SIC1+SIC2)*WID/(F20*F20)
      VC(NMS)=VC(NMS)+FVS*(PG1(NMS,M,N)*QF+SIC3*PD1(M,N))
      DO 85 L=1,NV
      QA=QF*PG1(L,M,N)
      VC(L)=VC(L)+QA
   85 CONTINUE
   75 CONTINUE
      OLD=PD2(I,J)
      PD2(I,J)=PDW2(I,J)-CF
      DO 95 L=1,NMS
      PG2(L,I,J)=PGW2(L,I,J)-VC(L)
      RER=ABS(1.0-OLD/PD2(I,J))
      IF(RER.GE.GG) GG=RER
   95 CONTINUE
   65 CONTINUE
      IF(GG.LT.1.E-2) GO TO 100
      GO TO 50
  100 RETURN
      END
      SUBROUTINE SAM1D
C     THIS SUBROUTINE COMPUTES THE PRESSURES AND PRESSURE
C     GRADIENTS AT (NS) SAMPLING POINTS.
      DIMENSION DUMB(20),ZZ(3),BG1(20),BG2(20)
      COMMON/SS2/SM(2),WE1,WE2,HAP,T,DEP,AS,NV,NS,NXO,NZO,
     *NIN,HPI,A1,A2,A3,A4,D(3),Z(3),CS(3),CZR(3),SUSP,
     *T1,T2,T3
      COMMON/SS3/PRES(11),PRG(11,7),PD1(1,10),PD2(1,10),
     *PG1(7,1,10),PG2(7,1,10)
      COMMON/SS4/CC(6),A(6,6)
      COMMON/SS5/WID
      COMMON/SS6/RDS(11),DX(11),DDX(11),DRS(11,6),DR1(11,6),DR2(11,6)
      COMMON/SS15/DMC,DMF
C     RDS(I)=VALUE OF RADIUS AT THE ITH PRESSURE SAMPLING POINT
C     DX(I)=FIRST ANGULAR DERIVATIVE OF RDS(I)
C     SECOND ANGULAR DERIVATIVE OF RDS(I)
C     DRS(I,J)=DERIVATIVE OF RDS(I) WITH RESPECT TO RADIAL PARAMETER J
C     DR1(I,J)=DREIVATIVE OF DX(I) WITH RESPECT TO JTH RADIAL PARAMETERS
C     DR2(I,J)=DERIVATIVE OF DDX(I) WITH RESPECT TO JTH RADIAL PARAMETE
      NMS=NV+1
C     INITIATION OF ARRAYS
      DO 40 I=1,NS
```

```
      F14=SQRT(F12)
      F15=SQRT(F13)
      F16=P2*F4*(1.0/F14-1.0/F15)
      F17=-F1*ALOG((F9+F14)/(F10+F15))
      F18=F8+F1*F11
      F19=F11+F7
      F20=-F18*(F9/F14-F10/F15)/F19
      PD2(I,J)=PD2(I,J)+D(K)*(F20+F17+F16)*FVS
      F21=(-F9*F4*P2-F16)/(F12*F14)
      DO 40 L=1,NV
      PG2(L,I,J)=PG2(L,I,J)+FVS*D(K)*DR(L)*F21
   40 CONTINUE
      PD2(I,J)=PD2(I,J)-SUSP*D(3)*P17
      F22=P2-RA*F2
      F23=F4*(1.0/F14-1.0/F15)
      F24=-P2*F4*(F22/(F12*F14)-P2/(F13*F15))
      F25=-F1*((-F2+F22/F14)/(F9+F14)-(-F2+P2/F15)/(F9+F15))
      F26=-F18*(-F2/F14+F2/F15-F22*F9/(F12*F14)-P2*P2*F2/(F13*F15))/F19
      F27=-F9/F14-P2*F2/F15
      F28=2.0*P2*(-F3*F18/(F19*F19)+(F1-F5)/F19)
      PG2(NMS,I,J)=PG2(NMS,I,J)+FVS*DIFR*D(K)*(F23+F24+F25+F26+F28)
   30 CONTINUE
      RETURN
      END
      SUBROUTINE SAM1C
C     THIS SUBROUTINE SOLVES THE TWO COUPLED INTEGRAL
C     THIS SUBROUTINE SOLVES A SET OF DISCRETIZED INTEGRAL EQUATIONS
C     OF THE FREDHOLM TYPE FOR THE MUTUAL CORRECTION OF THE
C     INDUCED POLE DENSITY AND POLE DENSITY GRADIENTS.
      DIMENSION VC(20)
      DIMENSION PDW1(1,40),PDW2(1,10),PGW1(7,1,10),PGW2(7,1,10)
      COMMON/SS2/SM(2),WE1,WE2,HAP,T,DEP,AS,NV,NS,NXO,NZO,
     *NIN,HPI,A1,A2,A3,A4,D(3),Z(3),CS(3),CZR(3),SUSP,
     *T1,T2,T3
      COMMON/SS3/PRES(11),PRG(11,7),PD1(1,10),PD2(1,10),
     *PG1(7,1,10),PG2(7,1,10)
      COMMON/SS4/CC(6),A(6,6)
      COMMON/SS5/WID
      COMMON/SS6/RDS(11),DX(11),DDX(11),DRS(11,6),DR1(11,6),DR2(11,6)
      NMS=NV+1
      DO 2 I=1,NZO
      DO 2 J=1,NXO
      PDW1(I,J)=PD1(I,J)
      PDW2(I,J)=PD2(I,J)
      DO 2 L=1,NMS
      PGW1(L,I,J)=PG1(L,I,J)
      PGW2(L,I,J)=PG2(L,I,J)
    2 CONTINUE
   50 GG=0.0
C     CORRECTION OF POLES,AND GRADIENT DISTR. ON FACE(1)
      DO 60 I=1,NZO
      DO 60 J=1,NXO
      DO 55 L=1,NMS
      VC(L)=0.0
   55 CONTINUE
      CY1=DEP*(I-0.5)/NZO
      PHI=(J-1)*A2
      DCZ1=-TAN(PHI)
      F1=(WID-AS)*TAN(PHI)
      CF=0.0
```

```
C       CORRECTION OF ONE POINT
        DO 70 M=1,NZO
        DO 70 N=1,NXO
        FVS=DEP*(WID+AS)/3.0
        FVS=FVS*SUSP
        IF(MOD(N,2).EQ.0) FVS=2.0*FVS
        PHI=(N-1)*A2
        DCZ2=TAN(PHI)
        F20=COS(PHI)
        F2=(WID+AS)*TAN(PHI)
        CY2=DEP*(M-0.5)/NZO
        F3=F1-F2
        F4=F1+F2
        F5=CY1-CY2
        F6=4.0*WID*WID
        F7=F5*F5+F6
        F8=F7+F3*F3
        F9=F7+F4*F4
        B1=1.0/(F8**1.5)
        B2=1.0/(F9**1.5)
        QF=B1+B2
        QF=QF*2.0*WID*FVS/(F20*F20)
        QA=QF*PD2(M,N)
        CF=CF+QA
        SIC1=3.0*B1*F3*(DCZ1-DCZ2)/F8
        SIC2=3.0*B2*F4*(DCZ1+DCZ2)/F9
        SIC3=2.0*(SIC1+SIC2)+WID/(F20*F20)
        VC(NMS)=VC(NMS)+FVS*(QF*PG2(NMS,M,N)+PD2(M,N)*SIC3)
        DO 80 L=1,NV
        QA=QF*PG2(L,M,N)
        VC(L)=VC(L)+QA
   80   CONTINUE
   70   CONTINUE
        OLD=PD1(I,J)
        PD1(I,J)=PDW1(I,J)-CF
        DO 90 L=1,NMS
        PG1(L,I,J)=PGW1(L,I,J)-VC(L)
        RER=ABS(1.0-OLD/PD1(I,J))
        IF(RER.GE.GG) GG=RER
   90   CONTINUE
   60   CONTINUE
C       CORRECTION OF POLE AND GRAD. DISTR. ON FACE(2)
        DO 65 I=1,NZO
        DO 65 J=1,NXO
        CF=0.0
        DO 45 L=1,NMS
        VC(L)=0.0
   45   CONTINUE
        CY1=DEP*(I-0.5)/NZO
        PHI=(J-1)*A2
        DCZ1=TAN(PHI)
        F1=(WID+AS)*TAN(PHI)
        CF=0.0
C       CORRECTION OF ONE POINT
        DO 75 M=1,NZO
        DO 75 N=1,NXO
        FVS=DEP*(WID-AS)/3.0
        FVS=FVS*SUSP
        IF(MOD(N,2).EQ.0) FVS=FVS*2.0
        PHI=(N-1)*A2
```

```
C       INITIATION OF ARRAYS
        DO 10 I=1,NZO
        DO 10 J=1,NXO
        PD2(I,J)=0.0
        DO 10 L=1,NMS
        PG2(L,I,J)=0.0
   10   CONTINUE
        DO 30 I=1,NZO
        DO 30 J=1,NXO
        PHI=(J-1)*A2
        P1=COS(PHI)
        ZZ(3)=DEP*(I-0.5)/NZO
        ZZ(2)=DEP-ZZ(3)
        ZZ(1)=T-ZZ(2)
        P2=ABS((WID+AS)/P1)
        DIFR=1.0/P1
        P3=ZZ(3)*ZZ(3)
        P4=ZZ(2)*ZZ(2)
        P5=0.1*DEP/2.0
        P6=P5*P5
        P7=2.0*WID-P5
        P8=P7*P7
        P9=ALOG((P3+P6)*(P4+P8)/((P4+P6)*(P3+P8)))
        P10=2.0*WID+P5
        P11=P10*P10
        P12=2.0*WID+3.0*P5
        P13=P12*P12
        P14=ALOG((P3+P13)*(P4+P11)/((P3+P11)*(P4+P13)))
        P15=2.0*ATAN(P5/ZZ(3))-ATAN(P12/ZZ(3))+ATAN(P10/ZZ(3))
        P16=2.0*ATAN(P5/ZZ(2))-ATAN(P12/ZZ(2))+ATAN(P10/ZZ(2))
        P17=(-ZZ(3)*P15+ZZ(2)*P16)/P5+P9+P10*P14/P5
        DO 30 I1=1,NIN
        FVS=2.0*A4*SUSP/3.0
        IF(MOD(I1,2).EQ.0) FVS=2.0*FVS
        RA=0.
        DO 33 N=1,NV
        DR(N)=0.0
   33   CONTINUE
        Q=(I1-1)*A4
        Q=2.0*HPI-Q
        DO 35 M=1,NV
        F1=COS((M-1)*Q)
        RA=RA+CC(M)*F1
        DO 35 N=1,NV
        DR(N)=DR(N)+A(M,N)*F1
   35   CONTINUE
        F1=COS(Q)
        F2=COS(Q-PHI)
        F3=1.0-F2*F2
        F4=COS(2.0*Q-PHI)
        F5=COS(3.0*Q-2.0*PHI)
        F6=RA*RA+P2*P2-2.0*RA*P2*F2
        F7=P2*P2*F3
        F8=P2*P2*(F1-F5)
        F10=-P2*F2
        F9=RA+F10
        DO 30 K=1,3
        F11=ZZ(K)*ZZ(K)
        F12=F6+F11
        F13=P2*P2+F11
```

```
      DR(N)=0.0
   33 CONTINUE
      Q=(I1-1)*A4
      DO 35 M=1,NV
      F1=COS((M-1)*Q)
      RA=RA+CC(M)*F1
      DO 35 N=1,NV
      DR(N)=DR(N)+A(M,N)*F1
   35 CONTINUE
      F1=COS(Q)
      F2=COS(Q-PHI)
      F3=1.0-F2*F2
      F4=COS(2.0*Q-PHI)
      F5=COS(3.0*Q-2.0*PHI)
      F6=RA*RA+P2*P2-2.0*RA*P2*F2
      F7=P2*P2*F3
      F8=P2*P2*(F1-F5)
      F10=-P2*F2
      F9=RA+F10
      DO 30 K=1,3
      F11=ZZ(K)*ZZ(K)
      F12=F6+F11
      F13=P2*P2+F11
      F14=SQRT(F12)
      F15=SQRT(F13)
      F16=P2*F4*(1.0/F14-1.0/F15)
      F17=-F1*ALOG((F9+F14)/(F10+F15))
      F18=F8+F1*F11
      F19=F11+F7
      F20=-F18*(F9/F14-F10/F15)/F19
      PD1(I,J)=PD1(I,J)+D(K)*(F20+F17+F16)*FVS
      F21=(-F9*F4*P2-F18)/(F12*F14)
      DO 40 L=1,NV
      PG1(L,I,J)=PG1(L,I,J)+FVS*D(K)*DR(L)*F21
   40 CONTINUE
      PD1(I,J)=PD1(I,J)-SUSP*D(3)*P17
      F22=P2-RA*F2
      F23=F4*(1.0/F14-1.0/F15)
      F24=-P2*F4*(F22/(F12*F14)-P2/(F13*F15))
      F25=-F1*((-F2+F22/F14)/(F9+F14)-(-F2+P2/F15)/(F9+F15))
      F26=-F18*(-F2/F14+F2/F15-F22*F9/(F12*F14)-P2*P2*F2/(F13*F15))/F19
      F27=-F9/F14-P2*F2/F15
      F28=2.0*P2*(-F3*F18/(F19*F19)+(F1-F5)/F19)
      PG1(NMS,I,J)=PG1(NMS,I,J)+FVS*DIFR*D(K)*(F23+F24+F25+F26+F28)
   30 CONTINUE
      RETURN
      END
      SUBROUTINE SAM18
C     THIS SUBROUTINE COMPUTES THE INDUCED POLE DENSITY AND
C     POLE DENSITY GRADIENTS ON THE CHANNEL WALL(2)
      DIMENSION ZZ(3),DR(6)
      COMMON/SS2/SM(2),WE1,WE2,HAP,T,DEP,AS,NV,NS,NXO,NZO,
     *NIN,HPI,A1,A2,A3,A4,D(3),Z(3),CS(3),CZR(3),SUSP,
     *T1,T2,T3
      COMMON/SS3/PRES(11),PRG(11,7),PD1(1,10),PD2(1,10),
     *PG1(7,1,10),PG2(7,1,10)
      COMMON/SS4/CC(6),A(6,6)
      COMMON/SS5/WID
      COMMON/SS6/RDS(11),DX(11),DDX(11),DRS(11,6),DR1(11,6),DR2(11,6)
      NMS=1+NV
```

```
      DO 676 JK=1,NV
      GC(JK,J)=0.0
      GC(JK,(J+NV))=0.0
      IF(JK.EQ.J) GC(JK,J)=1.0
      IF(JK.EQ.J) GC(JK,(J+NV))=-1.0
  678 CONTINUE
      WRITE(6,500) (C(I),I=1,12)
  500 FORMAT(/,2X,*CONSTRAINTS*,/,4(E14.6))
      CALL FMIMAX(7,12,13,F,G,GF,C,GC,U,AV,TT,TP)
      RETURN
      END
      SUBROUTINE SAM1A
C     THIS SUBROUTINE COMPUTES THE INDUCED POLE DENSITY AND
C     POLE DENSITY GRADIENTS ON THE CHANNEL SIDE WALL,1)
      DIMENSION ZZ(3),DR(6)
      COMMON/SS2/SM(2),WE1,WE2,HAP,T,DEP,AS,NV,NS,NXO,NZO,
     *NIN,HPI,A1,A2,A3,A4,D(3),Z(3),CS(3),CZR(3),SUSP,
     *T1,T2,T3
      COMMON/SS3/PRES(11),PRG(11,7),PD1(1,10),PD2(1,10),
     *PG1(7,1,10),PG2(7,1,10)
      COMMON/SS4/CC(6),A(6,6)
      COMMON/SS5/WID
      COMMON/SS6/RDS(11),DX(11),DDX(11),DRS(11,6),DR1(11,6),DR2(11,6)
      NMS=1+NV
C     INITIATION OF ARRAYS
      DO 10 I=1,NZO
      DO 10 J=1,NXO
      PD1(I,J)=0.0
      DO 10 L=1,NMS
      PG1(L,I,J)=0.0
   10 CONTINUE
      DO 30 I=1,NZO
      DO 30 J=1,NXO
      PHI=(J-1)*A2
      P1=COS(PHI)
      ZZ(3)=DEP*(I-0.5)/NZO
      ZZ(2)=DEP-ZZ(3)
      ZZ(1)=T-ZZ(2)
      P2=ABS((WID-AS)/P1)
      DIFR=-1.0/P1
      P3=ZZ(3)*ZZ(3)
      P4=ZZ(2)*ZZ(2)
      P5=0.1*DEP/2.0
      P6=P5*P5
      P7=2.0*WID-P5
      P8=P7*P7
      P9=ALOG((P3+P6)*(P4+P8)/((P4+P6)*(P3+P8)))
      P10=2.0*WID+P5
      P11=P10*P10
      P12=2.0*WID+3.0*P5
      P13=P12*P12
      P14=ALOG((P3+P13)*(P4+P11)/((P3+P11)*(P4+P13)))
      P15=2.0*ATAN(P5/ZZ(3))-ATAN(P12/ZZ(3))+ATAN(P10/ZZ(3))
      P16=2.0*ATAN(P5/ZZ(2))-ATAN(P12/ZZ(2))+ATAN(P10/ZZ(2))
      P17=(-ZZ(3)*P15+ZZ(2)*P16)/P5+P9+P10*P14/P5
      DO 30 I1=1,NIN
      FVS=2.0*A4*SUSP/3.0
      IF(MOD(I1,2).EQ.0) FVS=2.0*FVS
      RA=0.
      DO 33 N=1,NV
```

```
      CALL MINV(A,NV,DET,L5,M5)
C     COMP. OF FOURIER COEFS.
      DO 20 I=1,NV
      CC(I)=0.0
      DO 20 J=1,NV
      CC(I)=CC(I)+A(I,J)*X(J)*BECC
   20 CONTINUE
      WRITE(6,891) (CC(I),I=1,NV)
  891 FORMAT(//,2X,*FOURIER COEFFICIENTS*,/,4(E14.6))
C     OBJECTIVE FUNCTIONAL AND FUNCTIONAL GRADIENTS
      CALL SAM1A
C     PO1(I,J)=POLE DENSITY INDUCED  AT ITH DEPTH AND JTHPOINT
C     ALONG THE CHANNEL SIDE WALL (1)
      WRITE(6,40) ((PO1(I,J),J=1,NXO),I=1,NZO)
C     PG1(L,I,J)=POLE DENSITY GRADIENT  WITH RESPECT TO LTH VARIABLE
C     OF THE POINT ON CHANNEL WALL,U. AT AN ITH DEPTH ANDJTH LOCATION
C     ALONG THE CHANNEL
      WRITE(6,50) (((PG1(L,I,J),J=1,NXO),I=1,NZO),L=1,NMS)
   40 FORMAT(/,2X,*POLE DENSITY FACE(1)*,/,5(E14.6))
   50 FORMAT(/,2X,*POLE DENSITY GRADIENTS FACE(2)*,/,5(E14.6))
      CALL SAM1B
C     PO2(I,J)=POLE DENSITY INDUCED AT ITH DEPTH AND JTH POINT
C     ALONG THE CHANNEL SIDE WALL(2)
      WRITE(6,60) ((PO2(I,J),J=1,NXO),I=1,NZO)
   60 FORMAT(/,2X,*POLE DENSITY FACE(2)*,/,5(E14.6))
C     PG2(L,I,J)=POLE DENSITY GRADIENT WITH RESPECT TO LTH VARIABLE
C     OF THE POINT ON THE CHANNEL WALL(2),AT THE ITH DEPTH
C     AND JTH LOCATION ALONG THE CHANNEL
      WRITE(6,70) (((PG2(L,I,J),J=1,NXO),I=1,NZO),L=1,NMS)
   70 FORMAT(/,2X,*POLE DENSITY GRADIENTS FACE(2)*,/,5(E14.6))
      CALL SAM1C
      CALL SAM1D
      WRITE(6,80) (PRES(I),I=1,NS)
   80 FORMAT(/,2X,*PRESSURES AT THE NS SAMPLING POINTS*,/,4(E14.6))
      WRITE(6,90) ((PRG(I,J),J=1,NMS),I=1,NS)
   90 FORMAT(/,2X,*PRESSURE GRADIENTS*,/,5(E14.6))
      F=0.0
C     NUMERICAL SCALING FACTOR
      HUB=1.E-8
      DO 400 J=1,NMS
      GF(J)=0.0
      DO 400 I=1,NS
      IF(J.NE.1) GO TO 420
      F=F+PRES(I)*PRES(I)*HUB
  420 CONTINUE
      GF(J)=GF(J)+HUB*BECC*PRES(I)*PRG(I,J)
  400 CONTINUE
C     CONSTRAINTS ON RADIAL VARIABLES TO CONFINE THE RADIAL
C     VARIABLES INSIDE THE CHANNEL BOUNDARY.
      DO 678 J=1,NV
      C(J)=X(J)
      ANGL=(2.0*J-1)*A1
      KA=1.0
      IF(ANGL.GT.HPI) KA=2.0
      XTR=4.E-5
      DIVA=(WID+XTR+(2.0*KA-3.0)*AS)/(BECC*COS(ANGL))
      DIVA=ABS(DIVA)
      C(J+NV)=DIVA-X(J)
      GC(NMS,J)=0.0
      GC(NMS,(NV+J))=(2.0*KA-3.0)/ABS(COS(ANGL))
```

```
      T2=-T2
      T3=F2*D(3)
      CZR(1)=D(1)/(2.0*T)
      CZR(2)=D(2)/(2.0*T)
      CZR(3)=D(3)/(2.0*T)
      SUSP=1.0/(HPI*2+0.0)
      SUSP=-SUSP
      DMC=0.0
      DMF=0.0
      DO 1 I=1,3
      DMC=DMC+2.0*HPI*CS(I)
      DMF=DMF+2.0*HPI*CS(I)*Z(I)
    1 CONTINUE
C     CONSTANTS FOR PROGRAM THAT SOLVES NON-LINEAR
C     CONSTRAINED PROBLEMS.
C     NUMBER OF VARIABLES IN OPTIMIZATION(N=NS+1)
      N=7
C     NUMBER OF CONSTRAINTS
      NC=12
      MM=1
      IGK=0
      IK=1
C     SOLUTION OF CONSTRAINED NON-LINEAR PROBLEM
      DO 111 IH=1,IK
      CALL FLNL(N,NC,MM,IGK,X,G,H,W,EPS,XE,IH,IK,XB,IFINIS)
  111 CONTINUE
      STOP
      END
      SUBROUTINE FUNCT(X,F,G,U)
      DIMENSION X(7),G(7),C(12),GF(7),GC(7,12),AV(13),TT(13),TP(13)
      DIMENSION LS(20),MS(20)
      COMMON/SS2/SM(2),WE1,WE2,HAP,T,UEP,AS,NV,NS,NXO,NZO,
     *NIN,HPI,A1,A2,A3,A4,D(3),Z(3),CS(3),CZR(3),SUSP,
     *T1,T2,T3
      COMMON/SS3/PRES(11),PRG(11,7),PU1(1,10),PO2(1,10),
     *PG1(7,1,10),PG2(7,1,10)
      COMMON/SS4/CC(6),A(6,6)
      COMMON/SS5/WID
      COMMON/SS6/RDS(11),DX(11),DDX(11),DRS(11,6),DR1(11,6),DR2(11,6)
      NMS=NV+1
      BECC=1.E-4
C     AXIAL SHIFT OF BUBBLE Z-CYLINDRICAL CO-ORDINATE AXIS
C     WITH RESPECT TO THE CHANNEL AXIS OF SYMMETRY
      AS=BECC*X(5)
C     INITIATION OF ARRAYS
      DO 11 I=1,NS
C     PRES(I)=PRESSURES AT ITH SAMPLING POINT
      PRES(I)=0.0
      DO 11 J=1,NMS
C     PRG(I,J)=PRESSURE GRADIENTS OF ITH SAMPLING POINTS
C     WITH RESPECT TO THE NV RADIAL VARIABLES AND THE BUBBLE AXIAL SHIFT
      PRG(I,J)=0.0
   11 CONTINUE
C     GENERATION OF THE MATRIX ELEMENTS A(I,J)
      DO 10 I=1,NV
      DO 10 J=1,NV
      Q=(2.0*I-1)*A1
      A(I,J)=COS((J-1)*Q)
   10 CONTINUE
C     INVERSION OF A(I,J) TO A(I,J)
```

```
      L(K)=I
      M(K)=J
   20 CONTINUE
C
C        INTERCHANGE ROWS
C
      J=L(K)
      IF(J-K) 35,35,25
   25 KI=K-N
      DO 30 I=1,N
      KI=KI+N
      HOLD=-A(KI)
      JI=KI-K+J
      A(KI)=A(JI)
   30 A(JI) =HOLD
C
C        INTERCHANGE COLUMNS
C
   35 I=M(K)
      IF(I-K) 45,45,38
   38 JP=N*(I-1)
      DO 40 J=1,N
      JK=NK+J
      JI=JP+J
      HOLD=-A(JK)
      A(JK)=A(JI)
   40 A(JI) =HOLD
C
C        DIVIDE COLUMN BY MINUS PIVOT (VALUE OF PIVOT ELEMENT IS
C        CONTAINED IN BIGA)
C
   45 IF(BIGA) 48,46,48
   46 D=0.0
      RETURN
   48 DO 55 I=1,N
      IF(I-K) 50,55,50
   50 IK=NK+I
      A(IK)=A(IK)/(-BIGA)
   55 CONTINUE
C
C        REDUCE MATRIX
C
      DO 65 I=1,N
      IK=NK+I
      IJ=I-N
      DO 65 J=1,N
      IJ=IJ+N
      IF(I-K) 60,65,60
   60 IF(J-K) 62,65,62
   62 KJ=IJ-I+K
      A(IJ)=A(IK)*A(KJ)+A(IJ)
   65 CONTINUE
C
C        DIVIDE ROW BY PIVOT
C
      KJ=K-N
      DO 75 J=1,N
      KJ=KJ+N
      IF(J-K) 70,75,70
   70 A(KJ)=A(KJ)/BIGA
```

```
   75 CONTINUE
C
C          PRODUCT OF PIVOTS
C
      D=D*BIGA
C
C          REPLACE PIVOT BY RECIPROCAL
C
      A(KK)=1.0/BIGA
   80 CONTINUE
C
C          FINAL ROW AND COLUMN INTERCHANGE
C
      K=N
  100 K=(K-1)
      IF(K) 150,150,105
  105 I=L(K)
      IF(I-K) 120,120,108
  108 JQ=N*(K-1)
      JR=N*(I-1)
      DO 110 J=1,N
      JK=JQ+J
      HOLD=A(JK)
      JI=JR+J
      A(JK)=-A(JI)
  110 A(JI) =HOLD
  120 J=M(K)
      IF(J-K) 100,100,125
  125 KI=K-N
      DO 130 I=1,N
      KI=KI+N
      HOLD=A(KI)
      JI=KI-K+J
      A(KI)=-A(JI)
  130 A(JI) =HOLD
      GO TO 100
  150 RETURN
      E N D
      SUBROUTINE FLNL(N,NC,MM,IGK,X,G,H,W,EPS,XE,IH,IK,XB,
     *IFINIS)
C     THIS SUBROUTINE SOLVES CONSTRAINED PROBLEMS
C     USING THE LEAST P(TH) APPROXIMATION.
C
      COMMON /WY1/ IFN,KO
      COMMON /WY2/ ALFA,IA,IC,IM
      COMMON /WY4/ P,EPSC
      DIMENSION X(1), G(1), H(1), W(1), EPS(1), XE(N,IK,1), XB(1)
      IFINIS=0
      IF (MM.EQ.0) GO TO 2
C     DATA INPUT FOR OPTIMIZATION PROGRAM
      MAX=100
      IPT=2
      EST=1.E-20
      EPSC=1.E-6
      AO=1.0
      PO=4.0
      X(1)=2.8
      X(2)=2.8
      X(3)=2.8
      X(4)=2.8
```

```
      X(5)=2.8
      X(6)=2.8
      X(7)=3.0
      EPS(1)=1.E-8
      EPS(2)=1.E-8
      EPS(3)=1.E-8
      EPS(4)=1.E-8
      EPS(5)=1.E-8
      EPS(6)=1.E-8
      EPS(7)=1.E-10
      JPRINT=1
      P=PO
      ALFA=AO
      MODE=0
C     GRADIENT CHECK                                                    A
C                                                                       A
      IF (IGK.EQ.1) CALL GROCHK (N,X,G,W)                               A
2     CONTINUE                                                          A
      P=PO                                                              A
      IF (IPT.EQ.0) GO TO 3                                             A
      WRITE (6,34)                                                      A
      WRITE (6,35)                                                      A
      WRITE (6,36)                                                      A
3     IM=0                                                              A
      IT=0                                                              A
      CALL SECOND (T1)                                                  A
4     IC=0                                                              A
C                                                                       A
C     MINIMIZATION                                                      A
C                                                                       A
      CALL QUASIN (N,X,U,G,H,W,EST,EPS,MODE,MAX,IPT,IEXIT)              A
      IC=1                                                              A
      IM=1                                                              A
      MODE=3                                                            A
      CALL FUNCT (X,F,G,U)                                              A
      IF (IA.EQ.0.OR.IEXIT.EQ.3) GO TO 6                                A
      IF (IT.EQ.5) GO TO 5                                              A
      ALFA=ALFA*10.0                                                    A
      IT=IT+1                                                           A
      GO TO 4                                                           A
5     KO=0                                                              A
      PRINT 15                                                          A
6     CALL SECOND (T2)                                                  A
C                                                                       A
C     SOLUTION OUTPUT                                                   A
C                                                                       A
      CALL FINAL (N,X,F,G,NC,U)                                         A
      PRINT 20, P                                                       A
      IF (IT.EQ.5) CALL EXIT                                            A
      DO 7 I=1,N                                                        A
      G(I)=X(I)                                                         A
7     CONTINUE                                                          A
C                                                                       A
15    FORMAT (*0THE PARAMETER ALPHA HAS BEEN INCREASED 5 TIMES, NO FEASI A
     1BLE SOLUTION HAS BEEN FOUND.*)                                    A
16    FORMAT (5I5)                                                      A
17    FORMAT (1H0/1H ,*INITIAL VALUE OF THE PARAMETER ALPHA*,18(*.*),*AO A
     1 =*,E14.6)                                                        A
18    FORMAT (1H0/1H ,*HIGHEST ORDER OF ESTIMATES USED IN EXTRAPOLATION* A
     1,*..JORDER =*,I4)                                                 A
```

```
19    FORMAT (1H0/1H ,*MULTIPLYING FACTOR IN P VALUE*,21(*.*),*FACTOR =*
     1,E14.6)
20    FORMAT (1H0,15X,*VALUE OF THE PARAMETER P =*,E16.8)
21    FORMAT (1H0/1H0,*ESTIMATES OF THE MINIMAX SOLUTION BY EXTRAPOLATIO
     1N*/1H ,50(*-*)/)
22    FORMAT (1H0,*ORDER*,I3)
23    FORMAT (1H0,*X(*,I2,*) =*,E16.8)
24    FORMAT (5E16.6)
25    FORMAT (1H1,*INPUT DATA*/,1H ,10(*-*),//)
26    FORMAT (1H0,*NUMBER OF INDEPENDENT VARIABLES*,24(*.*),*N =*,I4,/)
27    FORMAT (1H0,*MAXIMUM NUMBER OF ALLOWABLE ITERATIONS*,15(*.*),*MAX
     1=*,I4,/)
28    FORMAT (1H0,*INTERMEDIATE PRINTOUT AT EVERY IPT ITERATIONS*,8(*.*)
     1,*IPT =*,I4,/)
29    FORMAT (1H0,*STARTING VALUE FOR VECTOR X(I)*,21(*.*),*X( 1) =*,E14
     1.6)
30    FORMAT (1H0,51X,*X(*,I2,*) =*,E14.6)
31    FORMAT (1H0/1H ,*TEST QUANTITIES TO BE USED*,23(*.*),*EPS( 1) = ,E
     114.6)
32    FORMAT (1H0,49X,*EPS(*,I2,*) =*,E14.6)
33    FORMAT (1H0/1H ,*ESTIMATE OF LOWER BOUND OF FUNCTION TO BE MINIMIZ
     1ED*,2(*.*),*EST =*,E14.6)
34    FORMAT (1H1)
35    FORMAT (1H0,*OPTIMIZATION BY FLETCHER METHOD*/,1H ,31(*-*),/)
36    FORMAT (1H0,*ITER.*,2X,*FUNCT.*,6X,*ALPHA*,8X,*OBJECTIVE*,6X,*VARI
     1ABLE*,7X,*GRADIENT*/1H0,1X,*NO.* ,3X,*EVALU.*,19X,*FUNCTION*,8X, VE
     2CTOR X(I)*,4X,*VECTOR G(I)*,/)
37    FORMAT (1H0,14X,*EXECUTION TIME IN SECONDS =*,F7.3)
38    FORMAT (1H0/1H ,*THE MARGIN BY WHICH CONSTRAINTS MAY BE VIOLATED*,
     15(*.*),*EPSC =*,E14.6)
      END
      SUBROUTINE FMIMAX (N,NC,NT,F,G,GF,C,GC,U,A,TT,TP)
C
C     THIS SUBROUTINE TRANSFORMS THE CONSTRAINED
C     PROBLEM INTO AN UNCONSTRAINED OBJECTIVE
C     USING THE BANDLER-CHARALAMBOUS TECHNIQUE.
C
      COMMON /WY2/ ALFA,IA,IC,IM
      COMMON /WY3/ PC(100)
      COMMON /WY4/ P,EPSC
      DIMENSION GF(N), C(NC), GC(N,NC), G(N), A(NT), TT(NT), TP(NT)
      Q=P
      AE=0.0
      IA=0
      IF (NC.EQ.0.OR.ALFA.EQ.0.0) GO TO 12
      FA=F/ALFA
      DO 1 I=1,NC
      A(I)=FA-C(I)
1     CONTINUE
      AM=A(1)
      A(NT)=FA
      DO 2 I=2,NT
      AM=AMAX1(AM,A(I))
2     CONTINUE
      IF (AM.LE.0.0) Q=-Q
      SUM1=0.0
      DO 6 I=1,NT
      IF (AM) 5,3,4
3     AE=1.E-10
      GO TO 5
```

```
4       IF (A(I).LE.0.0) GO TO 6                                          B
5       TT(I)=(A(I)-AE)/(AM-AE)                                           B
        TP(I)=TT(I)**Q                                                    B
        SUM1=SUM1+TP(I)                                                   B
6       CONTINUE                                                          B
        SUMT=ALFA*SUM1**(1./Q)                                            B
        U=(AM-AE)*SUMT                                                    B
        DO 11 I=1,N                                                       B
        XX=GF(I)/ALFA                                                     B
        SUM2=0.0                                                          B
        DO 10 J=1,NT                                                      B
        IF (AM) 6,8,7                                                     B
7       IF (A(J).LE.0.0) GO TO 10                                         B
8       YY=TP(J)/TT(J)                                                    B
        ZZ=XX*YY                                                          B
        IF (J.EQ.NT) GO TO 9                                              B
        SUM2=SUM2+ZZ-YY*GC(I,J)                                           B
        GO TO 10                                                          B
9       SUM2=SUM2+ZZ                                                      B
10      CONTINUE                                                          B
        G(I)=(SUMT*SUM2)/SUM1                                             B
11      CONTINUE                                                          B
        GO TO 14                                                          B
12      U=F                                                               B
        DO 13 I=1,N                                                       B
        G(I)=GF(I)                                                        B
13      CONTINUE                                                          B
14      IF (IC.EQ.0.OR.NC.EQ.0) GO TO 16                                  B
        DO 15 I=1,NC                                                      B
        PC(I)=C(I)                                                        B
        CT=C(I)+EPSC                                                      B
        IF (CT.LT.0.0) IA=1                                               B
15      CONTINUE                                                          B
16      RETURN                                                            B
        END                                                               B
        SUBROUTINE GRDCHK (N,X,G,W)                                       C
C                                                                         C
C       THIS SUBROUTINE PERFORMS GRADIENT CHECK                           C
C                                                                         C
        DIMENSION X(N), G(N), W(N)                                        C
        JJJ=0                                                             C
        CALL FUNCT (X,F,G,U)                                              C
        WRITE (6,3)                                                       C
        WRITE (6,4)                                                       C
        DO 1 I=1,N                                                        C
        Z=X(I)                                                            C
        DX=1.E-4*X(I)                                                     C
        IF (ABS(DX).LT.1.E-10) DX=1.E-10                                  C
        X(I)=Z+DX                                                         C
        CALL FUNCT (X,F,W,U2)                                             C
        X(I)=Z-DX                                                         C
        CALL FUNCT (X,F,W,U1)                                             C
        Y=0.5*(U2-U1)/DX                                                  C
        X(I)=Z                                                            C
        IF (ABS(Y).LT.1.E-14) Y=1.E-14                                    C
        IF (ABS(G(I)).LT.1.E-14) G(I)=1.E-14                              C
        YP=ABS((Y-G(I))/Y)*100.0                                          C
        WRITE (6,5) G(I),Y,YP                                             C
        IF (YP.GT.10.0) JJJ=1                                             C
1       CONTINUE                                                          C
```

```
      IF (JJJ.EQ.1) GO TO 2
      WRITE (6,6)
      RETURN
2     WRITE (6,7)
      CALL EXIT
C
C
C
3     FORMAT (1H1,/1H ,*GRADIENT CHECK AT STARTING POINT*/1H ,32(*-*))
4     FORMAT (///,1H0,5X,*ANALYTICAL GRADIENTS*,5X,*NUMERICAL GRADIENTS*
     1,5X,*PERCENTAGE ERROR*)
5     FORMAT (1H0,8X,E14.6,10X,E14.6,8X,E14.6)
6     FORMAT (1H0,///1H ,*GRADIENTS ARE O.K.*)
7     FORMAT (1H0,///1H ,*YOUR PROGRAM HAS BEEN TERMINATED BECAUSE GRADI
     1ENTS ARE INCORRECT*/1H0,*PLEASE CHECK IT AGAIN*)
      END
      SUBROUTINE QUASIN (N,X,U,G,H,W,EST,EPS,MODE,MAX,IPT,IEXIT)
C
C     THE FLETCHER(1972) METHOD OF MINIMIZATION
C
      DIMENSION X(1), G(1), H(1), W(1), EPS(1)
      COMMON /WY1/ IFN,KO
      COMMON /WY2/ ALFA,IA,IC,IM
      KO=0
      IF (IM.EQ.1) GO TO 1
      ITN=0
      IFN=1
1     CONTINUE
      NP=N+1
      N1=N-1
      NN=N*NP/2
      IS=N
      IU=N
      IV=N+N
      IB=IV+N
      IEXIT=0
      IF (MODE.EQ.3) GO TO 7
      IF (MODE.EQ.2) GO TO 4
      IJ=NN+1
      DO 3 I=1,N
      DO 2 J=1,I
      IJ=IJ-1
      H(IJ)=0.
2     CONTINUE
      H(IJ)=1.
3     CONTINUE
      GO TO 7
4     CONTINUE
      IJ=1
      DO 6 I=2,N
      Z=H(IJ)
      IF (Z.LE.0.) RETURN
      IJ=IJ+1
      I1=IJ
      DO 6 J=I,N
      ZZ=H(IJ)
      H(IJ)=H(IJ)/Z
      JK=IJ
      IK=I1
      DO 5 K=I,J
```

```
      JK=JK+NP-K
      H(JK)=H(JK)-H(IK)*ZZ
      IK=IK+1
5     CONTINUE
6     IJ=IJ+1
      IF (H(IJ).LE.0.) RETURN
7     CONTINUE
      IJ=NP
      DMIN=H(1)
      DO 8 I=2,N
      IF (H(IJ).GE.DMIN) GO TO 8
      DMIN=H(IJ)
8     IJ=IJ+NP-I
      IF (DMIN.LE.0.) RETURN
      Z=EST
      CALL FUNCT (X,F,G,U)
      DF=U-EST
      IF (DF.LE.0.0) DF=1.0
9     CONTINUE
      IF (IPT.EQ.0) GO TO 10
      IF (MOD(ITN,IPT).NE.0) GO TO 10
      PRINT 45, ITN,IFN,ALFA,U,((X(I),G(I)),I=1,N)
10    CONTINUE
      ITN=ITN+1
      W(1)=-G(1)
      DO 12 I=2,N
      IJ=I
      I1=I-1
      Z=-G(I)
      DO 11 J=1,I1
      Z=Z-H(IJ)*W(J)
      IJ=IJ+N-J
11    CONTINUE
      W(I)=Z
12    CONTINUE
      W(IS+N)=W(N)/H(NN)
      IJ=NN
      DO 14 I=1,N1
      IJ=IJ-1
      Z=0.
      DO 13 J=1,I
      Z=Z+H(IJ)*W(IS+NP-J)
      IJ=IJ-1
13    CONTINUE
      W(IS+N-I)=W(N-I)/H(IJ)-Z
14    CONTINUE
      GS=0.
      DO 15 I=1,N
      GS=GS+W(IS+I)*G(I)
15    CONTINUE
      IEXIT=2
      IF (GS.GE.0.) GO TO 37
      GS0=GS
      ALPHA=-2.*DF/GS
      IF (ALPHA.GT.1.) ALPHA=1.
      DF=U
      TOT=0.
16    CONTINUE
      IEXIT=3
      IF (ITN.EQ.MAX) GO TO 37
```

```
      ICON=0
      IEXIT=1
      DO 17 I=1,N
      Z=ALPHA*W(IS+I)
      IF (ABS(Z).GE.EPS(I)) ICON=1
      X(I)=X(I)+Z
17    CONTINUE
      CALL FUNCT (X,F,W,UY)
      IFN=IFN+1
      GYS=0.
      DO 18 I=1,N
      GYS=GYS+W(I)*W(IS+I)
18    CONTINUE
      IF (UY.GE.U) GO TO 19
      IF (ABS(GYS/GS0).LE..9) GO TO 21
      IF (GYS.GT.0.) GO TO 19
      TOT=TOT+ALPHA
      Z=10.
      IF (GS.LT.GYS) Z=GYS/(GS-GYS)
      IF (Z.GT.10.) Z=10.
      ALPHA=ALPHA*Z
      U=UY
      GS=GYS
      GO TO 16
19    CONTINUE
      DO 20 I=1,N
      X(I)=X(I)-ALPHA*W(IS+I)
20    CONTINUE
      IF (ICON.EQ.0) GO TO 37
      Z=3.*(U-UY)/ALPHA+GYS+GS
      ZZ=SQRT(Z*Z-GS*GYS)
      GZ=GYS+ZZ
      Z=1.-(GZ-Z)/(ZZ+GZ-GS)
      ALPHA=ALPHA*Z
      GO TO 16
21    CONTINUE
      ALPHA=TOT+ALPHA
      U=UY
      IF (ICON.EQ.0) GO TO 35
      DF=DF-U
      DGS=GYS-GS0
      LINK=1
      IF (DGS+ALPHA*GS0.GT.0.) GO TO 23
      DO 22 I=1,N
      W(IU+I)=W(I)-G(I)
22    CONTINUE
      SIG=1./(ALPHA*DGS)
      GO TO 30
23    CONTINUE
      ZZ=ALPHA/(DGS+ALPHA*GS0)
      Z=DGS*ZZ-1.
      DO 24 I=1,N
      W(IU+I)=Z*G(I)+W(I)
24    CONTINUE
      SIG=1./(ZZ*DGS*DGS)
      GO TO 30
25    CONTINUE
      LINK=2
      DO 26 I=1,N
      W(IU+I)=G(I)
```

```
26      CONTINUE                                                          D
        IF (DGS+ALPHA*GS0.GT.0.) GO TO 27                                 D
        SIG=1./GS0                                                        D
        GO TO 30                                                          D
27      CONTINUE                                                          D
        SIG=-ZZ                                                           D
        GO TO 30                                                          D
28      CONTINUE                                                          D
        DO 29 I=1,N                                                       D
        G(I)=W(I)                                                         D
29      CONTINUE                                                          D
        GO TO 9                                                           D
30      CONTINUE                                                          D
        W(IV+1)=W(IU+1)                                                   D
        DO 32 I=2,N                                                       D
        IJ=I                                                              D
        I1=I-1                                                            D
        Z=W(IU+I)                                                         D
        DO 31 J=1,I1                                                      D
        Z=Z-H(IJ)*W(IV+J)                                                 D
        IJ=IJ+N-J                                                         D
31      CONTINUE                                                          D
        W(IV+I)=Z                                                         D
32      CONTINUE                                                          D
        IJ=1                                                              D
        DO 33 I=1,N                                                       D
        IVI=IV+I                                                          D
        IBI=IB+I                                                          D
        Z=H(IJ)+SIG*W(IVI)*W(IVI)                                         D
        IF (Z.LE.0.) Z=CMIN                                               D
        IF (Z.LT.OMIN) OMIN=Z                                             D
        H(IJ)=Z                                                           D
        W(IBI)=W(IVI)*SIG/Z                                               D
        SIG=SIG-W(IBI)*W(IBI)*Z                                           D
        IJ=IJ+NP-I                                                        D
33      CONTINUE                                                          D
        IJ=1                                                              D
        DO 34 I=1,N1                                                      D
        IJ=IJ+1                                                           D
        I1=I+1                                                            D
        DO 34 J=I1,N                                                      D
        W(IU+J)=W(IU+J)-H(IJ)*W(IV+I)                                     D
        H(IJ)=H(IJ)+W(IB+I)*W(IU+J)                                       D
34      IJ=IJ+1                                                           D
        GO TO (25,28), LINK                                               D
35      CONTINUE                                                          D
        DO 36 I=1,N                                                       D
        G(I)=W(I)                                                         D
36      CONTINUE                                                          D
37      CONTINUE                                                          D
        IF (IEXIT.EQ.1) KO=1                                              D
        IF (IPT.EQ.0) GO TO 38                                            D
        PRINT 45, ITN,IFN,ALFA,U,((X(I),G(I)),I=1,N)                      D
38      IF (IEXIT.EQ.0) GO TO 39                                          D
        GO TO 40                                                          D
39      PRINT 46, IEXIT                                                   D
        GO TO 44                                                          D
40      GO TO (41,42,43), IEXIT                                           D
41      PRINT 47, IEXIT                                                   D
        GO TO 44                                                          D
```

```
42      PRINT 48, IEXIT
        GO TO 44
43      PRINT 49, IEXIT
44      CONTINUE
        RETURN
C
C
C
45      FORMAT (1H ,I3,5X,I3,6X,E10.3,1X,E14.6,1X,80(E14.6,1X,E14.6/44X))
46      FORMAT (1H1,*IEXIT =*,I2/1H0,*THE ESTIMATE OF THE HESSIAN MATRIX I
       1S NOT POSITIVE DEFINITE*)
47      FORMAT (1H1,*IEXIT =*,I2/1H0,*CRITERION FOR OPTIMUM (CHANGE IN VEC
       1TOR X .LT. EPS) HAS BEEN SATISFIED*)
48      FORMAT (1H1,*IEXIT =*,I2/1H0,*EPS CHOSEN IS TOO SMALL*)
49      FORMAT (1H1,*IEXIT =*,I2/1H0,*MAXIMUM NUMBER OF ALLOWABLE ITERATIO
       1NS HAS BEEN REACHED*)
        END
        SUBROUTINE FINAL (N,X,F,G,NC,U)
C
C       THIS SUBROUTINE OUTPUTS THE OPTIMAL SOLUTION
C
        DIMENSION X(N), G(N)
        COMMON /WY1/ IFN,KO
        COMMON /WY2/ ALFA,IA,IC,IM
        COMMON /WY3/ PC(100)
        IF (KO.EQ.0) GO TO 1
        WRITE (6,4)
        GO TO 2
1       WRITE (6,5)
2       WRITE (6,6) U
        WRITE (6,9) F
        WRITE (6,7) (I,X(I),I,G(I),I=1,N)
        IF (NC.EQ.0) GO TO 3
        WRITE (6,10)
        WRITE (6,11) (I,PC(I),I=1,NC)
3       WRITE (6,8) IFN
        WRITE (6,12) ALFA
        RETURN
C
C
C
4       FORMAT (1H0,/1H0,*OPTIMAL SOLUTION FOUND BY FLETCHER METHOD*/1H ,4
       11(*-*))
5       FORMAT (1H0,/1H0,*RESULTS FOUND BY FLETCHER METHOD AT LAST ITERATI
       1ON*/1H ,50(*-*))
6       FORMAT (1H0,//4X,*ARTIFICIAL UNCONSTRAINED FUNCTION  U =*,E16.6)
7       FORMAT (1H0,3X,*X(*,I2,*) =*,E16.6,8X,*G(*,I2,*) =*,E16.6)
8       FORMAT (1H0,/1H ,9X,*NUMBER OF FUNCTION EVALUATIONS =*,I5)
9       FORMAT (1H0,11X,*ACTUAL OBJECTIVE FUNCTION  F =*,E16.6/)
10      FORMAT (1H0,/1H ,3X,*INEQUALITY CONSTRAINTS*)
11      FORMAT (1H0,3X,*C(*,I2,*) =*,E16.6)
12      FORMAT (1H0,5X,*FINAL VALUE OF THE PARAMETER ALPHA =*,E16.6)
        END
```